Optical properties of high-temperature superconductors

D.B. Tanner and T. Timusk

in

Physical Properties of High-Temperature Superconductors III,

edited by Donald M. Ginsberg

(World Scientific, Singapore, 1992)

pp. 363–469.

Optical Properties of High-Temperature Superconductors

D.B. Tanner

Department of Physics, University of Florida, Gainesville, Florida 32611

T. Timusk

Department of Physics, McMaster University, Hamilton, Ont., Canada L8S 4M1

TABLE OF CONTENTS

I. INTRODUCTION

It is now more than five years since the discovery of high-temperature superconductivity. During this time an enormous amount of labor has gone toward investigating the cuprate superconducting materials, yet they remain in many ways as surprising and as little understood as at the time of their discovery. This is particularly true of the infrared optical properties, despite nearly 300 published papers in the area. These properties are also sometimes controversial, and they remain a fascinating subject. In this review we discuss the infrared properties, focussing on the studies of the a-b-plane conductivity of crystals and thin films that have appeared since an earlier review.[1]

Over the last several years, there has been substantial progress made in preparing high-quality crystals and oriented films. In some cases these are even true "single" crystals, exhibiting no twinning of the a and b axes, allowing anisotropy in the CuO_2 layers to be studied. In contrast to our earlier review, which was mostly about polycrystalline samples (although some pioneering crystal work was included), here we will discuss almost exclusively studies of the a-b-plane of highly oriented material.

There have been various important advances in our understanding of these materials. For example, it is now generally agreed that the insulating "parent" phases of the cuprate superconductors are charge-transfer insulators,[2] with a gap of about 2 eV (16,000 cm^{-1}). This charge transfer gap is stabilized by the combination of a large on-site Hubbard U on copper, which prevents double electron occupancy of a Cu site, and by the difference in energies between the Cu $d_{x^2-y^2}$ and the O p_x and p_y orbitals. Second, it is also well-accepted that when holes are introduced onto the CuO_2 layers, they occupy oxygen sites for the most part. These holes also are the mobile charge carriers responsible for the superconductivity and for the unusual normal-state properties. In Section IIwe will see several examples of the way that the charge-transfer gap fills in as holes are added.

Third, the idea that the high temperature superconductors are "clean-limit" superconductors has achieved wide recognition. The clean limit occurs when the value of the electronic mean free path of the normal state lies between the superconducting coherence length and penetration depth: $\xi < \ell < \lambda$. This case differs from the situation of pure metals. Pure metals at low temperatures enter the anomalous skin effect regime, where the mean free path is much longer than the electromagnetic penetration depth, *i.e.*, $\delta < \ell$. The electrodynamics of the superconductor in the anomalous skin effect limit are essentially the same as in the dirty limit.[3] The difference between pure

metals and the copper oxide materials is that the latter have comparitively smaller coherence lengths and lower carrier concentrations, which means lower conductivity, hence, longer penetration depths and the normal skin effect limit. It is in this normal skin effect regime that the clean-limit case occurs.

The outline of this review is as follows. Following this introduction, we will jump right in to a discussion of recent results and their interpretation. We have not included in this review any tutorial material covering the general optical properties of solids. Formulas, approaches, and ideas will be introduced as needed, without detailed derivations. We provided some background in our earlier review and readers unfamiliar with optical measurements in superconductors should probably read Section II of Ref. 1. Section II describes the non-Drude "midinfrared" absorption, a feature that appears as soon as carriers are added to the copper-oxide layers. Section III reviews photoinduced absorption studies, in which carriers are added by photoexcitation of the insulating parent phases. In Section IV we address various models and theories that have been proposed for the normal-state properties and present analyses of data following these models. We turn to the superconducting state in Section V, describing the effect of superconductivity on the reflectance and optical conductivity and discussing evidence for and against various gap assignments. Section VI is about the nature and role of electron-phonon interactions in the optical spectra. Finally, there is a concluding Section where we try to give our perspective on the current state of affairs for the studies of the optical properties of the high temperature superconductors.

Other reviews have addressed the infrared and optical properties of high temperature superconductors. Vibrational spectroscopy, mostly Raman, has been described by Thomsen and Cardona.[4] Raman and infrared phonon spectroscopies have been discussed by Feile.[5] The optical properties (as well as transport, Raman, and photoemission) were included in a review by Kitazawa and Tajima.[6] Thomas[7] has recently reviewed infrared measurements, with a focus on low doping levels and the metal-insulator transition. Renk[8] has recently described far-infrared studies, with emphasis on the superconducting state as well as with some discussion of applications.

II. THE MIDINFRARED ABSORPTION

It is generally accepted that all of the high T_c superconductors show non-Drude behavior in the infrared region.[1,9–11] Four pieces of evidence lead to this conclusion:

1. The temperature dependence of the a-b-plane optical response in the infrared is very small. The dc conductivity changes by a factor of three between 100 and 300 K, while the midinfrared reflectance hardly changes at all. Yet, one expects for the Drude model that the width of the plasma edge should be determined by the relaxation rate of the carriers. A considerable broadening with increasing temperature should then occur, but does not.
2. At lower frequencies there is a definite temperature dependence, with the far-infrared conductivity (above T_c) in good agreement with the dc conductivity.[10–17]
3. Attempts to fit the data with a simple Drude model give extreme values for the scattering rate. Values as large as 1 eV (8000 cm^{-1}) have been reported, which would imply mean free paths no larger than the lattice constant.
4. The quality of the fits is not particularly good, with the Drude model predicting considerable curvature to the midinfrared reflectance, in contrast to the nearly linear drop observed.[18]

The midinfrared absorption has been explained in two ways, which we call "one-component" and "two-component" pictures. In a one-component picture,[11,13,17,19–24] all of the midinfrared absorption is viewed as due to the same carriers, the ones which are responsible for the dc/far-infrared conductivity and which become the superconducting condensate below T_c. The difference between the two regions is attributed to a strong frequency dependence in the scattering rate and the carrier effective mass. This approach requires that the frequency dependence be rather strong, because the far-infrared data imply a 100 K scattering rate of $1/\tau \sim 100$ cm^{-1} while the midinfrared data need $1/\tau \sim 5000$ cm^{-1}.

In the two-component picture,[9–12,14–16,18,25–34] the oxide superconductors are viewed as containing two types of carriers: free carriers, which are responsible for the dc conductivity and which condense to form the superfluid below T_c, and bound carriers, which have a semiconductor-like gap for excitations from their bound states. The free carriers have an essentially ω-independent relaxation rate $1/\tau$. The T-linear temperature dependence of the resistivity is assumed to come from the temperature dependence of $1/\tau$ since in the Drude model, $\rho = 4\pi/\omega_{pD}^2\tau$, where ω_{pD} is the plasma frequency of the free carriers. The bound carriers are in a broad, nearly T-independent

band throughout the midinfrared. The apparent semiconducting gap is found to be rather small, of order 150–300 cm^{-1}.

A. Overview

In the rest of this Section, we will consider the midinfrared conductivity in a variety of oxide superconductors. All show non-Drude infrared behavior, as do a number of other mixed-valence oxide conductors.[1] Most of the families of oxide superconductors are shown in Fig. 1, from Kim *et al.*[35] The reflectance drops in a nearly linear fashion throughout the infrared region. The principal difference is that the "plasma minimum" varies between 1 and 2 eV for the four materials.

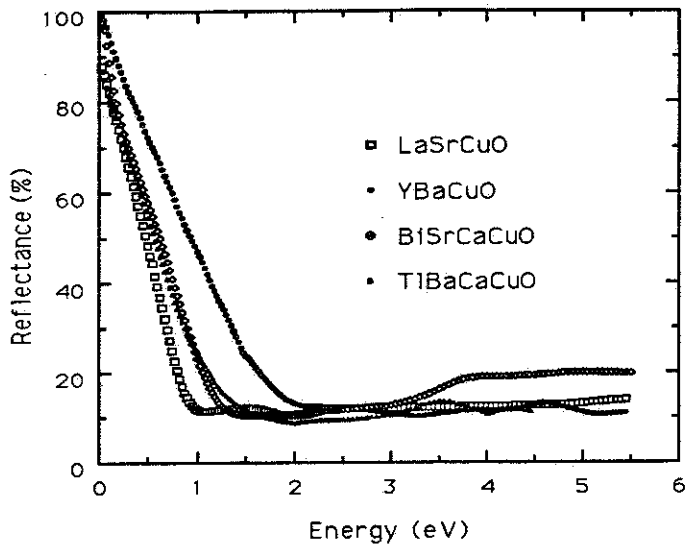

Fig. 1. Infrared–ultraviolet reflectance of four oxide superconductors: $La_{1.85}Sr_{0.15}CuO_4$, $YBa_2Cu_3O_{7-\delta}$, $Bi_2Sr_2CaCu_2O_8$, and $Tl_2Ba_2Ca_2Cu_3O_{10}$. [Ref. 35.]

In the following, we will first describe the three main cuprate families: the 2-1-4 material ($La_{2-x}Sr_xCuO_4$ and $Nd_{2-x}Ce_xCuO_4$), the bismuth, thallium, and lead-based systems (*e.g.*, $Bi_2Sr_2CaCu_2O_8$, $Tl_2Ba_2Ca_2Cu_3O_{10}$ and $Pb_2Sr_2LCu_3O_8$), and finally $YBa_2Cu_3O_{7-\delta}$. This sequence is chosen because it goes from the simplest to the most complicated material. In Section IV we will discuss the one- and two-component analyses which have been done for these materials.

B. $La_{2-x}Sr_xCuO_4$

$La_{2-x}Sr_xCuO_4$ is the simplest of the high temperature superconductors, with only one CuO_2 plane per formula unit (two per unit cell on account of the body-centered structure). In addition, the carrier concentration can be varied over a wide range $0 \lesssim x \lesssim 0.3$, taking it systematically from an antiferromagnetic insulator, through a superconductor, to a very unusual metal.

There were many early studies of ceramic samples,[1] including the first reports of midinfrared absorption bands.[36,37] One important result from these pellet studies was the discovery by Tajima *et al.*[38] that the plasmon minimum (which is quite similar in ceramics and in single crystals) does not shift with doping concentration.[39–42] This pinning of the plasmon minimum is unusual; in simple metals the minimum occurs near the screened plasma frequency

$$\tilde{\omega}_p = \sqrt{4\pi n e^2/m^*\epsilon_\infty} \tag{1}$$

and so should shift to higher frequencies as n is increased.

Another interesting early result from Tajima *et al.*[43] and Collins *et al.*,[44] based on the first single-crystal results, is the large anisotropy between the a-b plane and the c axis. Even when the a-b plane has a quite metallic appearance, the c axis remains insulating.

One problem for optical studies of $La_{2-x}Sr_xCuO_4$ is the well-known difficulty of producing large, homogeneously doped, single crystals. Thus, many of the early studies used crystals which either had rather low and broad superconducting transitions or were not superconducting at all. However, the room-temperature optical properties of good quality $La_{2-x}Sr_xCuO_4$ crystals have recently been reported by Uchida *et al.*[33,45] The samples had doping levels in the range $0 \le x \le 0.34$. The sample with $x = 0.15$ displayed a rather sharp superconducting transition at $T_c = 27$ K, somewhat below the expected 38 K value for this concentration. Two other samples ($x = 0.10$ and $x = 0.20$) were also superconducting, at 18 and 22 K, respectively.

1. Reflectance

Uchida *et al.*[33] measured the reflectance out to 30 eV. Fig. 2 shows the reflectance of these samples over 0.05–4 eV (400–32,000 cm^{-1}). A number of interesting features can be seen in these spectra. First, for $x = 0$, the reflectance is that of an insulator with a strong phonon near 700 cm^{-1} (≈ 0.09 eV in the figure), a nearly constant

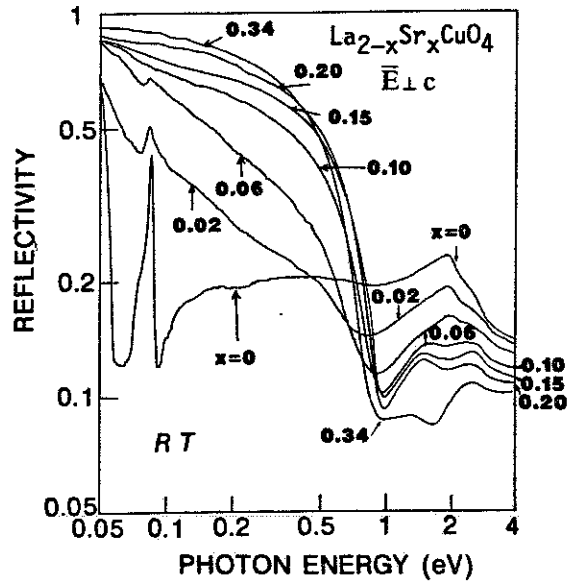

Fig. 2. Reflectance at 300 K of $La_{2-x}Sr_xCuO_4$ for compositions $0 \leq x \leq 0.34$. The electric field is polarized in the a-b plane. Note the logarithmic scales for both $\mathcal{R}$ and ω. [Ref. 33.]

midinfrared reflectance, and an electronic band (the Cu-O charge transfer band) peaked around 2 eV. Lower frequency phonons[43,44,46] at 140 and 360 cm^{-1} are not shown in this plot. Second, with doping, a broad absorption band grows in the midinfrared region, the phonon feature becomes obscured, and the charge transfer band becomes weaker. The position of the ~1 eV plasmon minimum between the midinfrared and charge transfer bands is nearly insensitive to doping.

Third, and not so easy to see, there is a weak shift in the plasmon minimum *to lower energies* in the case of the $x = 0.34$ sample. Because the plasmon minimum is related to the oscillator strength of the midinfrared and far-infrared regions (all else being equal), this suggests a diminution of oscillator strength in the heavily doped, non-superconducting materials.

2. Optical conductivity

These points can be seen more easily by inspecting the optical conductivity, shown in Fig. 3, obtained by Kramers-Kronig analysis of reflectance. The undoped material is an insulator, with a well-established charge-transfer absorption around 2 eV (16,000 cm^{-1}). The conductivity is very low below 1 eV. (There may be some minor problems with the measurements in the region below the charge transfer gap, as the conductivity gives every evidence of dipping below zero just below 1 eV and the contribution of

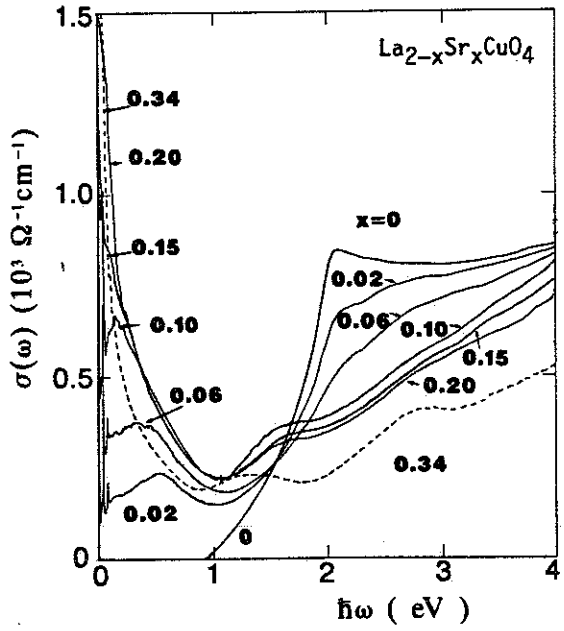

Fig. 3. Optical conductivity of $La_{2-x}Sr_xCuO_4$ at 300 K. Data are shown for $0 \leq x \leq 0.34$. [Ref. 33.]

the phonons is not shown.) With doping, the intensity of the charge-transfer band is reduced, and new features appear in the midinfrared region and around 1.5 eV.

The midinfrared band in Fig. 3 has a definite maximum in the lightly-doped samples, yielding evidence that it is a transition distinct from the low-frequency Drude absorption. The maximum is around 0.5 eV (4000 cm^{-1}) when $x = 0.02$; moves to 0.14 eV (1100 cm^{-1}) for $x = 0.1$; and is only a shoulder in the $x = 0.15$ sample. One reason that the midinfrared band is not as visible in the more highly doped samples is that the dc and far-infrared conductivity is increasing rapidly with doping. Nevertheless, there is clearly a midinfrared peak in $\sigma_1(\omega)$ for samples which are also superconducting.

It is interesting to note that the phonons (to the extent that they can be seen in Fig. 3) have about the same intensity at all doping levels while the electronic background increases. This would imply that these phonon modes are not screened in the ordinary sense of having their TO-LO splitting decrease to zero, but instead retain some ionic character, even in the conducting phase.

Finally, the dc conductivity increases rapidly with doping. The dc and far-infrared conductivities are in fair agreement. For example, Fig. 3 would suggest that the $x = 0.10$ sample has $\rho_{fir} \approx 1700$ $\mu\Omega$-cm while the measured a-b-plane resistivity is

ρ_{dc} = 900 $\mu\Omega$-cm. It is not uncommon to find such a factor of two between far-infrared and dc values for the resistivity; part of the discrepancy may be due to unknown contribution of the midinfrared band in this material at low frequency, part the combined experimental uncertainties of the two methods.

3. Dielectric function and energy-loss function

Two other optical functions presented by Uchida *et al.*[33] are shown in Figs. 4 and 5. These figures show respectively the real part of the dielectric function, $\epsilon_1(\omega)$, and the energy-loss function, $-\operatorname{Im} 1/\epsilon(\omega)$.

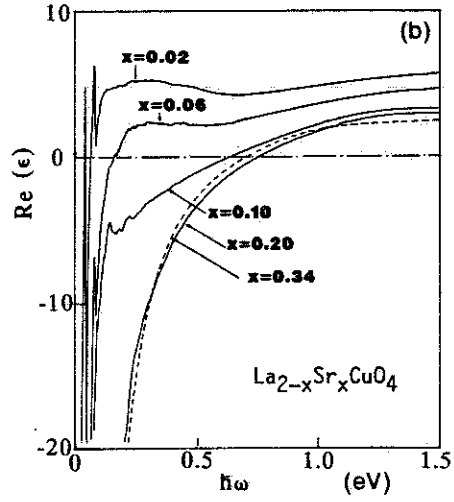

Fig. 4. The real part of the dielectric function of $La_{2-x}Sr_xCuO_4$ for Sr concentrations between 0.02 and 0.34. [Ref. 33.]

The dielectric function is negative at low frequencies, as expected for a metal, although the crossing for the lowest concentration occurs in the phonon region. For $0.10 \leq x \leq 0.34$, the zero in $\epsilon_1(\omega)$ occurs near 0.7 eV. This insensitivity of the zero-crossing to the dopant concentration is made even more remarkable by the fact that the high frequency limiting value of $\epsilon_1(\omega)$ decreases at the same time. This decrease is a consequence of the transfer of oscillator strength from the charge transfer band to the midinfrared and free-carrier absorption.

For either free or bound carriers with a large separation between the binding energy and the plasmon energy, the zero crossing in $\epsilon_1(\omega)$ occurs near the screened plasma frequency, given by Eq. 1. Thus one has $n/m^* = \epsilon_\infty \tilde{\omega}_p^2/4\pi e^2$. If this analysis applies to the data in Fig. 4, one would conclude that the ratio n/m^* does not change (or maybe even decreases) as x increases from 0.10 to 0.34.

A similar conclusion would come from considering the energy-loss function. The maximum in the loss function occurs in simple metals (or in insulators with energy gaps small compared to the plasmon energy) very close to the screened plasma frequency. Fig. 5 shows that the maximum in the loss function is only a weak function of Sr concentration. Typically the loss function maximum is a little above the zero in $\epsilon_1(\omega)$. The loss function may be written as $-\mathrm{Im}(1/\epsilon) = \left(\epsilon_2 + \epsilon_1^2/\epsilon_2\right)^{-1}$ where ϵ_1 and ϵ_2 are the real and imaginary parts of the dielectric function. In cases where $\epsilon_2(\omega)$ is a rapidly decreasing function of ω, the maximum in $-\mathrm{Im}(1/\epsilon)$ occurs above the zero in $\epsilon_1(\omega)$. Note that the maximum is sharp only if $|\epsilon_1| \gg \epsilon_2$ on either side of its zero.

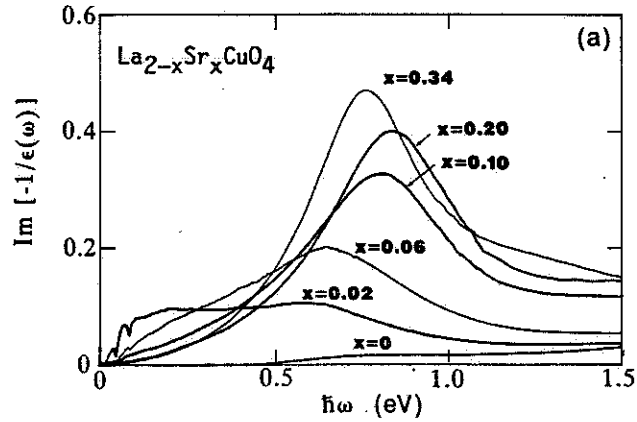

Fig. 5. The energy-loss function of $La_{2-x}Sr_xCuO_4$ for Sr concentrations between 0 and 0.34. [Ref. 33.]

4. Sum rule

Evaluation of the partial sum rule for the optical conductivity leads to rather different conclusions about the number of carriers than inspection of $\epsilon_1(\omega)$ or the loss function. Fig. 6 shows the evaluation by Uchida *et al.*[33] of

$$N_{eff}(\omega) = \frac{2V_c m_e}{\pi e^2} \int_0^{\omega} \sigma_1(\omega')\, d\omega', \tag{2}$$

the effective number of carriers with mass $m^* = m_e$ per formula unit participating in optical excitations for frequencies up to ω. The other quantities in Eq. 2 are m_e, the free-electron mass, and V_c, the volume of one formula unit. (Often, the left hand side of Eq. 2 is written as $N_{eff}\, m_e/m^*$, because optical experiments measure the ratio of carrier concentration to effective mass.)

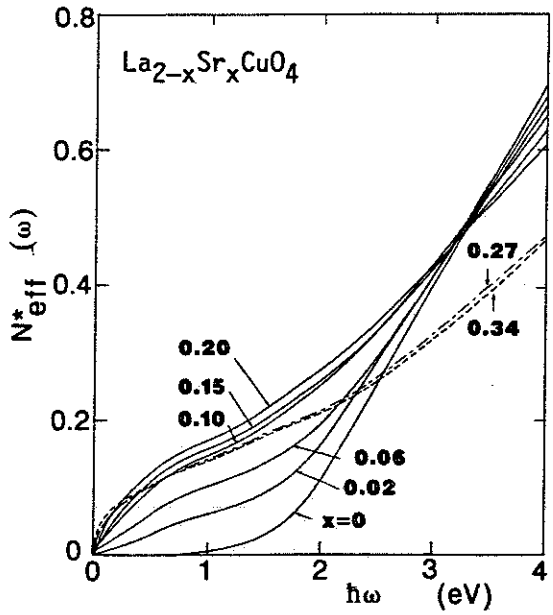

Fig. 6. Effective number of carriers per formula unit for $La_{2-x}Sr_xCuO_4$ at doping levels from 0 to 0.34. The data for $x = 0.27$ and $x = 0.34$ are shown as dashed lines. [Ref. 33.]

N_{eff} is zero up to 1 eV for the $x = 0$ sample, on account of its insulating character. For the conducting samples, N_{eff} increases in the far infrared, and shows a tendency to saturate above 1 eV, but then increases rapidly, beginning just below 2 eV as the charge-transfer and higher energy transitions begin to become important. The plateau value increases quickly up to $x = 0.1$, rises very slowly between $x = 0.1$ and $x = 0.2$, and actually seems to decrease at higher concentrations. The values of N_{eff} are somewhat larger than the dopant concentration, especially at $x < 0.1$, indicating that some charge-transfer oscillator strength has been redistributed to the midinfrared and free-carrier bands. This point was first made by Cooper *et al.*[28] from a study of $Pr_{2-x}Ce_xCuO_4$, to which we now turn.

C. The T′ Re_2CuO_4 compounds

The "electron-doped" T′ materials, of which the prototype is Nd_2CuO_4 but which can be prepared with a number of rare earths *Re* replacing Nd, are structurally very similar to $La_{2-x}Sr_xCuO_4$. The principal difference is the relocation of the apical oxygen to form *Re*-O_2-*Re* layers between CuO_2 layers.

The optical properties of these materials have been investigated by a number of workers.[28,33,34,45,47] They are similar to $La_{2-x}Sr_xCuO_4$. Examples are shown in Fig. 7 from Cooper *et al.*[28] and Fig. 8 from Uchida *et al.*[33] These figures show the

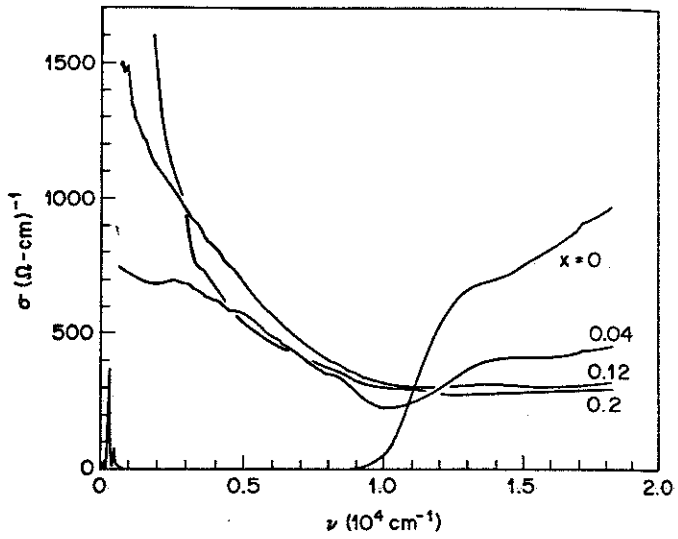

Fig. 7. Room temperature a-b-plane optical conductivity of $Pr_{2-x}Ce_xCuO_4$ for a series of Ce concentrations between 0 and 0.20. [Ref. 28.]

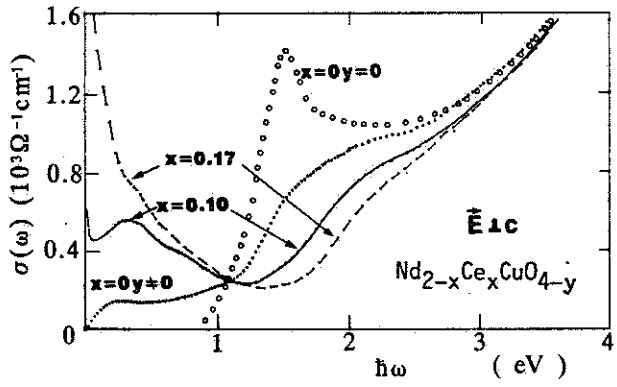

Fig. 8. Room temperature a-b-plane optical conductivity of $Nd_{2-x}Ce_xCuO_{4-y}$ for a series of Ce concentrations between 0 and 0.20. Note that data for two $x = 0$ samples are shown, one fully oxygenated and one somewhat reduced, with an unknown but small number of carriers. [Ref. 33.]

300 K a-b-plane optical conductivity from Kramers-Kronig analysis of reflectance for $Pr_{2-x}Ce_xCuO_4$ (Fig. 7) and for $Nd_{2-x}Ce_xCuO_{4-y}$ (Fig. 8).

If we assume that the $x = 0$ sample for the Pr series is comparable to the $x = 0$, $y \neq 0$ Nd sample, then there is reasonable agreement between the two measurements. First, the low energy oscillator strength grows at the expense of the ~1.5 eV (12,000 cm^{-1}) charge-transfer excitation. Second, there is a maximum (or shoulder) in $\sigma_1(\omega)$ at 3000-4000 cm^{-1} which is particularly noticeable at lower Ce concentrations. In the data from Uchida *et al.* (Fig. 8) this peak is seen up to $x = 0.17$ while Cooper

et al. observe a spectroscopically resolved feature only at $x = 0.04$. At higher concentrations, this midinfrared absorption merges into the low-frequency free-carrier absorption. Nevertheless, the midinfrared absorption shown in Fig. 7 differs substantially from the $1/\omega^2$ behavior expected for free carriers. A Drude conductivity scaled to the $\omega = 1000$ cm^{-1} data for $x = 0.12$ and having a relaxation rate of a few k_BT would decrease to the 60–100 Ω^{-1}cm^{-1} range by 5000 cm^{-1}, a conductivity roughly a factor of ten below the measured value of 600 Ω^{-1}cm^{-1}.

Close inspection of the $x = 0$, $y \neq 0$ data in Fig. 8 reveals the existence of a second low-energy maximum around 0.2 eV (1600 cm^{-1}). This feature can also be seen in the results of Zhang *et al.*[34] and has been studied in detail recently by Thomas *et al.*[48] who find it located at ~0.2 eV in several very lightly doped oxide superconductors. An example is shown in Fig. 9.

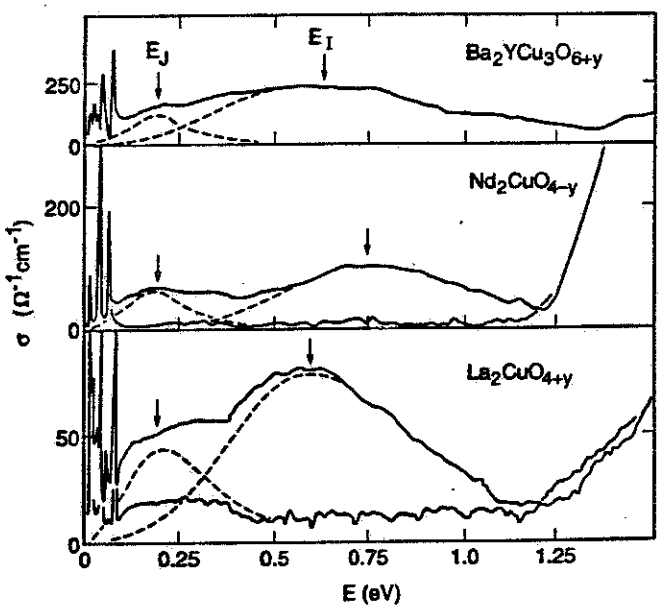

Fig. 9. Optical conductivity in the midinfrared region. of semi-insulating $YBa_2Cu_3O_{6+x}$ (upper panel), Nd_2CuO_{4-y} (center panel), and La_2CuO_4 (lower panel). The peak marked E_J is evident in a variety of oxide superconductors. [Ref. 48.]

In this figure, two bands appear in the midinfrared region. Thomas *et al.* argue that these data provide evidence for a distinct second component to $\sigma_1(\omega)$, in addition to the free carrier absorption. The latter is extremely weak in these samples on account of the high resistivity. Furthermore, the free carriers in these samples are frozen out at low temperatures, yet the midinfrared bands remain essentially unchanged between 10 and 300 K. The principal difference is some broadening,[49] by an

amount of order k_BT. In addition, the conductivity is rising from low frequencies, and more than one maximum is seen. All of these factors imply that it is not possible to argue that all of the midinfrared absorption is due to free carriers, as there is a residue, with substantial oscillator strength, in cases where there are no free carriers. Thomas *et al.* interpret the lower of the bands in Fig. 9 as characterized by the magnetic exchange J. The basic idea is that in the antiferromagnetic insulator, a charge transfer from one CuO_2 unit to an adjacent one costs energy J, because the motion upsets the antiferromagnetic order.

D. The bismuth-based materials

The Bi-based oxide superconductors are a family whose structure consists of 1, 2, or 3 CuO_2 layers, separated by Bi-O layers as well as by layers containing Sr^{+2} ions and apical oxygens. In the 2-layer material, $Bi_2Sr_2CaCu_2O_8$, Ca occupies the position between CuO_2 bilayers that Y does in $YBa_2Cu_3O_7$. Thus the two-layer material is very similar to $YBa_2Cu_3O_{7-\delta}$, with the exception that there are no one-dimensional Cu-O chains. The charge carriers (holes) in the CuO_2 layers are assumed to come from the Bi-O layer, either from defects or by charge transfer. This leaves open the possibility that the Bi-O layer itself could be conducting, as in fact band structure calculations predict.[50] However, scanning tunneling microscope measurements[51] and electron-energy loss studies[52] suggest that the Bi-O layers are insulators with a gap of order 4 eV. This is in agreement with photoelectron spectroscopy of well-annealed samples with the highest transition temperatures.[53] In what follows, we will assume that the Bi-O layers do not contribute significantly to the midinfrared and far-infrared optical spectra.

1. Comparison of the 1, 2, and 3-layer systems.

A direct comparison of the infrared reflectance of the three compounds (2201, 2212, and 2223) has been made on polycrystalline ceramic samples by Maeda *et al.*[54] Their results are shown in Fig. 10. The reflectance minimum is seen to shift upward as the number of layers increases. Fits to a Drude formula give the plasma frequencies shown by the arrows. These frequencies are for the screened plasmon and should be multiplied by $\sqrt{\epsilon_\infty}$ (which was not reported) to estimate the actual plasma frequency.

Maeda *et al.*[54] also studied the effect of Y doping in $Bi_2Sr_2CaCu_2O_8$. Replacing the Ca^{2+} with Y^{3+} reduces the number of holes on the CuO_2 planes and renders the system an insulator around 50% Y. Despite the change in free carrier concentration, the frequency of the plasmon minimum does not change with Y content; instead,

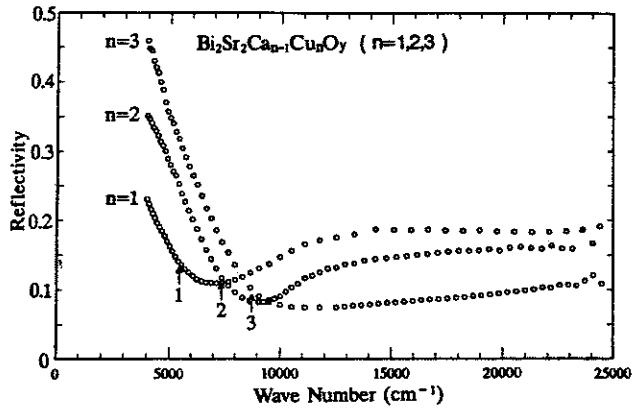

Fig. 10. Reflectance of ceramic samples of $Bi_{2.1}Sr_{1.9}CuO_y$ (2201), $Bi_2Sr_{1.8}Ca_{1.2}Cu_2O_y$ (2212) and $Bi_{1.85}Pb_{0.35}Sr_2Ca_{1.2}Cu_{3.1}O_y$ (2223). The arrows show the result for the plasma frequency from fits to the Drude formula. [Ref. 54.]

the magnitude of the low-frequency reflectance decreases steadily. This behavior is basically identical to what happens in $La_{2-x}Sr_xCuO_4$, and highlights the danger in attempting to estimate the carrier concentration from the value of the reflectance minimum.

2. *Reflectance of $Bi_2Sr_2CaCu_2O_8$*

The first single-crystal reflectance spectra of $Bi_2Sr_2CaCu_2O_8$ were reported by Reedyk *et al.*,[55] who measured the temperature dependence in the far infrared of samples with $T_c = 85$ K and determined the optical conductivity by Kramers-Kronig analysis. The reflectance over a broad frequency range is shown in Fig. 11, along with more recent data.[56] Similar data have been obtained by several groups.[29,35,57–60] The reflectance drops steadily throughout the infrared to a minimum around 10,000 cm^{-1} (1.3 eV). The data shown are for 300 K, but very little temperature dependence is observed above 1000 cm^{-1}.

Also visible in Fig. 11 is a band centered around 16,000 cm^{-1} (2 eV) as well as structure (with considerable sample-to-sample variation) spanning 28,000–32,000 cm^{-1} (3.5–4 eV). The lower band is interpreted as the Cu-O charge transfer band while the upper one is most likely associated with excitations of the Bi-O layers.

3. *Transmittance of $Bi_2Sr_2CaCu_2O_8$*

Perhaps the most detailed study of $Bi_2Sr_2CaCu_2O_8$ has been carried out by Romero *et al.*[61–63] by transmission measurements. As first shown by Forro *et al.*,[31]

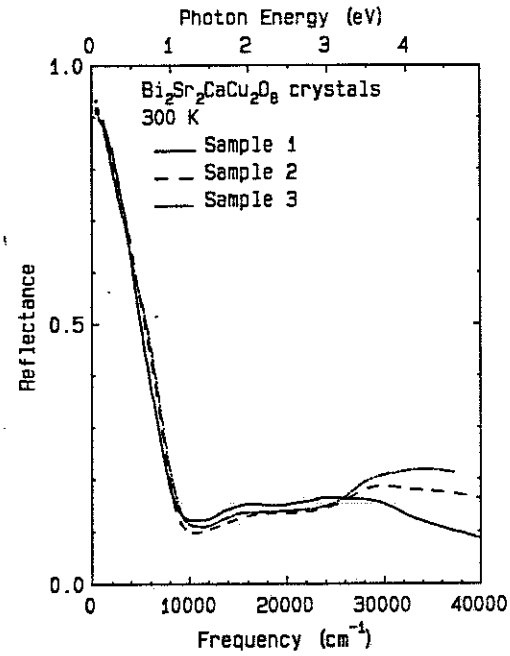

Fig. 11. Reflectance of three $Bi_2Sr_2CaCu_2O_8$ samples at 300 K. [Ref. 56.]

the micaceous nature of the bismuthates makes it possible to prepare thin free-standing flakes of $Bi_2Sr_2CaCu_2O_8$ that are as little as 1000 Å thick and to make infrared transmission studies of these flakes.

Because the samples are free standing, the transmittance may be measured over a wide frequency range without interference from a substrate. Romero *et al.*[61] measured the transmittance between 80 and 30,000 cm^{-1} at temperatures between 20 and 300 K. Fig. 12 shows the (unpolarized) transmittance $\mathcal{T}$ of a $Bi_2Sr_2CaCu_2O_8$ free-standing crystal at temperatures between 20 and 300 K. The transmittance is low overall, but increases with increasing frequency. The low frequency $\mathcal{T}$ is rather different above and below the superconducting transition, with a finite intercept for $T > T_c$ contrasting with $\mathcal{T} \propto \omega^2$ for $T < T_c$.

At higher frequencies, $\mathcal{T}$ increases quasi-linearly with ω out to ~2200 cm^{-1} (0.27 eV); above which it increases more quickly. There is a transmission maximum at 14,000 cm^{-1} (1.8 eV) and a second maximum at 25,000 cm^{-1}(3.1 eV). This linear increase is different from what is expected for a simple metal. The transmission of a thin film is approximately given by[64]

$$\mathcal{T} = \frac{1}{(1 + Z_0\sigma_1 d/2)^2 + (Z_0\sigma_2 d/2)^2} \tag{3}$$

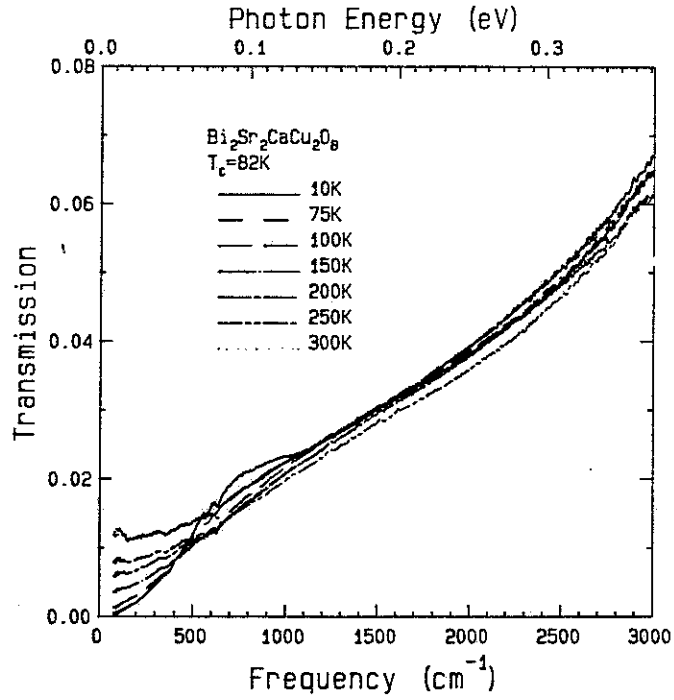

Fig. 12 Transmittance of a 1340 Å crystal of $Bi_2Sr_2CaCu_2O_8$. [Ref. 61.]

where $Z_0 = 377\ \Omega$ is the impedance of free space, d the film thickness, and $\sigma_1 + i\sigma_2 = \sigma$, the complex conductivity of the film. If $\mathscr{T} \ll 1$, then Eq. 3 further simplifies to $\mathscr{T} \approx 4/|Z_0\sigma d|^2$. Above T_c the $\omega = 0$ intercept is then a direct measure of the dc conductivity. (In an ordinary metal, $\sigma_2 \ll \sigma_1$ at low frequency.) Below T_c the inductive response of the superfluid dominates the absorptive part at low frequencies, as discussed in Section V.

At high frequencies ($\omega \gg 1/\tau$), free carriers have a conductivity

$$\sigma = \frac{\omega_p^2 \tau}{4\pi(1 - i\omega\tau)} \approx i\frac{\omega_p^2}{4\pi\omega} \tag{4}$$

If Eq. 4 is substituted into Eq. 3, one finds that $\mathscr{T} \approx \omega^2$ is the expected behavior for the Drude carriers of an ordinary metal once $\omega > 1/\tau$. Thus, the quasi-linear frequency dependence of $\mathscr{T}$ is further evidence for the non-Drude nature of the midinfrared conductivity.

An additional feature in the transmittance spectra of Fig. 12 is the shoulder that develops near 700 cm^{-1} (90 meV). The shoulder is associated with the superconductivity, to which we will return in Section V. However, the shoulder is also connected to

the midinfrared absorption, because it can be explained within a two-component picture as a sort of pass band between the midinfrared absorption and the low-frequency free-carrier absorption. The reason for this pass band can be seen by modeling both midinfrared and free-carrier absorption as oscillators centered at ω_e and zero frequency, respectively, and by neglecting damping. In this case, the dielectric function is purely real, except for delta functions in the imaginary part at $\omega = 0$ and $\omega = \omega_e$:

$$\epsilon = -\frac{\omega_{pD}^2}{\omega^2} + \frac{\omega_{pe}^2}{\omega_e^2 - \omega^2} + \epsilon_\infty \tag{5}$$

where ω_{pD} is the free carrier plasma frequency or oscillator strength and ω_{pe} is the same quantity for the midinfrared oscillator.

Eq. 5 has poles at $\omega = 0$ and at $\omega = \omega_e$ and zeros at

$$\omega_\pm^2 = \frac{(\omega_{pD}^2 + \omega_{pe}^2 + \epsilon_\infty \omega_e^2) \pm \left[(\omega_{pD}^2 + \omega_{pe}^2 + \epsilon_\infty \omega_e^2)^2 - 4\epsilon_\infty \omega_{pD}^2 \omega_e^2\right]^{1/2}}{2\epsilon_\infty} \tag{6}$$

When ω_e is small compared to the two plasma frequencies, as is the case for two-component fits to the copper oxide superconductors, then Eq. 6 reduces to

$$\omega_+ \approx \sqrt{\frac{\omega_{pD}^2 + \omega_{pe}^2}{\epsilon_\infty}} \tag{7}$$

and

$$\omega_- \approx \frac{\omega_{pD}\omega_e}{\sqrt{\omega_{pD}^2 + \omega_{pe}^2}} \tag{8}$$

The dielectric function is negative at low frequencies, positive between ω_- and ω_e, negative between ω_e and ω_+, and positive at high frequencies. The frequencies where $\epsilon > 0$ are the places were the system is transparent. Both of the zeros correspond to plasmon frequencies. The one at ω_+ is a combined plasmon of free carriers and midinfrared carriers while the one at ω_- is a plasmon of the free carriers alone, strongly screened by the midinfrared oscillator.

The actual system does not have zero damping, of course, and there is considerable absorption throughout the midinfrared region. However, if the damping of the free carrier component is suddenly reduced (as, for example, by the onset of superconductivity), then there should be a corresponding increase in the transmittance

between ω_- and ω_e. This argument relies heavily on the presence of a midinfrared component; if there are only free carriers then only one pole and one zero exist. Note that such a transmission band in the superconducting state was predicted by Bonn *et al.*[65] in 1987.

4. Conductivity of $Bi_2Sr_2CaCu_2O_8$

Romero *et al.*[62,63] determined the optical conductivity of $Bi_2Sr_2CaCu_2O_8$ by Kramers-Kronig analysis. It can be shown that $\theta(\omega)$, the change of phase upon transmission, θ, is related to $\mathcal{T}$ by a Kramers-Kronig integral, just like the reflectance.[66] Once θ is known, the complex refractive index can be obtained by numerical solution of

$$\sqrt{\mathcal{T}}\, e^{i\theta} = \frac{4N}{(N+1)^2 e^{-i\delta} - (N-1)^2 e^{i\delta}} \tag{9}$$

where $N = \sqrt{\epsilon}$ is the complex refractive index, $\epsilon = \epsilon_1(\omega) + 4\pi\sigma_1(\omega)/\omega$ is the complex dielectric function, and $\delta = \omega N d/c$, with d the thickness of the film. The only added complication is that the phase shift the radiation would have travelling through a thickness d of vacuum, $\omega d/c$, has to be added to θ prior to solving Eq. 9 for N.

Results of Romero *et al.*[62,63] for the optical conductivity over 150–3000 cm^{-1} are shown in Fig. 13. In the normal state the low-frequency conductivity approaches the dc conductivity and falls with increasing frequency as expected for the Drude response of free carriers. However, above ~300 cm^{-1} the decrease in $\sigma_1(\omega)$ is closer to ω^{-1} than the ω^{-2} behavior expected for free carriers. Furthermore, the T-dependence of $\sigma_1(\omega)$ at high frequencies is much smaller than at dc or low-frequencies. Thus $Bi_2Sr_2CaCu_2O_8$ displays the non-Drude conductivity that is a common feature of the high temperature superconductors. Below T_c, $\sigma_1(\omega)$ has a broad maximum around 1000 cm^{-1} (0.15 eV), with some structure in the phonon region. A slight dip in $\sigma_1(\omega)$ can be seen around 400 cm^{-1} (50 meV) although this anitresonance or "notch" is not as noticeable here as in the $YBa_2Cu_3O_{7-\delta}$ system. This feature will be discussed in Section VI.

5. Conductivity of $Bi_2Sr_2CuO_6$

$Bi_2Sr_2CuO_6$ is a very interesting compound because it exhibits conductivity with a "metallic" temperature dependence, yet is not superconducting, at least above 5 K.[67] The transmittance of free-standing flakes of $Bi_2Sr_2CuO_6$ has been measured recently by Romero *et al.*[62] and the optical conductivity determined by Kramers-Kronig

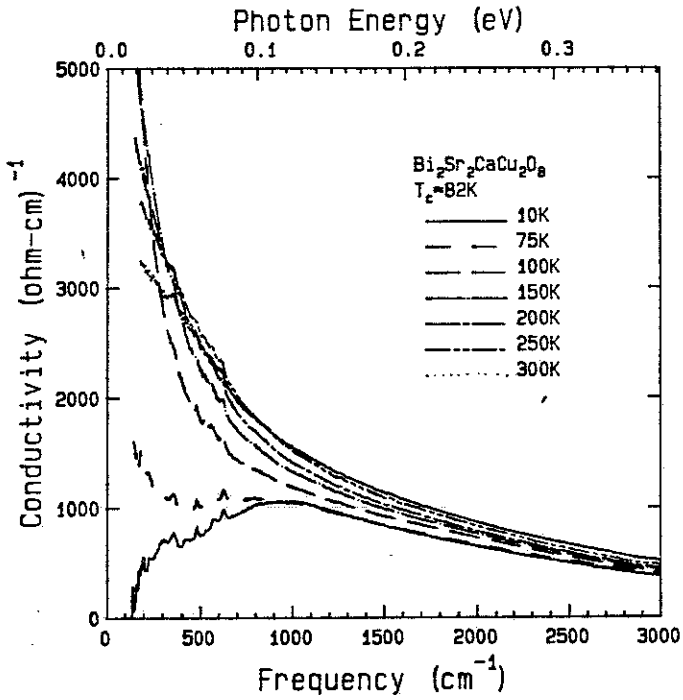

Fig. 13. Frequency-dependent conductivity of $Bi_2Sr_2CaCu_2O_8$ between 20 and 300 K. [Ref. 62.]

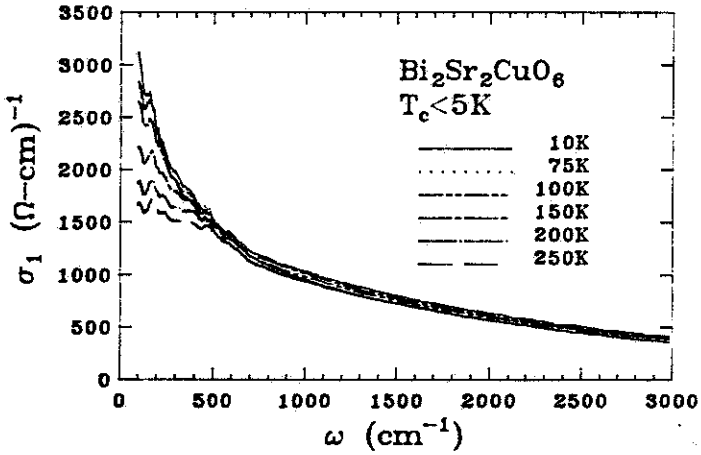

Fig. 14. Frequency-dependent conductivity of $Bi_2Sr_2CuO_6$ between 20 and 300 K. [Ref. 62.]

analysis. The spectrum of this "low-T_c" or "no-T_c" compound, shown in Fig. 14, is very similar to the above 90 K $\sigma_1(\omega)$ of $Bi_2Sr_2CaCu_2O_8$. The low-frequency infrared conductivity agrees with the dc conductivity both in magnitude and in temperature behavior. $\sigma_1(\omega)$ initially falls with increasing ω in a way consistent with a Drude response. However, at higher frequencies, the decrease goes over to ω^{-1} and the temperature dependence is much weaker. From these data it is clear that the non-Drude

optical behavior is not directly correlated with high-T_c, but instead with the presence of holes on CuO_2 layers.

E. The thallium system

Although the 2223 structure of the Tl-based oxide superconductors has the highest T_c yet reported, it has received the least attention from infrared spectroscopists. What few spectra are available[68,69] resemble closely the corresponding bismuthate.

The room temperature reflectance for $Tl_2Ba_2Ca_2Cu_3O_{10}$ as measured by Božović *et al.*[68] is shown in Fig. 1, above. The reflectance decreases steadily throughout the infrared to a broad minimum around 2 eV (16,000 cm^{-1}). The real part of the dielectric function, determined by a combination of Kramers-Kronig analysis and ellipsometry,[20] shows a zero crossing at 0.9 eV (7300 cm^{-1}) while the energy loss function, has a maximum at 1.2 eV.

The temperature dependent reflectance of $Tl_2Ba_2CaCu_2O_8$ has been measured by Foster *et al.*[30] The optical properties were determined by Kramers-Kronig analysis and analyzed within a two-component picture. Fig. 15 shows the frequency-dependent conductivity at four temperatures. The data above T_c show a narrow peak at zero frequency and a broad, nearly temperature-independent midinfrared absorption. There is good agreement between the dc conductivity and the low-frequency optical conductivity. Note that just above T_c, there is a weak minimum between the zero frequency peak and the midinfrared band.

Fig. 16 shows the corresponding curves for $\epsilon_1(\omega)$. Below T_c, $\epsilon_1(\omega)$ follows ω^{-2}, as indicated in the inset. Above T_c, $\epsilon_1(\omega)$ is mostly negative, but only slightly so at 300 K. There seems to be a tendency for $\epsilon_1(\omega)$ to become positive at low frequencies as if the negative free-carrier contribution in the normal state, which in a Drude model is $\epsilon_{1D} = -\omega_{pD}^2\tau^2$ were not strong enough to overcome the positive contribution from the midinfrared band, which is $\epsilon_{1mir} = +\omega_{pe}^2/\omega_e^2$, assuming an oscillator at ω_e.

F. $Pb_2Sr_2LCu_3O_8$

$Pb_2Sr_2LCu_3O_8$, where L is a rare earth, usually partially substituted by Ca or Sr, shares structural elements with both $Bi_2Sr_2CaCu_2O_8$ and $YBa_2Cu_3O_{7-\delta}$. Between CuO_2 bilayers, common to all three materials, is a PbO-CuO_δ-PbO sequence. The PbO layers are analogous to the BiO layers in $Bi_2Sr_2CaCu_2O_8$ while the CuO_δ structure is reminiscent of the oxygen-deficient chain layer in $YBa_2Cu_3O_6$. The maximum T_c is 75 K, found originally when L=($Y_{0.5}$ + $Ca_{0.5}$). It has recently been

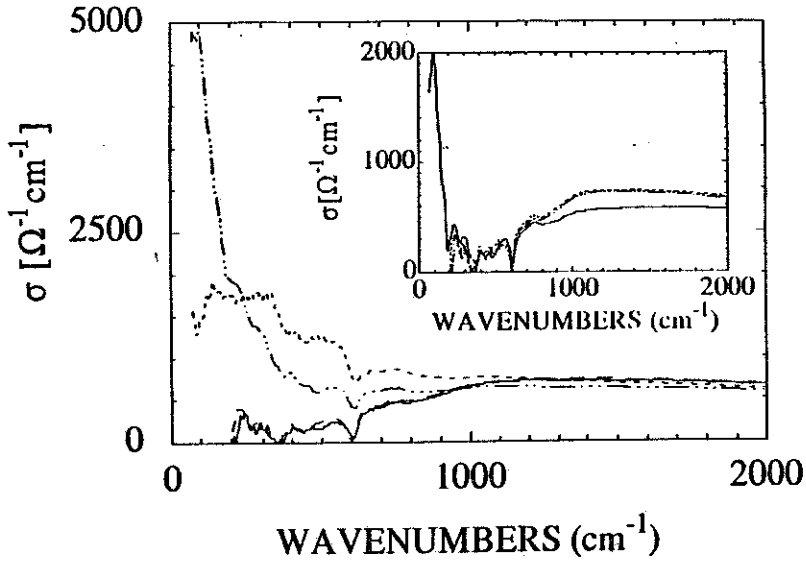

Fig. 15. Frequency-dependent conductivity for $Tl_2Ba_2CaCu_2O_8$ at 300 K (short dash), 125 K (dash dot), 60 K (long dash), and 10 K (solid). The inset compares $\sigma_s(\omega)$ at 60 K (short dash), and 10 K (dash-dot) with $[\sigma_n(\omega) - \sigma_D(\omega)]$, the normal state conductivity with the Drude term subtracted. [Ref. 30].

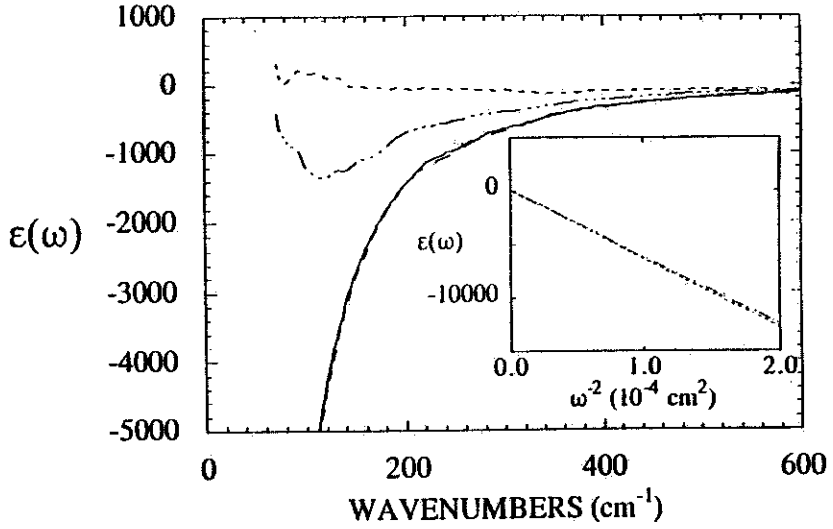

Fig. 16. Real part of the dielectric function for $Tl_2Ba_2CaCu_2O_8$ at 300 K (short dash), 125 K (dash dot), 60 K (long dash), and 10 K (solid). The insert shows the data below T_c vs. ω^{-2}. [Ref. 30].

discovered that a progression from an insulator to a high temperature superconductor occurs in Ca-free material as the size of the rare earth decreases. Thus, nominally $Pb_2Sr_2PrCu_3O_8$ is an insulator, whereas $Pb_2Sr_2DyCu_3O_8$ has $T_c \approx 75$ K.

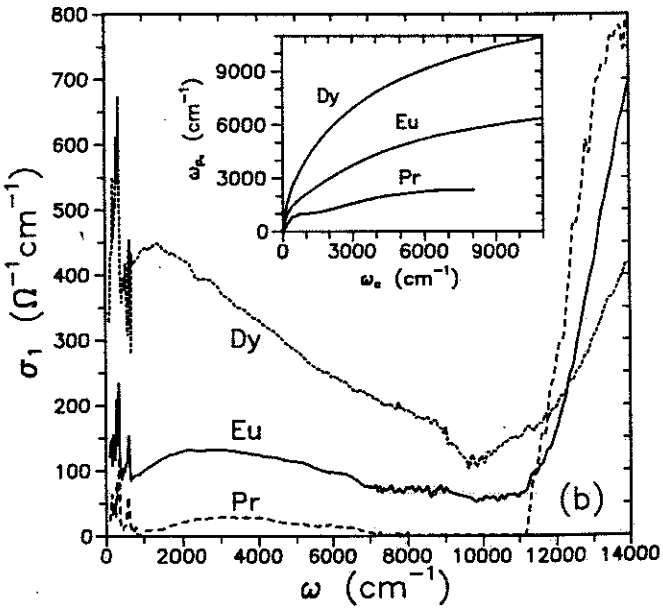

Fig. 17. Room-temperature optical conductivity for three $Pb_2Sr_2LCu_3O_8$ samples. The inset shows the partial sum rule, expressed as an effective plasma frequency, for the three samples. [Ref. 70.]

The reflectance of a series of $Pb_2Sr_2LCu_3O_8$ crystals has been measured by Reedyk *et al.*,[70] with the optical conductivity determined by Kramers-Kronig analysis. Results are shown in Fig. 17. The main figure shows $\sigma_1(\omega)$ at 300 K for three materials. The Pr compound is an insulator, with strong phonons dominating the far-infrared region. There is a weak band centered at 3200 cm^{-1} (0.4 eV) and a strong charge transfer excitation above 12,000 cm^{-1} (1.5 eV). With increased dc conductivity and higher T_c, which also means (one assumes) increased Cu-O carrier concentration, there is a shift of oscillator strength from the charge-transfer band to the midinfrared and far-infrared regions. There is also a shift of the midinfrared maximum to lower energies. This maximum is clearly seen in the midinfrared region, even in the $T_c = 75$ K Dy crystal.

The inset to Fig. 17 shows an evaluation of the partial sum rule, Eq. 2, expressed in this case as an effective plasma frequency, ω_{p_c}. $N_{eff}(\omega)$ is related to this plasma frequency by $N_{eff} = m_e V_{cell} \omega_{p_c}^2 / 4\pi e^2$; the saturation values in the inset correspond to 0.11, 0.04, and 0.005 free holes per CuO_2 unit for Dy, Eu, and Pr, respectively. It is interesting that, even though T_c is as high as 75 K in these crystals, the effective far- and midinfrared carrier concentration is one of the smallest of the high temperature superconductors.

G. $YBa_2Cu_3O_{7-\delta}$

By far the most effort at determining the optical properties of the high-T_c superconductors has gone into studies of $YBa_2Cu_3O_{7-\delta}$. On the one hand, this is unfortunate, because $YBa_2Cu_3O_{7-\delta}$ is probably the most complicated superconductor of all, on account of (a) the presence of both quasi-two-dimensional ("planes") and quasi-one-dimensional ("chains") Cu-O layers, (b) the microtwinning of most samples which gives only an a-b-plane average , and (c) the variable oxygen content, which leads to variations in carrier concentration. On the other hand, some of the best samples (in terms of crystalline perfection, homogeneity, sharpness of T_c, *etc.*) are crystals and oriented films of $YBa_2Cu_3O_{7-\delta}$. In the following, we will first describe results on twinned samples and then discuss more recent (and less detailed) measurements of untwinned crystals.

Many groups have presented measurements of the a-b-plane infrared spectra of $YBa_2Cu_3O_{7-\delta}$, with perhaps the most detailed results from groups at (alphabetically) AT&T Bell Labs,[11,27,25] Florida/McMaster/Bellcore,[10,15,32,71,72] IBM,[73,13,17] and Regensburg/Siemens.[14,16,74–76]

1. a-b-plane reflectance

The first complete (in terms of wavelength and temperature coverage) study of the a-b-plane infrared properties of $YBa_2Cu_3O_7$ was reported by Schutzman *et al.*[14] The main part of Fig. 18 shows the reflectance over 50–1200 cm^{-1} (0.006–0.15 eV) of an epitaxial $YBa_2Cu_3O_{7-\delta}$ film at temperatures between 20 and 300 K. Data at two temperatures out to 8000 cm^{-1} (1 eV) are given in the inset. The sample had $T_c = 91$ K, about the maximum that is observed for $YBa_2Cu_3O_7$ thin films. Later results for similar samples have been presented by Renk *et al.*[16,76]

The data in the inset show that the reflectance drops steadily (but not quite linearly) throughout the infrared. There is a obvious shoulder around 4000 cm^{-1} (0.5 eV), which, as we shall see from measurements on single-domain crystals, is probably associated with excitations on the b-axis-oriented chains.

A nearly parallel downward shift of the reflectance with increasing temperature above 100 K, is also seen at all but the very lowest and highest frequencies. The value of the reflectance at 800 cm^{-1} (0.1 eV) and $T = 100$ K is 91%, which is close to the highest value observed in $YBa_2Cu_3O_{7-\delta}$ samples.

There is a dip or minimum in the 20 K reflectance around 800 cm^{-1}, so the reflectance is actually smaller below T_c than above in this frequency region. This

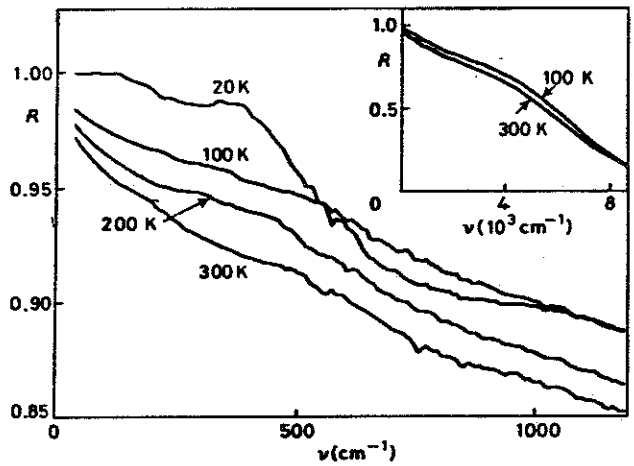

Fig. 18. Reflectance of a $YBa_2Cu_3O_{7-\delta}$ film prepared on $SrTiO_3$ by laser evaporation. The inset shows the reflectance out to 8000 cm^{-1} (1 eV). [Ref. 14.]

effect has also been seen by other groups.[15,17,73] The minimum develops only below T_c, and corresponds closely to the transmission maximum in Fig. 12. It can be understood in the same way as the transmission maximum by considering the effect on the dielectric function of two intense absorption bands, one at zero frequency and one in the midinfrared. Both bands give a pole in the dielectric response; there is a zero in $\epsilon(\omega)$ between the two poles. If $\epsilon(\omega)$ were purely real, there would be a deep reflectance minimum at a frequency just above the zero. When $\epsilon(\omega)$ has a large imaginary part, this minimum becomes washed out. However, if one component loses its dissipative part, a weak reflectance minimum develops. With the onset of superconductivity, for example, much (if not all) of the free-carrier component of $\epsilon(\omega)$ collapses to a delta function at the origin (as discussed in detail in Section V). This decreases the imaginary part of $\epsilon(\omega)$ at finite frequencies and leads to the formation of the weak minimum in the reflectance seen in Fig. 18.

The other obvious feature in Fig. 18 is the structure around 500 cm^{-1}. It is most obvious in the 20 K data, but can also be discerned above T_c. The 100, 200, 300 K curves all have a feature at this frequency which could be described as a "knee" or "shoulder," where the reflectance lies above the trend above and below 500 cm^{-1}. This feature, which has been discussed by a number of authors[25,15,27] is a signature of the non-Drude behavior of the reflectance, because a Drude reflectance which fit the data below 200 cm^{-1} would have a nearly constant value in the 400–1200 cm^{-1} range.[10]

Thomas *et al.*,[11] Cooper *et al.*,[25] and Orenstein *et al.*[27] have studied a series of high-quality $YBa_2Cu_3O_{7-\delta}$ twinned crystals which have different values of δ. Fig. 19 shows the reflectance of four crystals of $YBa_2Cu_3O_{7-\delta}$, measured at 100 K. The samples are characterized by their transition temperatures. The sample with T_c = 90 K is presumed to have $\delta \approx 0$ whereas the one with $T_c = 30$ K (which also contains some Al) has $\delta \approx 0.5$.[1] The reflectance of each sample drops steadily (but not quite linearly) throughout the infrared, with a sort of plasmon minimum around 10,000 cm^{-1} in all cases. As oxygen is removed, reducing the carrier concentration on both the CuO_2-planes and the *b*-axis-oriented chains, the reflectance in the midinfrared is substantially reduced. However, as in other doping studies, this reduction in n has little effect on the frequency location of the plasmon minimum.

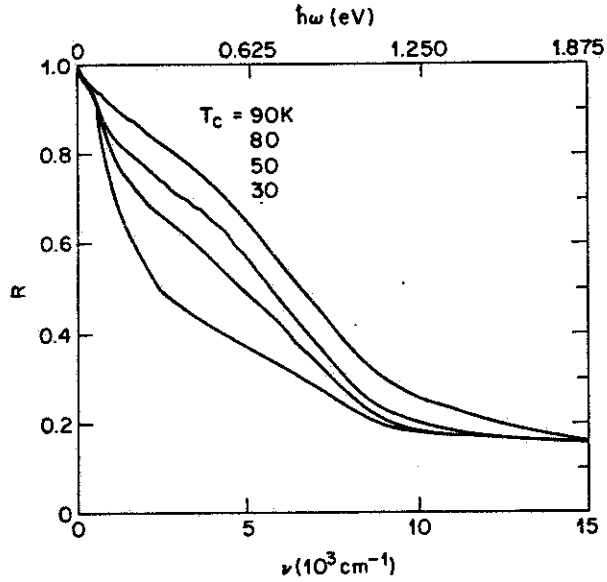

Fig. 19. Reflectance of four $YBa_2Cu_3O_{7-\delta}$ crystals having different values of δ. The superconducting T_c is indicated, with the most reflecting sample having the highest T_c. (The sample with $T_c = 30$ K was Al-doped as well as oxygen deficient.) Sample temperature is 100 K. [Ref. 27.]

At low frequencies, the reflectance is high, being above 90% for all four samples for $\omega \lesssim 500$ cm^{-1}, as expected for a conducting material. The three reduced-T_c samples clearly have a break or shoulder in this normal-state reflectance at $\omega \sim 500$ cm^{-1}, similar to that in Fig. 18. In fact, the dominant effect of reducing the oxygen content appears to be a substantial reduction of the midinfrared reflectance, with the effects in the far infrared being more modest.

The reflectance at several temperatures of these samples is shown in Fig. 20, which shows frequencies below 2000 cm^{-1} (0.25 eV). It is evident from these data that most of the temperature dependence occurs below 800 cm^{-1} (0.1 eV), except for the $T_c = 90$ K sample, where there is a systematic decrease in $\mathscr{R}$ at all frequencies at 200 K, the highest temperature shown for this sample.

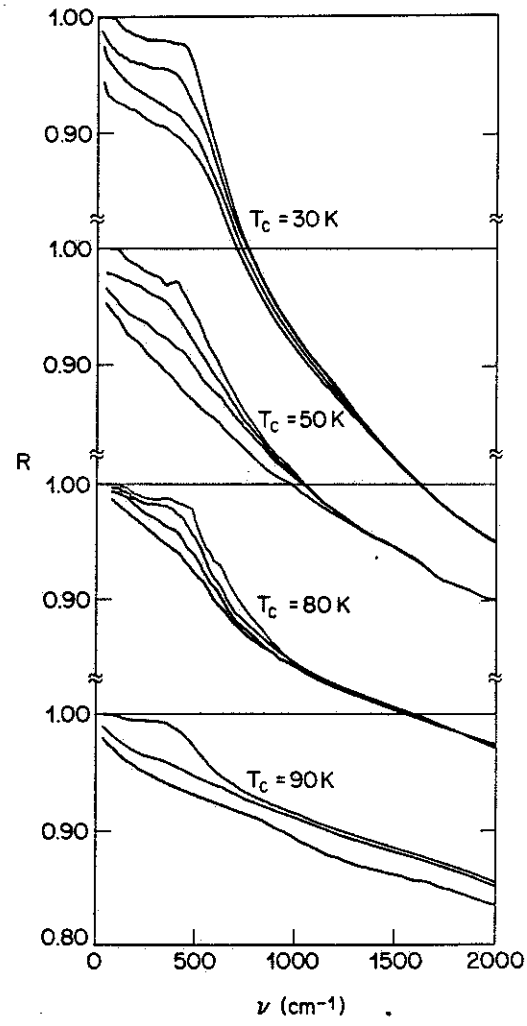

Fig. 20. Reflectance at several temperatures for the same crystals as in Fig. 19. The temperatures are as follows: $T_c = 30$ K—10, 100, 150, 250 K; $T_c = 50$ K—10, 100, 150, 250 K; $T_c = 80$ K—10, 40, 80, 150 K; $T_c = 90$ K—20, 100, 200 K. [Ref. 27.]

The 500 cm^{-1} "shoulder" or "knee" that was discussed above is quite obvious in these data as well. It occurs in all four samples at the same location and can be seen up to 150–250 K in the reduced-T_c samples.

The reflectance of a "fully-oxygenated" $YBa_2Cu_3O_{7-\delta}$ crystal with $T_c = 93$ K has been reported by Collins *et al.*[73,77] and Schlesinger *et al.*[17] Their results are shown in Fig. 21. The 105 K, 800 cm^{-1} (0.1 eV) reflectance (89%) is somewhat smaller than the 92% for the $T_c = 90$ K sample shown in Fig. 20.

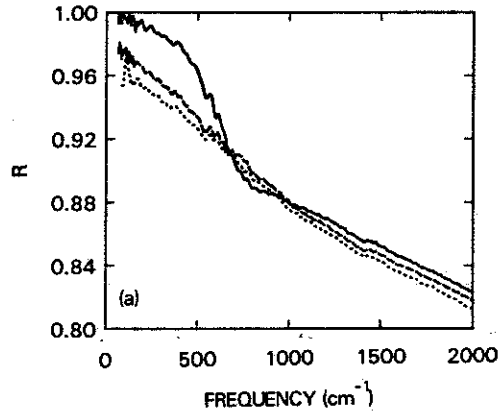

Fig. 21. Reflectance of a $T_c \approx 93$ K $YBa_2Cu_3O_{7-\delta}$ crystal at $T = 45$, 105, and 150 K. [Ref. 17.]

There is a noticeable dip or minimum in the 45 K reflectance around 800 cm^{-1}, similar to the data in Fig. 18. As discussed above, this can be qualitatively understood as a result of the collapse below T_c of the free-carrier component of $\epsilon(\omega)$ to a delta function.

A final example of the reflectance of $YBa_2Cu_3O_{7-\delta}$ is shown in Fig. 22 from the work of Kamarás *et al.*.[15] This figure shows the *a*-*b*-plane reflectivity of two $YBa_2Cu_3O_{7-\delta}$ films prepared by laser evaporation. One (upper panel) had $T_c \approx 91$ K; the other (lower panel) had $T_c \approx 89$ K. The reflectance, shown out to 800 cm^{-1}, was measured at 20, 100, and 300 K.

When compared to the results of Fig. 20, these films would appear to fall between the $T_c = 80$ K and the $T_c = 90$ K crystal spectra. The 800 cm^{-1} reflectance at $T = 100$ K is 89% and 88% for the two samples while the crystals had reflectances of ~87% and ~92%, respectively. Note that the 20 K and 100 K reflectances are nearly the same around 800 cm^{-1} (0.1 eV), while the 300 K reflectance is systematically lower than the 100 K reflectance at all frequencies, as in the case of the 90 K sample of Fig. 20.

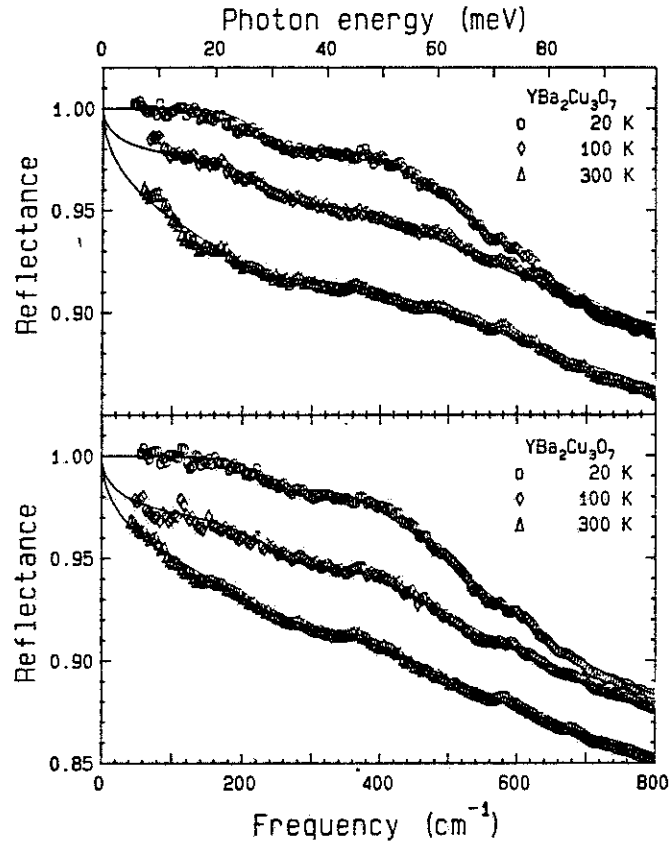

Fig. 22. a-b-plane reflectance of two $YBa_2Cu_3O_{7-\delta}$ films at 20, 100, and 300 K. The film in the upper panel had $T_c = 91$ K; the other had $T_c = 89$ K. The lines show fits to a model two-component dielectric function. [Ref. 15.]

2. The a-b-plane conductivity

The optical conductivity $\sigma_1(\omega)$ of $YBa_2Cu_3O_{7-\delta}$ has been determined by Kramers-Kronig analysis of the reflectance by a number of groups. We will show several examples. The low-frequency extrapolations needed to complete the Kramers-Kronig integral are most critical in the case of the superconducting state, as we will discuss in Section V. Typically, a Hagen-Rubens extrapolation $\mathcal{R} = 1 - A\sqrt{\omega}$ is satisfactory for the normal state.

Fig. 23 shows the conductivity at four temperatures, as presented by Kamarás *et al.*,[15] while Fig. 24 shows the conductivity at four temperatures as presented by Schützmann *et al.*[14] The corresponding reflectances were shown above in Figs. 22 and 18. The data are quite similar, with $\sigma_1(\omega)$ agreeing within about 10% over most of the range shown. The far-infrared conductivity is strongly temperature dependent but there is only a small change in the midinfrared above about 800 cm^{-1}. An

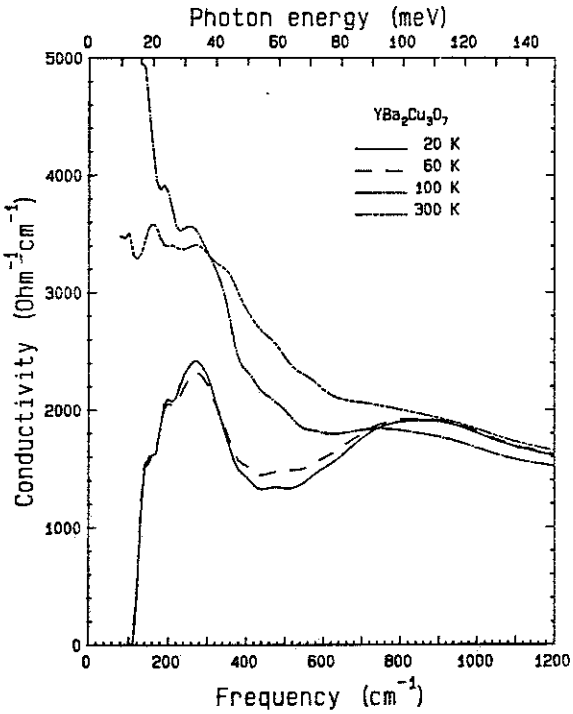

Fig. 23. Frequency dependent conductivity of a $T_c = 91$ K film of $YBa_2Cu_3O_{7-\delta}$ at 20, 60, 100, and 300 K. [Ref. 15.]

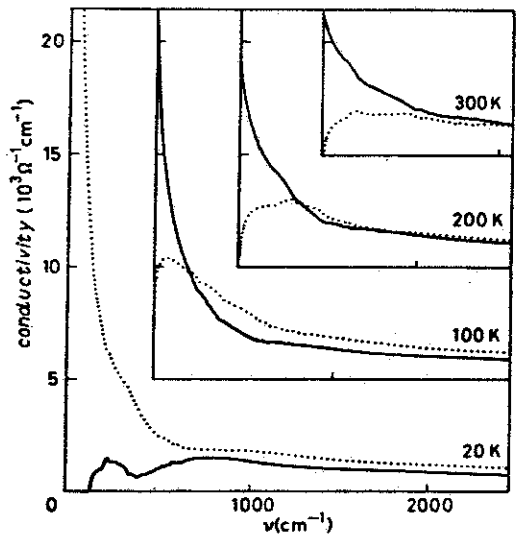

Fig. 24. Solid lines: optical conductivity $\sigma_1(\omega)$ of a $T_c = 92$ K film of $YBa_2Cu_3O_{7-\delta}$ at 20, 100, 200, and 300 K. Dotted lines: Imaginary conductivity $\sigma_2(\omega)$. [Ref. 14.]

obvious feature in the conductivity is the minimum around 430 cm^{-1} (0.54 eV). This feature is easily seen in the below-T_c spectra but can also be discerned in the 100, 200, and (weakly) in the 300 K spectra. It will be the subject of Section VI, where it is identified as a signature of strong coupling of the midinfrared carriers to phonons.

The conductivity of a $YBa_2Cu_3O_{7-\delta}$ crystal at three temperatures, as reported by Schlesinger *et al.*,[17] from Kramers-Kronig analysis of the data in Fig. 21, is shown in the upper panel of Fig. 25. The lower panel shows $\epsilon_1(\omega)$, the real part of the dielectric function. The optical conductivity is generally like that in Figs. 23 and 24, except for a magnitude about 20% larger. There is one interesting qualitative difference, however: the complete absence of temperature dependence in $\sigma_1(\omega)$ above 800 cm^{-1}. This should be compared to a small but nonzero variation with T in the conductivity of Schützmann *et al.*[14] and Kamarás *et al.*[15] According to Schlesinger *et al.*, the absence of any T-variation in $\sigma_1(\omega)$ extends to 10,000 cm^{-1} and to 250 K. In contrast, both the measured reflectance (Fig. 21) and $\epsilon_1(\omega)$ (lower panel of Fig. 25) do show some temperature dependence. Because $\sigma_1(\omega)$ and $\epsilon_1(\omega)$ are related by Kramers-Kronig relations, a temperature variation in one generally leads to temperature variation in the other, so these results are surprising.

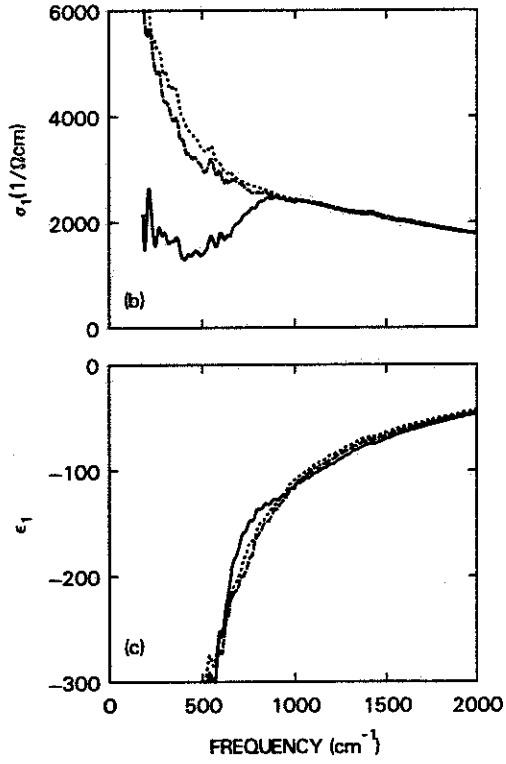

Fig. 25. Upper panel: optical conductivity of a $T_c \approx 93$ K $YBa_2Cu_3O_{7-\delta}$ crystal at 45, 105, and 150 K. Lower panel: corresponding $\epsilon_1(\omega)$. [Ref. 17.]

Fig. 26 shows the conductivity at 100 K over a wide frequency range for five $YBa_2Cu_3O_{7-\delta}$ crystals with different values of δ, from Ref. 27. One sample (the lowest

trace) is insulating while the other four are superconducting. Their reflectance was shown in our Fig. 19. The insulator has obvious phonon features at low frequencies, a weak midinfrared absorption, and the onset of the charge-transfer absorption at about 12,000 cm^{-1} (1.5 eV). With increased oxygen content, the absorption in the midinfrared increases and appears to shift to lower energies. The samples with T_c = 30, 50, and 80 K all have a minimum at 430 cm^{-1} (0.43 eV) clearly visible in their $\sigma_1(\omega)$ spectra. Below that minimum, the conductivity turns up toward its dc value.

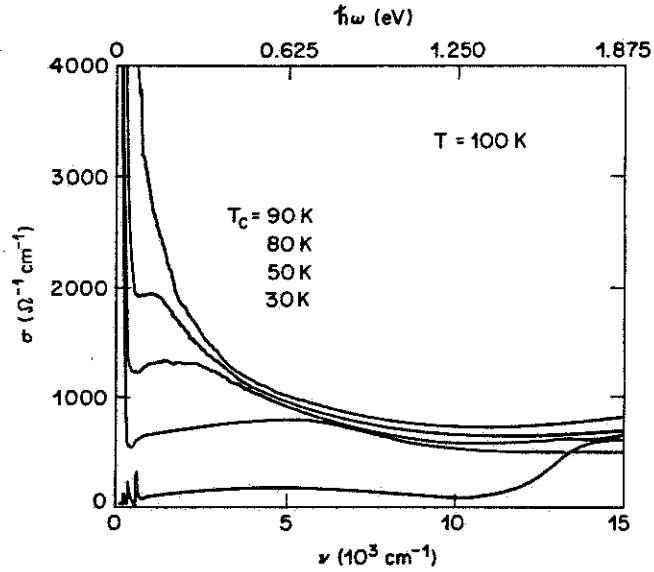

Fig. 26. Optical conductivity of five $YBa_2Cu_3O_{7-\delta}$ crystals over 0–15,000 cm^{-1} (0–1.9 eV). Values of δ range from ~0.8 for the lowest curve to ~0 for the highest. [Ref. 27.]

Fig. 27 shows the evaluation of the partial oscillator-strength sum rule for these samples. N_{eff}, the number of free carriers per formula unit, increases rapidly at low frequencies, on account of the high dc conductivity, and continues to increase in the midinfrared region. The value of N_{eff} at 11,000 cm^{-1} gives an approximate measure of the far-infrared and midinfrared oscillator strength; from this one estimates $N_{eff} \approx$ 0.6, 0.75, 0.8, and 1.1 per formula unit for the T_c = 30, 50, 80, and 90 K samples, respectively. These carriers are distributed among the two CuO_2 planes and the CuO chain. The value of 1.1 for the $T_c = 90K$ sample is in rough accord with the estimate of 1 carrier per formula unit that one would make from the chemical formula, assuming Cu^{+2} and O^{-2} for all sites.

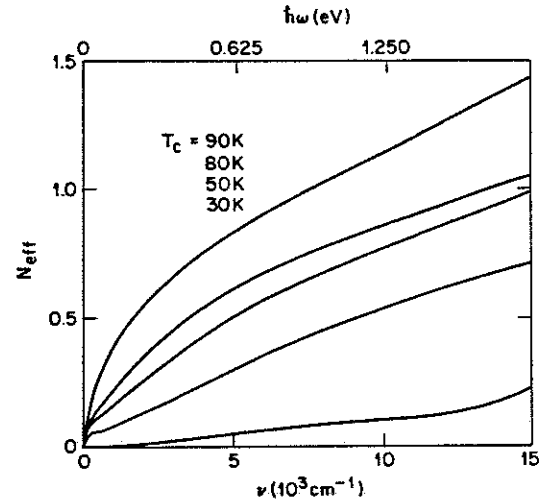

Fig. 27. Evaluation of the partial oscillator strength sum rule for four $YBa_2Cu_3O_{7-\delta}$ crystals with T_c between 30 and 90 K and for one insulating crystal (lowest trace). [Ref. 27.]

H. *a-b*-plane anisotropy

1. $YBa_2Cu_3O_{7-\delta}$

The as-grown $YBa_2Cu_3O_{7-\delta}$ material is usually twinned in the *a-b*-plane with alternating strip-like domains of *a*- and *b*-axis oriented material. Thus any optical measurement gives an average of the properties in the two directions. Because the material is orthorhombic, the optical properties in the two directions should be different. Added to this is the contribution associated with the chains that peaks in the midinfrared[78,79,26,19,80] and that may have a tail extending to the far infrared. (The observation that the dc conductivity is anisotropic in the *a-b*-plane[81,82] suggests that the chain conductivity extends to zero frequency and the chains are metallic. This is in accord with NMR measurements.[83])

In recent years, large single-domain crystals of $YBa_2Cu_3O_{7-\delta}$ have become available, and several measurements of such crystals have been reported. The first measurements over a wide frequency range were by Koch *et al.*,[26] who reported on the room temperature *a*- and *b*-axis polarized reflectance. The crystals, slightly Al doped with $T_c \approx 85$ K, were single domain as grown. The reflectance for the two polarizations are shown in Figs. 28 and 29. The reflectances are nearly the same at low frequencies, but the *a*-axis reflectance begins to fall and reaches its plasmon minimum sooner than the *b*-axis reflectance. There are several bands at higher energies. At 3

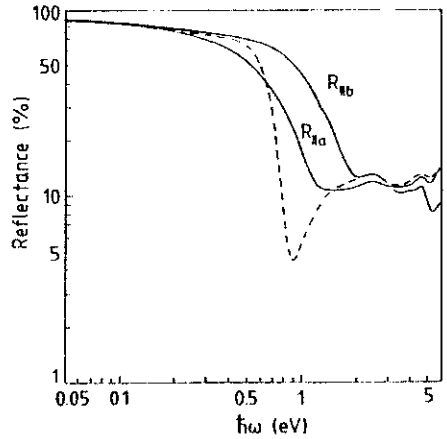

Fig. 28. Room-temperature reflectance of the (001) surface over 0.05–6 eV (400–48,000 cm^{-1}) for $\vec{E} \parallel a$ and $\vec{E} \parallel b$ of a $YBa_2Cu_3O_{7-\delta}$ single crystal. The dashed line is a model calculation. Note the logarithmic energy scale. [Ref. 26.]

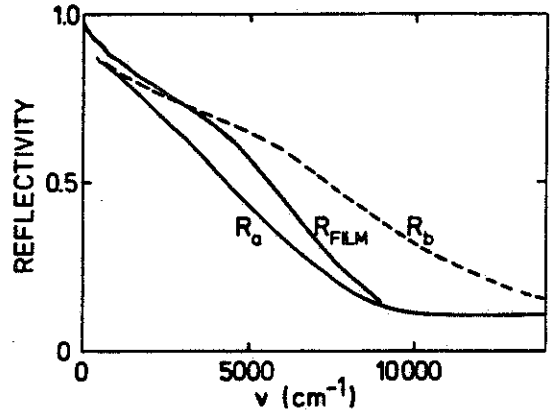

Fig. 29. Room-temperature reflectance of a single-domain crystal of $YBa_2Cu_3O_{7-\delta}$ for $\vec{E} \parallel a$ and $\vec{E} \parallel b$ as well as the reflectance of an epitaxial film. [Ref. 16.]

eV the two reflectances are equal, with the b-axis reflectance being smaller than the a-axis reflectance at higher frequencies.

In Fig. 29 the same data are plotted on a linear wavenumber scale and compared to the a-b-plane reflectance of an epitaxial thin film. The film reflectance is between that of the a- and b-axis polarizations, although the minimum occurs close to the minimum for the a-axis polarization. Note that the decrease in reflectance for $\vec{E} \parallel a$ is nearly linear with ω while that for $\vec{E} \parallel b$ has a shoulder around 5000 cm^{-1} (0.6 eV) on account of the excitations in the chains mentioned above.

Koch *et al.*[26] find that the loss function maxima and the zero crossings of $\epsilon_1(\omega)$ occur at about 1 eV for $\vec{E} \parallel a$ and at about 1.5 eV for $\vec{E} \parallel b$, indicating about twice as large oscillator strength along b. The conductivity is also larger along b, as illustrated

by Fig. 30, which shows the conductivity over 400–48,000 cm^{-1} (0.05–6 eV) for the two polarizations.

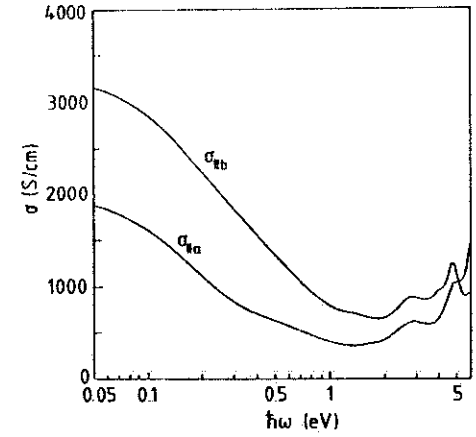

Fig. 30. Room-temperature optical conductivity from Kramers-Kronig analysis of reflectance polarized $\|$ a and $\|$ b of a $YBa_2Cu_3O_{7-\delta}$ single crystal. Note the logarithmic energy scale. [Ref. 26.]

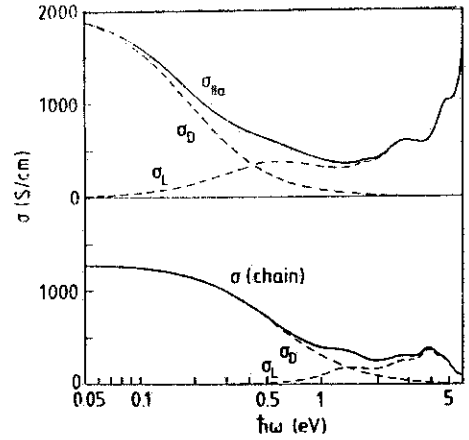

Fig. 31. Full line: difference between the b-axis and a-axis optical conductivity of a $YBa_2Cu_3O_{7-\delta}$ crystal at room temperature. The dashed lines show fits to sum of Drude shape and Lorentz oscillators. [Ref. 26.]

Koch *et al.*[26] interpret the additional conductivity along b as due to carriers on the chains. By calculating the difference between the b- and the a-axis conductivity, they extract the "chain" contribution shown in Fig. 31. According to this analysis, the chain conductivity is a broad Drude-like band band that extends to 0.5 eV (4000 cm^{-1}). However, as pointed out by Koch *et al.*, the additive nature of the chains

and planes is obviously violated at high frequencies where $\mathcal{R}_a > \mathcal{R}_b$. This inequality implies that the dielectric function is *smaller* parallel to the chains than perpendicular to them at high frequencies. It is probably too simple to assume that the b-axis conductivity is the superposition of an isotropic (2-dimensional) a-b-plane component and a quasi-one-dimensional b-axis chain component.

The temperature dependence of the a- and b-axis reflectance has been measured by Schlesinger *et al.*[19] on a crystal which was mechanically detwinned. Their results for both reflectance and conductivity at 100 K are shown in Fig. 32. At this lower temperature, the dc conductivity is larger, and the upturn to the dc conductivity at low frequencies is much more obvious. The b-axis appears to have a broad band in the midinfrared, while the variation along the a-axis is much smoother. A well-defined maximum at 2000 cm^{-1} (0.25 eV) is seen in the difference spectrum, $\sigma_b - \sigma_a$. This difference represents $\sigma_1(\omega)$ for the chains only if the assumptions hold that the conductivity can be decomposed into chain and plane components and that the plane conductivity is isotropic.

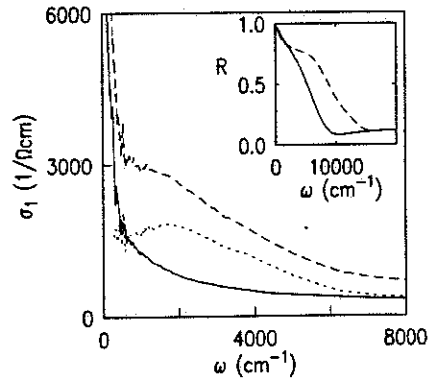

Fig. 32. The 100 K optical conductivity for $\vec{E} \parallel a$ (full line) and $\vec{E} \parallel b$ (dashed line). The difference $\sigma_{1b} - \sigma_{1a}$ is shown as the dotted line. The inset shows the a- and b-axis reflectances. [Ref. 19.]

2. $Bi_2Sr_2CaCu_2O_8$

That the a-b plane itself is not isotropic is illustrated by Fig. 33, which shows the polarized transmittance of a single-domain $Bi_2Sr_2CaCu_2O_8$ crystal at four temperatures, measured by Romero *et al.*[61,63] The anisotropy is substantial, despite the pseudo-tetragonal crystal structure of this material and the absence of chains. At all temperatures the a axis is more transparent (less conducting) than the b axis; however, most qualitative features (such as the shoulder at 700 cm^{-1} and the quasi-linear

increase in $\mathscr{T}$ with ω) are seen in both polarizations. The anisotropy in the conductivity is quite comparable to that in $YBa_2Cu_3O_{7-\delta}$ in this frequency region. This anisotropy is evidence against the interpretation of the $YBa_2Cu_3O_{7-\delta}$ anisotropy, which is attributed[19,26] to the presence of chains along b, because there are no chains in $Bi_2Sr_2CaCu_2O_8$. It is entirely possible that the a-b plane is itself anisitropic due to the different Cu-O bond lengths in the two directions.

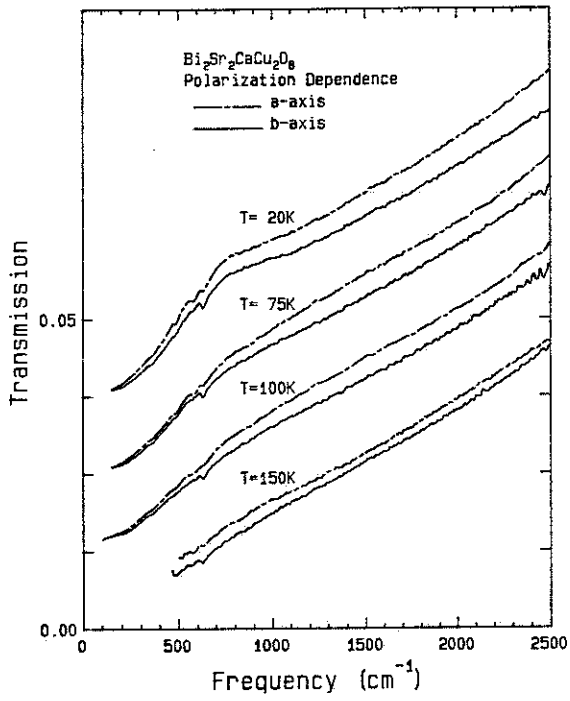

Fig. 33. The polarized transmittance of a single-domain $Bi_2Sr_2CaCu_2O_8$ crystal at four temperatures. [Ref. 61.]

3. $YBa_2Cu_4O_8$

A version of $YBa_2Cu_3O_{7-\delta}$ with double copper chains between the planes, $YBa_2Cu_4O_8$ has been prepared in single-domain form, and was studied in the 0.3 eV to 3.2 eV region by Bucher *et al.*[84] The material exhibits considerable anisotropy: the b-axis reflectance is 65% at 1 eV, a higher value than is seen in the best samples of $YBa_2Cu_3O_{7-\delta}$, which typically has a reflectance of less than 60%. It appears that the extra response comes from the midinfrared spectral weight associated with the extra chains. The authors fit Lorentz oscillators in both a and b directions, in addition to the Drude term.

I. Other metallic perovskites

1. $BaPb_{1-x}Bi_xO_3$

A midinfrared band is not a peculiarity of the two-dimensional copper oxygen plane; it is also present in the cubic $BaPb_{1-x}Bi_xO_3$ superconductor. This system can be doped over the whole concentration range from what appears to be a normal metal at $x = 0$ to a superconductor for $0.05 < x < 0.30$ and an insulator for $x > 0.33$. Tajima *et al.*[85] studied the infrared spectrum of a series of compositions x ranging from $x = 0.05$ to $x = 1.00$. For $x = 0.2$, in the superconducting range of composition, they fit their reflectance data to a combined Drude-Lorentz model with a Drude plasma frequency of 5400 cm^{-1} and an oscillator with a plasma frequency of 7600 cm^{-1} centered at 5400 cm^{-1}.

The overall infrared spectral weight scales well with the chemical doping under the assumption that each bismuth atom donates an electron to the system. Also, unlike in the copper oxides, the near-infrared plasma edge in the bismuthate scales with the concentration in the expected way.[85] This may be due to the greater energy of the charge transfer gap, estimated to be above 3 eV in this system.

2. Non-superconducting oxides

As we saw for $Bi_2Sr_2CuO_6$ the presence of a midinfrared band in a conducting oxide does not make it a superconductor. At low doping levels, a broad band in the 0.5 eV range develops in many oxides. $BaTiO_3$ with low carrier concentration develops a conductivity peak at 0.6 eV that the authors attributed to a deep impurity state associated with oxygen vacancies.[86] Bi *et al.*[87] find that $La_{2-x}Sr_xNiO_4$ also has a midinfrared peak, at 0.6 eV (4800 cm^{-1}). Only 3% of the spectral weight is attributed to the free carriers. Similarly Crandles *et al.*[88] find a broad midinfrared band peaking in the 0.4 eV region in the barely metallic $LaTiO_3$. Watanabe *et al.*[89] have studied a series of non-superconducting analogs of the $Bi_2Sr_2CaCu_2O_8$ compounds with Fe, Co and Mn replacing the Cu. Fig. 34 shows typical conductivity curves for these non-superconducting transition metal oxides. A midinfrared band is present in every case.

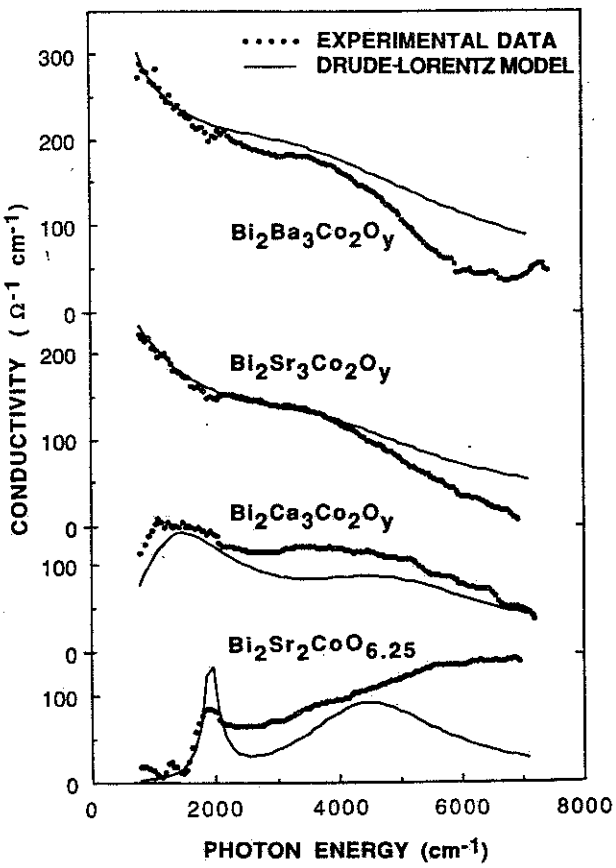

Fig. 34. Optical conductivity of a series of transition metal analogs of the superconducting $Bi_2Sr_2CaCu_2O_8$ cuprate. Solid curves are Drude-Lorentz models. [Ref. 89.]

III. PHOTOINDUCED ABSORPTION

A. Introduction

Subjected to intense illumination in the visible region of the spectrum, the insulating parent compounds of the high temperature superconductors develop absorption bands in the midinfrared. These resemble closely the bands in the corresponding superconductors obtained by chemical doping. This photoinduced absorption was first seen by Kim *et al.*[90] in $La_{2-x}Sr_xCuO_4$ and since then in most high T_c superconducting materials.[91–98]. Two features stand out: a broad continuous absorption in the midinfrared, similar to the midinfrared band seen in the doped materials, and a series of sharp bands in the phonon region, 100–600 cm^{-1}. The midinfrared continuum is always observed as an increase in the absorption, while the phonon bands can have either sign: photoabsorption or photobleaching. Fig. 35 shows the photoinduced spectrum for a series of high T_c superconductors, from the work of Foster *et al.*[94]

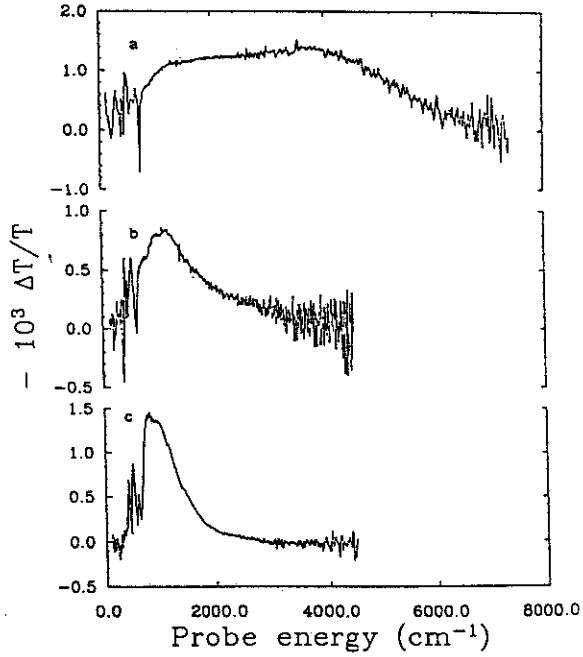

Fig. 35. Photoinduced absorption in three insulating parent compounds of the high temperature superconductors. Top curve La_2CuO_4, middle curve $YBa_2Cu_3O_{6.25}$, bottom curve, $Tl_2Ba_2Ca_{1-x}Gd_xCu_2O_8$. Under intense laser irradiation the insulating compounds develop absorption bands that resemble those of the corresponding doped superconducting materials. [Ref. 94.]

B. Experimental method

The photoinduced absorption experiments are done on very finely powdered samples suspended in an infrared-transparent host material typically CsI or KBr, with a concentration of 1–2 wt. %. The micron-size grains of the non-superconducting oxide material are almost infrared transparent, except at the isolated reststrahlen bands of optically active phonons.

In the visible, where the laser excitation takes place, the materials are fairly opaque, the penetration depth of the 5440 Å Argon ion laser line is less than 1000 Å. The intensity of the infrared beam passing through the sample is measured alternately with the laser beam on and off, to give the quantity $1 - I/I_0 \equiv \Delta\mathcal{I}/\mathcal{I}$, called the photoabsorption. Here the intensity of the beam is I with the visible laser on and I_0 with the laser off. The value of $\Delta\mathcal{I}/\mathcal{I}$ in most experiments is quite small, of the order of 10^{-3}. Care has to be taken to avoid local heating of the grains by the laser by reducing the intensity and by comparing the presumed photoinduced spectra with thermal difference spectra.[92]

The absorption measurements are done with a Fourier transform infrared interferometer, time averaged over several hours to extract the weak absorption signals from the noise. The individual stroke of the interferometer may take several seconds, so an equilibrium is established between the generation of carriers by the laser and their decay. Similar experiments have been done with conventional grating spectrometers where the infrared signal is detected with a lock in amplifier and the laser modulated at frequencies from 5 Hz to 50 kHz. Somewhat different results are obtained with the high frequency modulation, particularly in the near infrared.[99]

C. The midinfrared band

The most striking result of the photoabsorption technique is the appearance of a broad midinfrared band, roughly at the frequency where a band is seen in the conductivity spectra of the corresponding doped systems. For example, the first experiments by Kim *et al.*[90] in La_2CuO_4 yielded a broad photoinduced band centered at 0.5 eV, very similar to the band seen in the a-b-plane conductivity[33] in $La_{2-x}Sr_xCuO_4$ with $x = 0.02$. In $YBa_2Cu_3O_{6.2}$ both the midinfrared band[27] and the photoinduced continuum[93,95] have maxima around 0.12 eV (1000 cm^{-1}). The trend of decreasing peak frequency with rising T_c is continued in the $Tl_2Ba_2CaCu_2O_8$ system where the photoinduced peak occurs[94] at 0.1 eV (800 cm^{-1}). This comparison of the absorption induced in the grains with the a-b-plane conductivity cannot be taken too far, since small particle optical effects can distort the spectra.[100]

Evidence that the bands correspond to mobile carriers (and not to the absorption by excitons, for example) is provided by the laser intensity dependence of the absorption. Both the electronic midinfrared continuum and the phonon bands vary in strength as the square root of the laser power. In a bimolecular recombination process the rate of change in the density of photogenerated carriers n is given by $dn/dt = \alpha I - \beta n^2$ where α and β are constants. In equilibrium $dn/dt = 0$ and $n = \sqrt{\alpha/\beta I}$. This square root behavior is observed in most cases.

D. The phonon bands

Two types of photoinduced bands appear with width and location consistent with the idea that phonons are involved. The first set are photo-bleaching bands, regions of frequency where the absorption is reduced as a result of the irradiation. The second set, the true photoabsorption bands, correspond to frequencies where new absorption bands appear as a result of the irradiation.

A comparison with transmission spectra shows that the bleaching bands are, as one might expect, at frequencies where the undoped parent compound has phonon bands, mainly polarized in the a-b-plane.[95] One interpretation of the phenomenon is that the added electrons are locally doping the material, and that a phase transition is taking place from the tetragonal phase, stable in the semiconducting state, to the orthorhombic, superconducting phase. Thus the tetragonal phonons are bleached as the orthorhombic ones are formed in their place.

An example of this process is seen in the photoabsorption spectra of Ye *et al.*[95] in $YBa_2Cu_3O_{7-\delta}$. Upon irradiation, a photobleaching line appears at 255 cm^{-1} along with an absorption line 273 cm^{-1}. These are to be compared with the infrared modes at 253 cm^{-1} in the $O_{6.3}$ and at 276 cm^{-1} in $O_{7.0}$.[101] Similar transfer from the tetragonal $O_{6.3}$ to the $O_{7.0}$ spectra are seen for other lines.

Another effect, suggested by Kim *et al.*,[90,93] is that the added carriers cause local changes in symmetry, activating modes that are not otherwise infrared active. In this picture the 0.5 eV absorption is a localized electronic state similar to the mid-gap absorption in polyacetylene which can be produced either by chemical doping or by photoexcitation.[102,103] The breakdown of translational symmetry due to the electronic defect causes Raman active modes to become infrared active vibrations (IRAV)[104,105] through coupling to an electronic continuum.

The coincidence of photoabsorption lines and Raman lines can be seen in Fig. 36 from Taliani *et al.*[92] in the oxygen vibration region of $YBa_2Cu_3O_{7-\delta}$. The most obvious feature is the bleaching of the strong 600 cm^{-1} band of the $O_{6.21}$ material. The two photoabsorption bands at 510 and 435 cm^{-1} correspond to the strong Raman bands, shown in the upper part of the figure of the O_7 superconducting material, although, as the authors point out, the 500 cm^{-1} photoabsorption band is considerably broader.

Another example is the $Tl_2Ba_2CaCu_2O_8$ system.[106,94] As in the other materials, an electronic band is seen along with three broad induced bands in the phonon region of the spectrum. Table 1 summarizes the frequencies of some of the infrared and Raman bands. We have also included, for comparison, the *minima* in the infrared conductivity that are a common feature of the optical conductivity of the doped materials in the phonon region (see Section II on the midinfrared absorption, above, and Fig. 56, below), and are particularly strong in this material. The strongest of these infrared minima occurs at 595 cm^{-1}, the position of the prominent Raman line at 595 cm^{-1}. There is good reason to believe that this is the frequency of a phonon

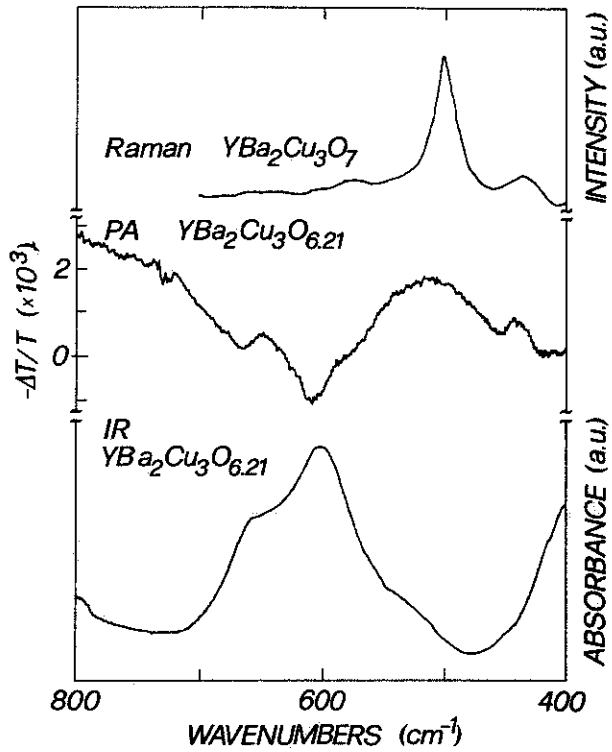

Fig. 36. Photoinduced absorption in the phonon region (middle trace) of $YBa_2Cu_3O_{7-\delta}$ at 34K. Raman (at 4K) and infrared spectra are also shown. There is a close correlation between photo absorption lines and Raman lines and photobleaching lines and infrared absorption lines in the *undoped* parent compound. [Ref. 92.]

that is strongly coupled to the electronic continuum.[107] It is also very close to the photoabsorption line at 578 cm^{-1}. A similar coincidence is seen for the 480 cm^{-1} photoabsorption line.

Thus it appears, at least in the case of the $Tl_2Ba_2CaCu_2O_8$ system, that there is a close correspondence between three sets of phonon lines: photoabsorption, infrared coupled phonons, and Raman lines. This behavior is not universal however. In the $YBa_2Cu_3O_{7-\delta}$ material the infrared coupled phonons[107] exhibit a very broad band centered on 450 cm^{-1}, whereas the photoabsorption shows bands at higher frequencies, agreeing in position with several Raman lines in the doped material.[92,97] The 600 cm^{-1} breathing mode appears in the infrared data of Pham *et al.*[108] as an optic phonon band with a conductivity *maximum* rather than an electronically coupled mode, *i.e.*, a conductivity *minimum,* as it is most other materials.

In summary, the photoinduced spectroscopies provide two important clues in the mystery of the infrared properties of the high temperature superconductors. First,

Table 1. Prominent Raman lines, IRAV modes and phonons seen to couple strongly to the midinfrared oscillator strength for $Tl_2Ba_2CaCu_2O_8$. The IRAV data are taken from Ref. 94 and the conductivity data from Ref. 30. The frequencies are in cm^{-1}.

Raman	IRAV	MID-IR $\sigma(\omega)$
691		
595	578	595
509	480	478
433	403	
221	188	

photoexcitation creates carriers that have a midinfrared absorption whose frequency location is in rough accord with the absorption due to chemical addition of holes to the CuO_2 planes. One can therefore conclude that localized carriers on the CuO_2 layers have a characteristic non-Drude midinfrared absorption. Second, photoexcitation of carriers changes the phonon spectrum. This is *prima facie* evidence for significant electron-phonon interaction, since there is no change in lattice structure or symmetry upon photoexcitation.

IV. ANALYSES OF THE INFRARED CONDUCTIVITY

There are two, seemingly different, approaches to analyzing of the infrared conductivity of the oxide superconductors. One, which we call the two-component approach, considers the conductivity to be due to a combination of free (Drude-like) and midinfrared (bound) carriers. Both contributions depend on there being holes on the CuO_2 planes—at least neither exists in the insulating parent compound—but may have different dependences on the hole concentration and on temperature. A key part of the two-component picture is that the free carriers condense into the superfluid below T_c, while the midinfrared carriers are relatively unaffected by the superconducting transition.

The other approach, the one-component picture, invokes only a single type of carrier. These carriers interact strongly with some type of optically inactive excitation in the material, giving a strong frequency dependence to the scattering rate and an enhanced low-frequency effective mass. This approach has been proposed by Anderson.[109] The "marginal Fermi liquid" ideas of Varma *et al.*[23,110] and Littlewood and Varma[111] and the "nested Fermi liquid" theory of Virosztek and Ruvalds[24,112] have both been used to discuss the optical conductivity within a one-component picture. In this picture, the onset of superconductivity leads to a gap in the conductivity spectrum; it is interesting that the optical gap may be at $\hbar\omega = 4\Delta$ rather than the $\hbar\omega = 2\Delta$ of Mattis-Bardeen theory.[111,113,114]

A. Two-component approaches

A two-component picture has been used extensively to discuss infrared absorption in ceramic samples[1] and has been also widely used in analyses of the *a*-*b*-plane conductivity in crystals and films. As an example, Fig. 37 shows the conductivity at 100 K of a $YBa_2Cu_3O_{7-\delta}$ film over a wide frequency range. Also shown is a fit to a model two-component dielectric function. The free-carrier component was fit to a Drude model, while the midinfrared and higher-energy components were fit by Lorentzian oscillators. The model dielectric function is

$$\epsilon(\omega) = \epsilon_1(\omega) + \frac{4\pi i}{\omega}\sigma_1(\omega) = -\frac{\omega_{pD}^2}{\omega^2 + i\omega/\tau} + \sum_{j=1,6} \frac{\omega_{pj}^2}{\omega_{ej}^2 - \omega^2 - i\omega\gamma_j} + \epsilon_\infty \qquad (10)$$

where ω_{pD} and $1/\tau$ are the plasma frequency and relaxation rate of the Drude carriers; ω_{ej}, ω_{pj}, and γ_j are the center frequency, strength, and width of the j^{th} Lorentzian contribution; and ϵ_∞ is the high-frequency limiting value of $\epsilon(\omega)$.

In Fig. 37 the fit is shown as a solid line, the Drude component as a dashed line, and the individual Lorentzian terms as dash-dotted lines. The high-frequency terms are due to various interband and charge-transfer transitions[115–117] occurring at 34,500 cm^{-1} (4.3 eV), 21,000 cm^{-1} (2.6 eV) and 11,200 cm^{-1} (1.4 eV). (The 1.7 eV charge transfer band of the insulating $YBa_2Cu_3O_6$ compound appears to split into two bands, 1.4 and 2.6 eV, in $YBa_2Cu_3O_7$. These are relatively weak in fully oxygenated samples, such as the one shown in Fig. 37.)

From the discussion of the *a*-*b*-plane anisotropy in Section II, we can conclude that the band at 3300 cm^{-1} (0.41 eV) is largely polarized in the *b* direction. Thus, it can be assigned to localized excitations associated with the chains.

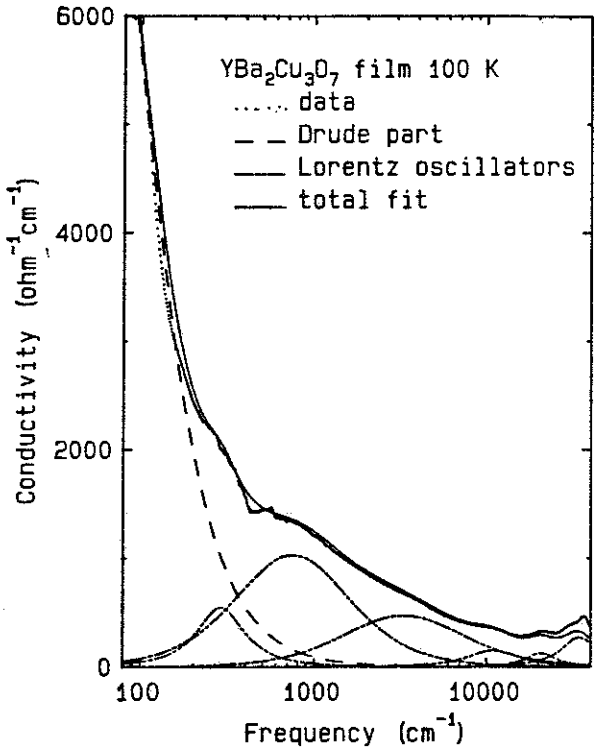

Fig. 37. Conductivity (as points) shown on a logarithmic frequency scale. The $\sigma_1(\omega)$ from fits to a sum of Drude (D) and Lorentzian (L) terms is shown, as well as the individual contributions to the sum. The Drude parameters are (in cm^{-1}): $\omega_{pD} = 8200$ and $1/\tau = 80$. The Lorentzian ω_{ej}, ω_{pj}, γ_j are: L_1—290, 3000, 250; L_2—740, 9800, 1550; L_3—3300, 14 500, 7500; L_4—11 200, 9300, 9500; L_5—21 000, 8600, 9500; L_6—34 500, 17 000, 18 000. [Ref. 71.]

The two lowest Lorentzian terms (740 and 290 cm^{-1} or 0.09 and 0.036 eV) are then the *a*-*b*-plane midinfrared conductivity. Two oscillators are needed to fit the data because of the minimum in the conductivity at 430 cm^{-1} (0.053 eV). In the fit, the wings of these terms are broader than the structure in $\sigma_1(\omega)$, indicating that Lorentzians are not particularly good model dielectric functions. As discussed in Section VI, the minimum or "notch" at 430 cm^{-1} is probably due to an electron-phonon interaction of an unusual type, and the midinfrared band can be viewed as a single feature with structure due to coupling of the midinfrared charge carriers to the phonons.

Fig. 38 shows another fit to the conductivity, from the work of Orenstein *et al.*[27] The data are for a crystal with $T_c = 50$ K. The calculated free-carrier conductivity includes a weak ($\lambda = 0.4$, in accord with estimates from resistivity[118] and infrared[15])

coupling to a band of excitations spanning 100–700 cm^{-1} (0.012–0.88 eV). The calculation used a free carrier plasma frequency of $\omega_{pD} = 8000$ cm^{-1} (1 eV). The fit is systematically higher than the low-frequency data, but even so falls well below the data above 400 cm^{-1}. The dashed line is the difference between the data (dots) and the free-carrier term (solid line). Orenstein *et al.* conclude that the midinfrared conductivity cannot be adequately described by a weak-coupling model, implying that the dashed line represents a second component in $\sigma_1(\omega)$.

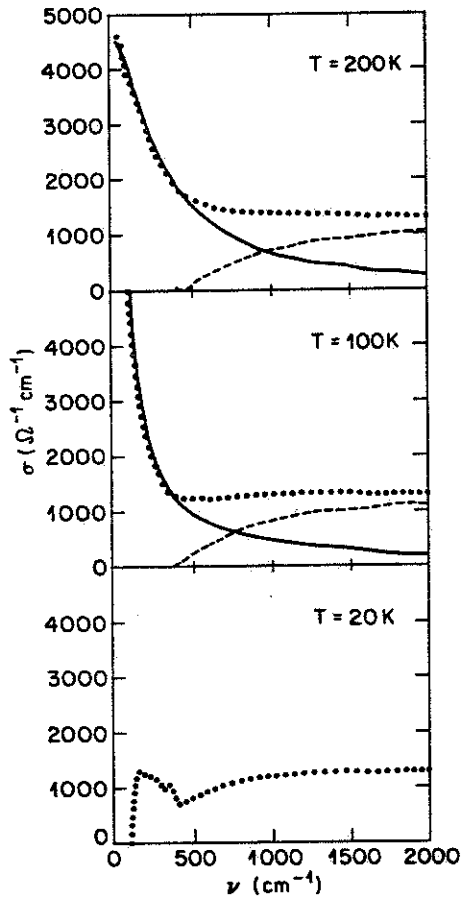

Fig. 38. Optical conductivity for a $T_c \approx 50$ K crystal at 200 (upper), 100 (middle), and 20 K (lower). The data are shown as a dotted line, with a weak coupling calculation shown as a solid line. [Ref. 27.]

1. The midinfrared conductivity

a. $YBa_2Cu_3O_{7-\delta}$

Kamarás *et al.*[15] used their fits to the reflectance to estimate the midinfrared part of their optical conductivity. The result is shown in Fig. 39. The curves in the

upper part of Fig. 39 were obtained by subtracting the Drude part of the conductivity, $\sigma_{1D} = \omega_{pD}^2/(1+\omega^2\tau^2)$, from the total conductivity. The curves in the lower part are the total conductivity below T_c (with nothing subtracted).

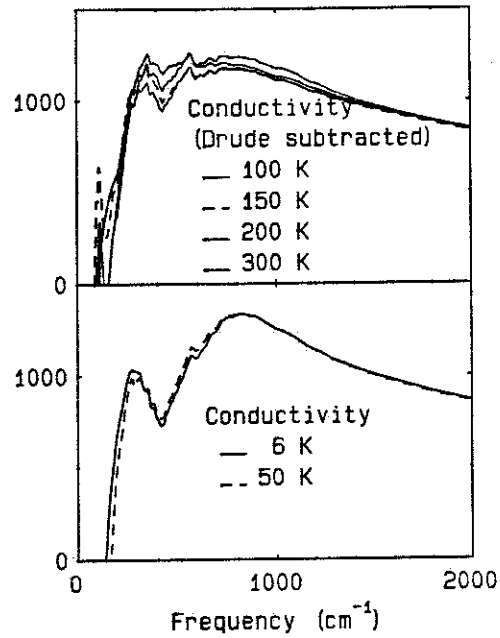

Fig. 39. Upper panel: Optical conductivity of a $T_c = 89$ K $YBa_2Cu_3O_{7-\delta}$ film above T_c, with the Drude contribution subtracted. Lower panel: Total conductivity below T_c. [Ref. 15.]

In Fig. 39 it can be seen that without the free carrier contribution, the normal state resembles the superconducting state: an onset near 140 cm^{-1}, a maximum around 350 cm^{-1}, a minimum at 430 cm^{-1}, and a second broad maximum near 750 cm^{-1}. With decreasing temperature the 430 cm^{-1} minimum grows deeper and the 140 cm^{-1} edge becomes a bit steeper; this trend continues below T_c. Because both the ~140 cm^{-1} onset and the minimum at 430 cm^{-1} are present in the normal state up to 300 K, they are unlikely to be associated with the superconducting gap. See the discussions in Sections V and VI for more about these features.

It is important to stress that the function which was subtracted from the data to obtain the results shown in Fig. 39 was a smoothly decreasing Drude conductivity, shown for $T = 100$ K in Fig. 37. The subtraction cannot build in any of the sharp features shown in Fig. 39; by suppressing the strong upturn associated with the free carriers, it only makes them easier to see. However, they clearly can be seen in the

total conductivity; for example there are obvious minima at 430 cm^{-1} in Figs. 23 and 26.

b. $Bi_2Sr_2CaCu_2O_8$

A similar determination of the midinfrared conductivity has been carried out for $Bi_2Sr_2CaCu_2O_8$ by Reedyk *et al.*[55,119] More recently, Romero *et al.*[62,63] have determined the free carrier and midinfrared components of $Bi_2Sr_2CaCu_2O_8$ by a procedure that begins by assuming that the line shape of the midinfrared conductivity can be approximated by the total conductivity at 20 K. (This approximation is accurate to about 10% of the maximum midinfrared conductivity.) A smooth free carrier contribution and a midinfrared contribution can be estimated by iteration. The midinfrared component is shown in Fig. 40.

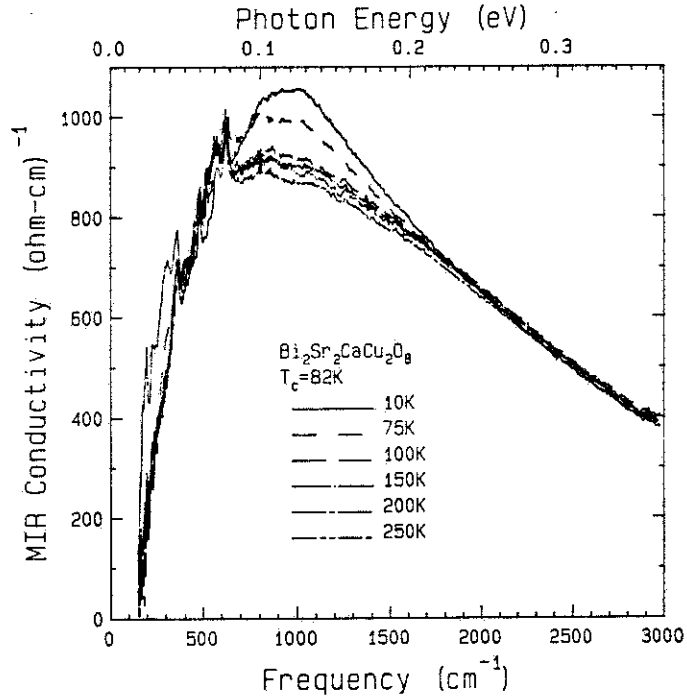

Fig. 40. The midinfrared contribution to the frequency-dependent conductivity of $Bi_2Sr_2CaCu_2O_8$ at temperatures between 20 and 300 K. The curves at and above 75 K were found by subtracting a Drude-model conductivity from the total conductivity of Fig. 13. The 20 K curve *is* the total conductivity. [Ref. 62.]

Fig. 40 agrees well with the results of Kamarás *et al.*[15] for $YBa_2Cu_3O_{7-\delta}$: there is an apparent onset of midinfrared conductivity around 150 cm^{-1} (0.019 eV), structure in the phonon region, and a broad maximum around 1000 cm^{-1} (0.12 eV).

Some of the phonons are ordinary in-plane vibrations, but a weak minimum is seen around 400 cm^{-1} (0.05 eV) that is probably of the same origin as the 430 cm^{-1} notch in $YBa_2Cu_3O_{7-\delta}$. This minimum is weaker and at higher frequency in the $Bi_2Sr_2CaCu_2O_8$ material, however.

2. T-dependence of the midinfrared conductivity

Let us turn to the temperature dependence of the midinfrared conductivity. In $Bi_2Sr_2CaCu_2O_8$ (Fig. 40) above T_c there is no T-dependence to the low-energy edge, some weak T-dependence between 700 and 1600 cm^{-1}, and no temperature dependence at higher energies. Below T_c the edge appears to shift to slightly *lower* frequencies and the T-dependence in the 700–1600 cm^{-1} region appears to be stronger.

For $YBa_2Cu_3O_{7-\delta}$ Kamarás *et al.*[15] used a sum of three Lorentzian oscillators to model the midinfrared and chain contribution to the dielectric function, finding some temperature variation in all of the nine Lorentz parameters. The data can also be fit with a temperature variation in line widths but with center frequencies and oscillator strengths held constant. The line widths have a linear temperature dependence, $\gamma(T) = \gamma(0) + k_BT$, just like the Drude $1/\tau$. It almost seems as if whatever is broadening the free carrier conductivity is also broadening the (already quite wide at $T = 0$ K) midinfrared conductivity. This linear temperature dependence of the broadening of the midinfrared band has recently been reported by Thomas *et al.*[49]

3. The free carrier conductivity

a. $YBa_2Cu_3O_{7-\delta}$

The free-carrier conductivity appears to be quite conventional: the plasma frequency is independent of temperature (or nearly so) while the scattering rate follows the T-dependence of the resistivity.[10] Fig. 41 shows the temperature dependence of the low-frequency Drude terms for a $T_c = 89$ K film, from the work of Kamarás *et al.*[15] and Herr *et al.*[72] Consistent with its slightly lower T_c, this sample had a lower free-carrier oscillator strength than the $T_c = 91$ K specimen discussed in the previous Section. The Drude plasma frequency $\omega_{pD} \approx 8200$ cm^{-1}, is nearly T-independent. The scattering rate is $1/\tau \approx 80$ cm^{-1} at 100 K and is essentially T-linear (like the resistivity), with zero intercept. The 100 K value corresponds to $\tau = 6.6 \times 10^{-14}$ sec and (if $v_F = 2 \times 10^7$ cm/sec) a mean free path of $\ell = 130$ Å.

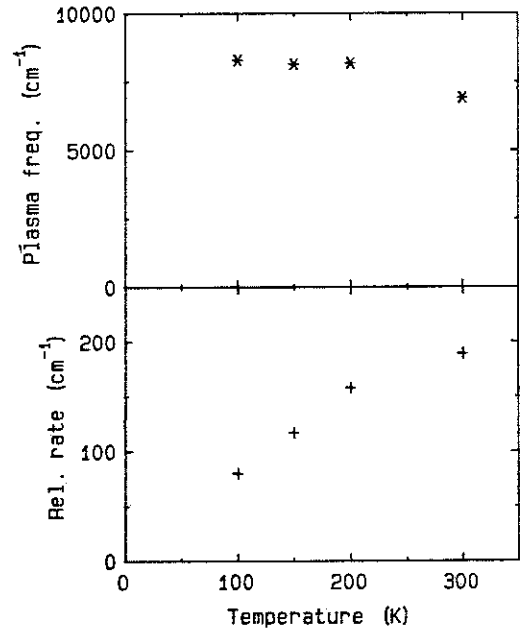

Fig. 41. Temperature dependence of the Drude plasma frequency and relaxation rate for $YBa_2Cu_3O_{7-\delta}$. [Ref. 71.]

b. $Bi_2Sr_2CaCu_2O_8$

Fig. 42 shows the free-carrier contribution to the *a-b*-plane conductivity of $Bi_2Sr_2CaCu_2O_8$ from the work of Romero *et al.*[62,63] The free carrier component is defined as the difference between the optical conductivity (shown in Fig. 13) and the *average* above-T_c midinfrared component. Above T_c, the Drude contribution has a nearly T-independent plasma frequency, $\omega_{pD} = 10,250 \pm 100$ cm^{-1} and a T-linear scattering rate, shown in the inset. Note that the intercept is almost zero at zero temperature.

This T-linear scattering rate combined with a T-independent plasma frequency is of course completely consistent with the dc conductivity. From the Drude fits, Romero *et al.* estimate a 100 K resistivity of 100 $\mu\Omega$-cm, in good agreement with the measured dc value of the samples studied.

4. Temperature dependence of τ above T_c

The scattering rate may be expressed as[121]

$$\hbar/\tau = 2\pi\lambda k_B T + \hbar/\tau_0 \tag{11}$$

where λ is the dimensionless coupling constant between the charge carriers and whatever T-dependent excitation is responsible for their scattering. Note that Eq. 11 is

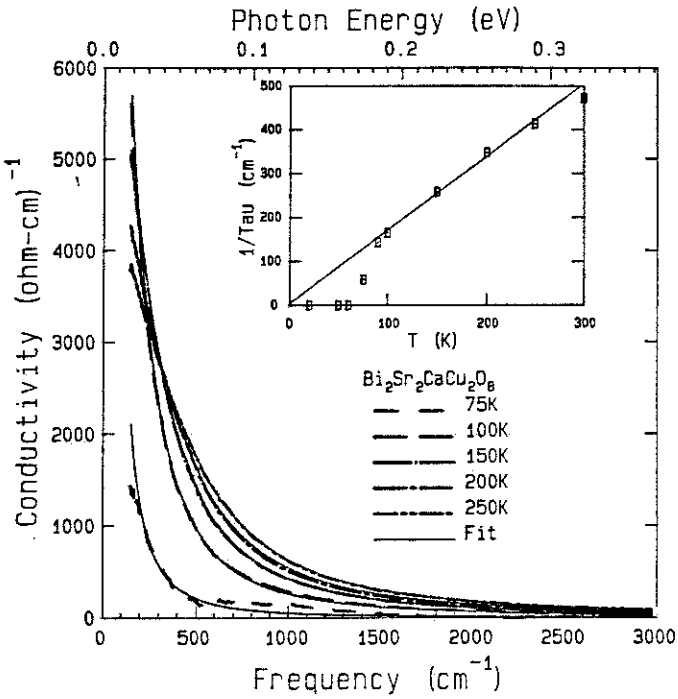

Fig. 42. The free carrier contribution to the a-b-plane conductivity of $Bi_2Sr_2CaCu_2O_8$ at temperatures between 75 and 300 K. The thin lines are the calculated Drude conductivity at each temperature. The inset shows the scattering rate *vs.* temperature found from the analysis. [Ref. 120.]

a high-temperature expression which assumes that the characteristic energy $\hbar\Omega$ of the excitation is small compared to T. In addition, the zero temperature value $1/\tau_0$ is assumed to result from elastic scattering by impurities that is additive to the T-dependent term. In the best high temperature superconductors the $T = 0$ intercept of resistivity, and hence $1/\tau_0$, appears to be zero.

A number of authors have evaluated transport and optical data within such a weak-coupling theory, finding $\lambda \approx 0.3 \pm 0.1$, a weak coupling value. Table 2 lists the results of these analyses. In this Table, the values from resistivity measurements are reported as upper limits on λ; $\hbar/\tau$ is then calculated from Eq. 11. The optical measurements yield $\hbar/\tau$, from which λ is calculated. The scattering rate is in units of k_BT.

Table 2. Scattering rate and λ for the free-carrier component.

Material	Scattering rate $\hbar/\tau k_B T$	Coupling constant λ	Temp. range (K)	Technique
$YBa_2Cu_3O_{7-\delta}$	1.9	0.3	130–600	Resistivity[118]
$Bi_2Sr_2CaCu_2O_8$	1.3	0.2	90–600	Resistivity[122]
$La_{2-x}Sr_xCuO_4$	0.6	0.1	50–1100	Resistivity[118]
$Bi_2Sr_2CuO_6$	0.5	0.08	7–700	Resistivity[67]
$Tl_2Ba_2CaCu_2O_8$	2.1	0.3	125–300	Infrared[30]
$YBa_2Cu_3O_7$	1.9	0.3	100–300	Infrared[14]
$YBa_2Cu_3O_7$	1.4	0.2	100–300	Infrared[15]
$YBa_2Cu_3O_7$	2	0.3	100–300	Infrared[27]
$YBa_2Cu_3O_7$	2.6	0.4	100–300	Infrared[32]
$YBa_2Cu_3O_{6+x}$	1.8	0.28	60–270	Infrared[11]
$Bi_2Sr_2CaCu_2O_8$	2.5	0.4	90–300	Infrared[31]
$Bi_2Sr_2CaCu_2O_8$	2.4	0.4	90–300	Infrared[61,62,63]
$Bi_2Sr_2CuO_6$	2.0	0.3	40–300	Infrared[62]

B. One-component analysis

1. Holstein model

As mentioned already, early attempts at one-component analyses, such as the use of a broad Drude oscillator[1,123,124] or a Holstein emission process,[11,13] were unsuccessful in accounting for both the far-infrared and dc conductivity and the midinfrared conductivity. A good example of the difficulties with the Holstein approach has been given by Orenstein *et al.*[27] Their result is shown in Fig. 43. The data, a-b-plane optical conductivity for a $T_c = 90$ K crystal, are shown as points together with two fits to a Holstein model, the dashed and the dotted cureves.

Ordinary metals are well described by the Holstein model.[1,125–127] Both the frequency and temperature dependence of the conductivity can be shown to depend

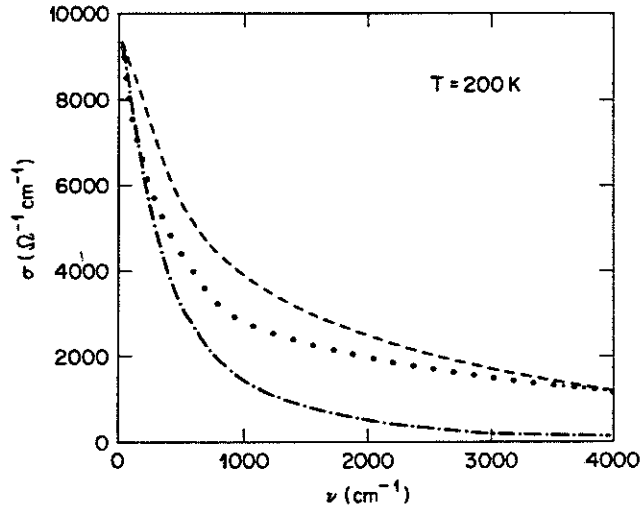

Fig. 43. The circles show the 200 K optical conductivity of a $T_c = 90$ K crystal of $YBa_2Cu_3O_{7-\delta}$. The dashed lines are fits to a Holstein model with the following parameters: dash-dotted curve: $\omega_p = 1.4$ eV; $\lambda = 0.4$; dashed curve: $\omega_p = 2.15$ eV, $\lambda = 2.0$. [Ref. 27.]

on $\alpha^2F(\omega)$, the electron-phonon spectral density, with a coupling constant λ given by

$$\lambda = 2\int_0^\infty \frac{\alpha^2F(\omega)}{\omega}\,d\omega \tag{12}$$

In contrast, Orenstein *et al.* tried to fit the conductivity of $YBa_2Cu_3O_{7-\delta}$ with a variety of functional forms for $\alpha^2F(\omega)$ but were basically unsuccessful. The curves in Fig. 43 show two such attempts. In them, $\alpha^2F(\omega)$ is 500 cm^{-1} wide and is centered at 330 cm^{-1} but has different magnitudes, giving different λ values; $\lambda = 0.4$ for the lower curve and $\lambda = 2.0$ for the upper curve.

The reason for the failure of the Holstein model to describe the optical conductivity is that the low-frequency optical conductivity combined with the linear-in-T dc resistivity implies a small value for λ while the broad, T-independent midinfrared absorption requires a large value of λ. Thus the data are not consistent with a one-component picture based on the Holstein emission process.

Another way to understand this is as follows. The Holstein emission process is one in which a charge carrier absorbs a photon of energy ω, emits an excitation of energy Ω, and scatters, giving rise to absorption. (The excitation is generally a phonon but in fact could be any boson that couples linearly to the charge carriers. We will use "electrons" and "phonons" for concreteness.) Momentum is conserved in the electron-phonon system; energy largely in the photon-phonon system. Only

phonons with energy less than the photon energy play a role. These considerations lead to the following expression for the $T = 0$ scattering rate[126]

$$1/\tau(\omega) = \frac{2\pi}{\omega}\int_0^{\omega} \alpha^2 F(\Omega)(\omega - \Omega)d\Omega \tag{13}$$

The scattering rate has a threshold at the phonon energy. It is possible to design, therefore, an $\alpha^2 F(\omega)$ that gives to the optical conductivity the observed low-temperature line shape, with a threshold for the non-Drude midinfrared absorption at some Ω_0 in the far-infrared and with free-carrier-like behavior below.[11,13,128] However, this $\alpha^2 F(\omega)$ is not in accord with the observed electrical resistivity; once $k_B T \approx \hbar\Omega_0$, the model predicts strong (on account of the large λ needed) deviations from T-linear behavior because the charge carriers interact strongly with thermally excited phonons. The signature of these deviations in the middle temperature range is that an extrapolation of resistivity along a linear T dependence does not go through the origin. Instead, its $T = 0$ intercept is at a negative resistivity on account of the large upward curvature of the low-T resistivity. (T-linear behavior can be simulated by adjusting the zero-T intercept, *i.e.*, by assuming a particular value of the residual resistivity. This assumption requires the residual resistivity of a large number of samples to be identical, a rather unlikely coincidence.)

2. The marginal Fermi liquid

Varma *et al.*[23] have proposed a phenomenological model for the oxide superconductors that they call a "marginal Fermi liquid." This model assumes that excited charge carriers interact with a spectrum of (optically inactive) excitations which is flat over $T < \omega < \omega_c$, where ω_c is a high energy scale that cuts off the spectrum. Evidence advanced in support of this hypothesis includes the Raman spectrum,[129,130] where a broad continuum of electronic excitations extending to 1 eV (8000 cm^{-1}) is observed, and the angle-resolved photoemission,[131,132] where a broad, asymmetric peak at the Fermi energy is seen.

According to Varma *et al.*[23] and Littlewood and Varma[111] the quasiparticle self energy Σ of the marginal Fermi liquid has an imaginary part which qualitatively goes as

$$-\operatorname{Im}\Sigma(\omega) \sim \begin{cases} \pi^2\lambda T, & \omega < T \\ \pi\lambda\omega, & \omega > T \end{cases} \tag{14}$$

where λ is defined by an equation like Eq. 12. There is a corresponding logarithmic (in ω/ω_c or T/ω_c, whichever is greater) upturn in the effective mass, with the mass enhancement proportional to λ.

The inverse lifetime (or scattering rate) of the charge carriers is given by the imaginary part of the self-energy, which at zero frequency is linear in T. This result is in accord with the measured resistivity. At high frequencies, there is no temperature dependence in Eq. 14 and the scattering rate is proportional to ω; the lifetime to $1/\omega$. Thus, at high frequencies the conductivity becomes $\sigma_1(\omega) = \omega_p^2\tau/4\pi(1+\omega^2\tau^2) \sim \omega_p^2/4\pi\omega$. It goes like $1/\omega$ in contrast to the $1/\omega^2$ dependence of an ordinary metal with frequency-independent scattering.

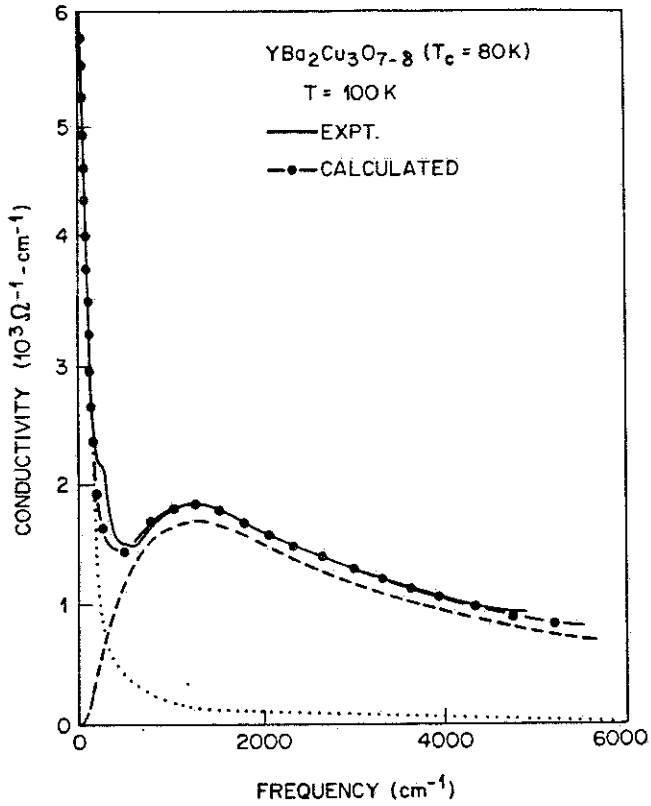

Fig. 44. The optical conductivity from Ref. 27 is shown as the solid line. The dash-dotted line is a sum of a marginal Fermi liquid contribution (dots) and a direct midinfrared absorption (dashes). [Ref. 23.]

Fig. 44 shows a comparison between the measured optical conductivity of Orenstein *et al.*[27] and a calculation within the marginal Fermi liquid approach.[23] The data are the solid line and the result of the calculation is the dash-dotted line. Note that in this calculation a second component, representing a second, optically active, direct absorption, has been added to $\sigma_1(\omega)$. Strictly speaking, therefore, this is not a pure one-component calculation. The direct absorption, the dashed line, has about 80%

of the infrared oscillator strength, while the the marginal Fermi liquid conductivity, the dotted line, has about 20%. The latter has most of its oscillator strength in the low frequency region [below the ~500 cm^{-1} minimum in $\sigma_1(\omega)$] with a relatively low contribution in the midinfrared region. In more recent calculations,[111] this second contribution has been dropped. The cutoff frequency, ω_c, is 1200 cm^{-1} (0.15 eV).

3. The nested Fermi liquid

Virosztek and Ruvalds[133,112] have discussed the unconventional nature of the normal state of the high temperature superconductors in terms of Fermi-surface nesting. According to this "nested Fermi liquid" approach, large parts of the 2-dimensional Fermi surface of the CuO_2 layers are spanned by common nesting wave vectors, which change qualitatively the susceptibility and quasiparticle self-energy of the charge carriers. The dominant scattering process in this nested Fermi liquid is electron-electron scattering (or hole-hole scattering) Instead of the $-\operatorname{Im}\Sigma \propto \omega^2 + T^2$ of the ordinary metallic system, the nested Fermi liquid has

$$-\operatorname{Im}\Sigma(\omega) = \alpha \max(\beta T, |\omega|) \tag{15}$$

where α is a dimensionless coupling constant ($\alpha \approx 0.5$–1) and β~1.2–1.5. Eq. 15 gives a scattering rate that is linear in T at low ω and linear in ω at high ω, *i.e.*, one just like that in Eq. 14. There is also a mass enhancement at low frequencies, $m^*/m = 1 + (2\alpha/\pi)\ln[\omega_c/\max(\beta T, \omega)]$, where ω_c is a cutoff of order the width of the conduction band.

Fig. 45 shows a comparison of the nested Fermi liquid theory to optical reflectance data.[112] The data for $YBa_2Cu_3O_{7-\delta}$ are from Watanabe *et al.*[18]; for $Bi_2Sr_2CaCu_2O_8$ from Kim *et al.*[134]. The fits are for $1/\tau = -\operatorname{Im}(\Sigma) = 0.9\omega$. (The data in Fig. 45 are in the high-frequency limit of Eq. 15.) Also shown as the dashed line is the reflectance of a Drude model (with no additional midinfrared contribution) that fails to describe the data.

C. Measurements of $1/\tau^*(\omega)$ and $\Sigma(\omega)$

A number of groups have determined the scattering rate and frequency dependent effective mass from optical data. Various theoretical formulae have been used, and it might be useful for us to digress for a moment and describe these formulae.

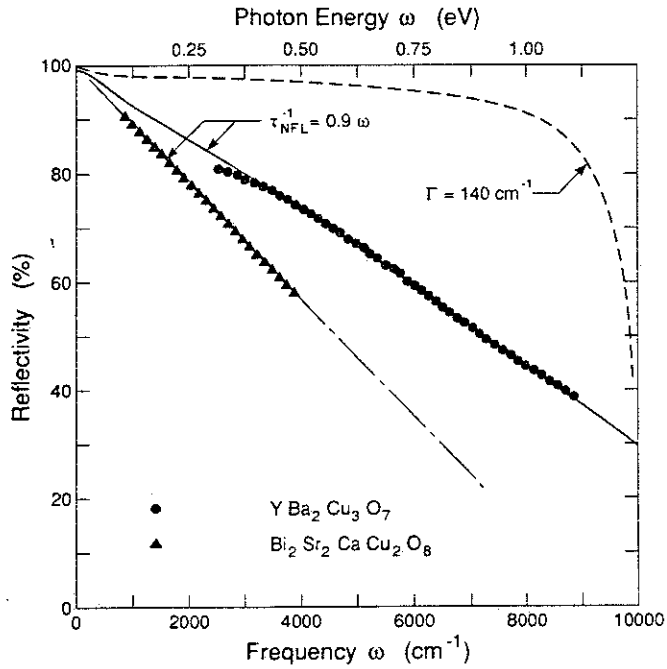

Fig. 45. 300 K reflectance of $YBa_2Cu_3O_{7-\delta}$ (dots) and $Bi_2Sr_2CaCu_2O_8$ (triangles) compared to a fit using the nested Fermi liquid approach. Parameters used are $\alpha = 0.9$ for both materials; $\omega_p = 16000\ cm^{-1}$ (2 eV) and 11000 cm^{-1} (1.4 eV) for $YBa_2Cu_3O_{7-\delta}$ and $Bi_2Sr_2CaCu_2O_8$, respectively. The dashed line is a Drude reflectance with $\omega_p = 9600\ cm^{-1}$ (1.2 eV) and $1/\tau = 140\ cm^{-1}$. [Ref. 112.]

1. Notation

We begin with the notion of a frequency-dependent scattering rate. Such frequency dependence can arise in a number of contexts such as the Holstein effect, other electron-boson interaction models, the marginal Fermi liquid, and the nested Fermi liquid. If a frequency-dependent scattering rate, $\gamma(\omega)$ is used in a generalized Drude model,[1,135]

$$\epsilon(\omega) = \epsilon_\infty - \frac{\omega_p^2}{\omega(\omega + i\gamma)}$$

(where ϵ_∞ represents interband contributions not involving the charge carriers and

$$\omega_p = \sqrt{4\pi n e^2/m^*}$$

is the plasma frequency, with n the carrier concentration and m^* the effective mass), then the real and imaginary parts of ϵ will not satisfy causality (*i.e.*, Kramers-Kronig) unless

(a.) γ is complex,

or

(b.) γ is real and ω_p or m^* is frequency dependent.

These two cases are equivalent, but lead to different functional forms for "scattering rates."

For the first case, we will write the complex damping function, also called a memory function, as $\gamma = R(\omega) + iI(\omega)$, and

$$\epsilon(\omega) = \epsilon_\infty - \frac{\omega_p^2}{\omega[\omega - I(\omega) + iR(\omega)]}. \tag{16}$$

For the second case, we will put the needed frequency dependence into the effective mass m^* and write

$$\epsilon(\omega) = \epsilon_\infty - \frac{\omega_p^2}{\omega(m^*(\omega)/m_b)[\omega + i/\tau^*(\omega)]}, \tag{17}$$

where $1/\tau^*(\omega)$ is the (renormalized) scattering rate. Finally, for the marginal Fermi liquid, Littlewood and Varma[111] have suggested writing the dielectric function in the following approximate form:

$$\epsilon(\omega) \approx \epsilon_\infty - \frac{\omega_p^2}{\omega[\omega - 2\Sigma(\omega/2)]} \tag{18}$$

where the factor of two appears because quasiparticle excitations (like in superconductors) are made in pairs and where Σ is the quasiparticle self-energy, given by:

$$\Sigma_{MFL} = 2\lambda\omega \log\left(\frac{\pi T - i\omega}{\omega_c}\right) - i\pi^2\lambda T. \tag{19}$$

Here, ω_c is a high-frequency cutoff and λ is a dimensionless coupling constant. Eq. 19 has the same limiting forms as Eqs. 14 and 15.

The quantity ω_p in Eqs. 16, 17, and 19 is the "bare" plasma frequency, given by $\omega_p^2 = 4\pi ne^2/m_b$ with m_b the band mass. An accurate value for ω_p needs to be supplied as part of the analysis to get $1/\tau^*$ or Σ. The other quantities can be related by equating real and imaginary parts of the denominators as follows:

$$\frac{m^*(\omega)}{m_b} = 1 - \frac{I(\omega)}{\omega} = 1 - \frac{2}{\omega}\,\mathrm{Re}\,\Sigma\left(\frac{\omega}{2}\right) \tag{20}$$

and

$$\frac{m^*(\omega)}{m_b} 1/\tau^*(\omega) = R(\omega) = -2\,\mathrm{Im}\,\Sigma\left(\frac{\omega}{2}\right) \tag{21}$$

Note that $1/\tau^*(\omega)$ is called the "renormalized" scattering rate, while $R(\omega)$ is the "unrenormalized" scattering rate is sometimes written as $1/\tau$.

Some of these distinctions disappear at zero frequency. In particular, the dc conductivity of Eq. 17 is

$$\sigma_{dc} = \omega_p^2(m_b/m_0^*)\tau_0^*/4\pi = \omega_p^2\tau_0/4\pi$$

which shows that the effect of the mass enhancement at low frequencies is cancelled by the renormalization of τ.

2. $Bi_2Sr_2CaCu_2O_8$

Romero *et al.*[62] have analyzed their optical conductivity for $Bi_2Sr_2CaCu_2O_8$ and $Bi_2Sr_2CuO_6$ to obtain Σ. Results are shown in Fig. 46 for $Bi_2Sr_2CaCu_2O_8$ and Fig. 47 for $Bi_2Sr_2CuO_6$. The insets show the dc resistivity and the far-infrared resistivity, defined as the inverse of the limiting low-frequency $\sigma_1(\omega)$.

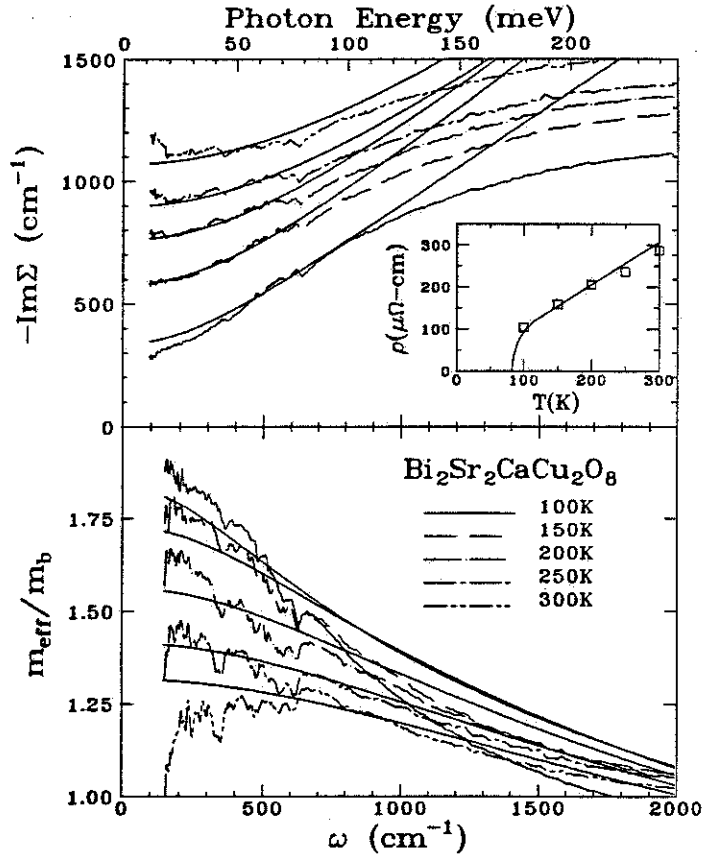

Fig. 46. Upper: Imaginary part of the quasiparticle self energy Σ for $Bi_2Sr_2CaCu_2O_8$. Lower: Effective mass as a function of frequency. The thin lines are fits to Eqs. 18 and 19. The inset shows the dc resistivity (continuous line) and the resistivity determined by far infrared means (open squares). [Ref. 62.]

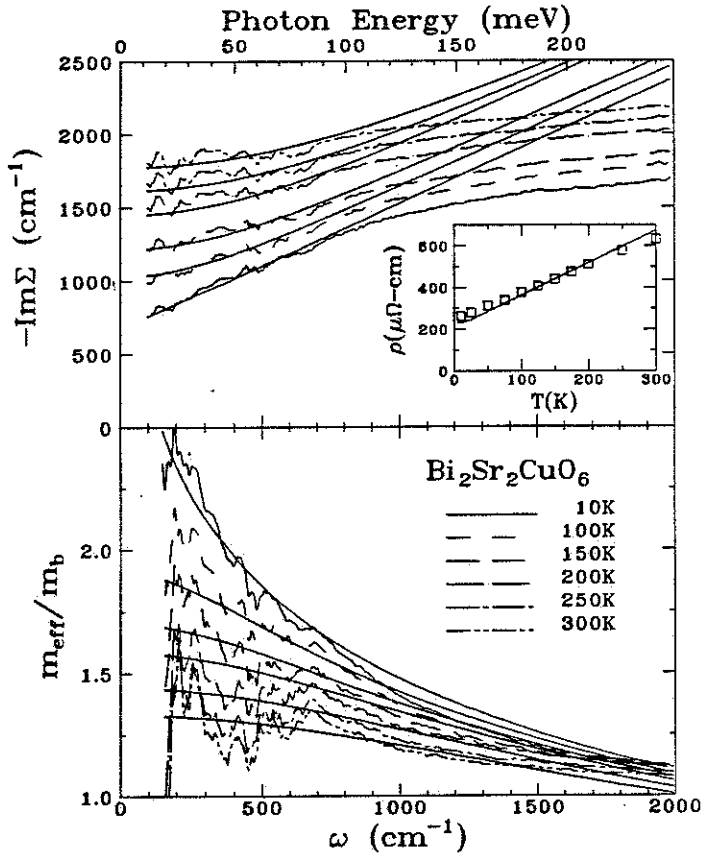

Fig. 47. Upper: Imaginary part of the quasiparticle self energy Σ for $Bi_2Sr_2CuO_6$. Lower: Effective mass as a function of frequency. The thin lines are fits to Eqs. 18 and 19. The inset shows the dc resistivity (continuous line) and the resistivity determined by far infrared means (open squares). [Ref. 62.]

Romero *et al.* made a fit to Eqs. 18 and 19, shown in Figs. 46 and 47. The fits gave $\omega_p = 14,700$ cm^{-1} (1.8 eV) for $Bi_2Sr_2CaCu_2O_8$ and $\omega_p = 12,800$ cm^{-1} (1.6 eV) for $Bi_2Sr_2CuO_6$. $\omega_c = 1200$ cm^{-1} (0.15 eV) and $\lambda = 0.27$ for both materials. (Note that the equation for this coupling constant, Eq. 14, differs from the equation used to calculate the λ's in Table 2 by a factor of $2/\pi$.) The calculations for the self-energy agree with the data in several important ways. First, both give a dc resistivity in agreement with experiment. Second, $-\mathrm{Im}\,\Sigma$ increases linearly with ω for $\omega > T$. Third, there is an enhancement of the effective mass at low frequencies by an amount that is larger at lower temperatures.

There are also some differences. The principal one is that the cutoff frequency is rather low; data and calculation agree only below 1000 cm^{-1} (0.12 eV). This conflicts with the high cutoff suggested by Raman[129,130] and photoemission[131] experiments.

The calculations deviate substantially from the data above the cutoff. Experimentally, the zero-frequency effective mass increases with decreasing T more rapidly than predicted. Finally, the conductivity spectrum has a substantial part of its oscillator strength above the cutoff, implying that not all the midinfrared absorption can be attributed to the carriers.

3. $Tl_2Ba_2CaCu_2O_8$

A low-frequency mass enhancement and quasi-linear in ω scattering rate have been observed by Jehl *et al.*[69] in a study of $Tl_2Ba_2CaCu_2O_8$. Their results are shown in Fig. 48. What Jehl *et al.* call γ, we called R in the discussion of notation, above. γ rises linearly up to about 1500 cm^{-1}, where the slope decreases suddenly; it saturates above 4000 cm^{-1} (0.5 eV). The mass enhancement in this 300 K data is about a factor of 10 larger than that obtained by Romero *et al.*; the reason for this large difference in very similar materials is not clear.

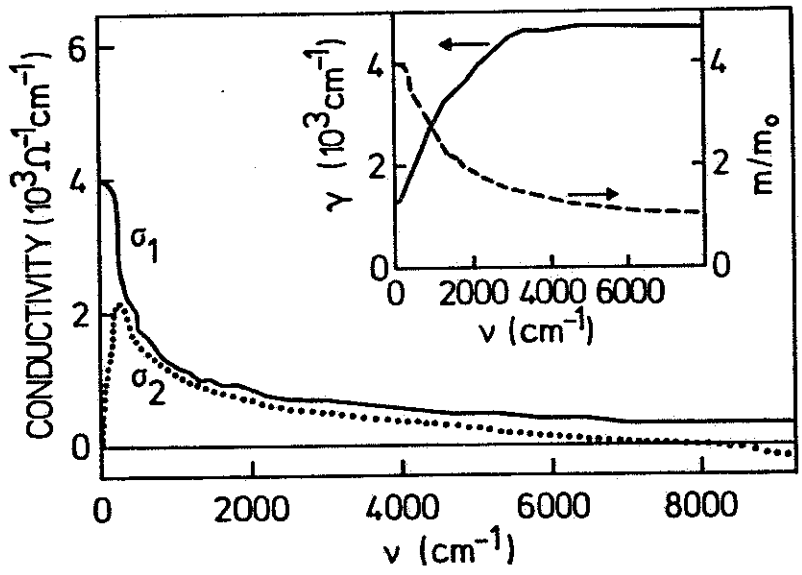

Fig. 48. The main panel shows the real and imaginary parts of the 300 K optical conductivity for $Tl_2Ba_2CaCu_2O_8$. The inset shows the scattering rate and the mass enhancement inferred from the conductivity. [Ref. 69.]

4. $YBa_2Cu_3O_{7-\delta}$

Schlesinger *et al.*[17,19] have calculated the scattering rate for both a-b-plane crystals and the a-axis polarization for single crystals of $YBa_2Cu_3O_{7-\delta}$. The result for the a-axis scattering rate, $1/\tau^*$, at 100 K, is shown in Fig. 49. The mass enhancement is substantial. The effective mass increases from near the free-carrier value at 2000

cm^{-1} to ~2.5 at low frequencies. The scattering rate is linear up to ~1200 cm^{-1} (0.15 eV), after which its slope starts to decrease. Note that if this figure shows the renormalized scattering rate, as appears to be the case, then it is not expected to be linear according to the marginal Fermi liquid ideas. If the unrenormalized scattering rate is linear, then the renormalized rate will have the same curvature as m^*/m_b and vice-versa.

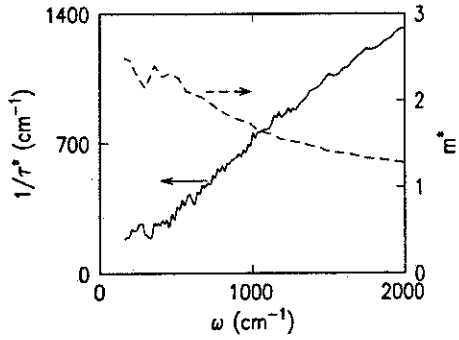

Fig. 49. Dashed line, right scale: Effective mass as a function of frequency determined from the a-axis polarized conductivity of a $YBa_2Cu_3O_{7-\delta}$ single crystal. The temperature is 100 K. Full line, left scale: The corresponding renormalized scattering rate, $1/\tau^*$. [Ref. 19.]

Cooper *et al.*[80] have recently measured the room-temperature optical conductivity of oxygen deficient $YBa_2Cu_3O_{6.6}$ single crystals as well as $YBa_2Cu_3O_7$ and have also extracted the scattering rate and mass enhancement. Their results are shown in Fig. 50. For the $YBa_2Cu_3O_7$, T_c~90 K sample, the effective mass increases to twice the free-carrier value by 400 cm^{-1} (0.05 eV) and the scattering rate appears linear up to 2400 cm^{-1} (0.3 eV).

Much more interesting are the data for the oxygen deficient sample. Both the slope of the scattering rate and the mass enhancement of this lower T_c (~66 K) sample are larger than for the fully oxygenated specimen. A similar result has recently been reported by Rotter *et al.*[136] These results are difficult to understand within a marginal Fermi liquid perspective. The mass enhancement and the scattering rate slope are both proportional to λ, implying that the higher T_c material has a smaller λ. The difficulty comes because the T_c is also supposed to be determined by λ, and strong coupling—large λ—should mean high T_c.

However, according to the discussion of the nested Fermi liquid picture,[112] an increased coupling (*i.e.*, a larger value of α) is expected as the carrier concentration

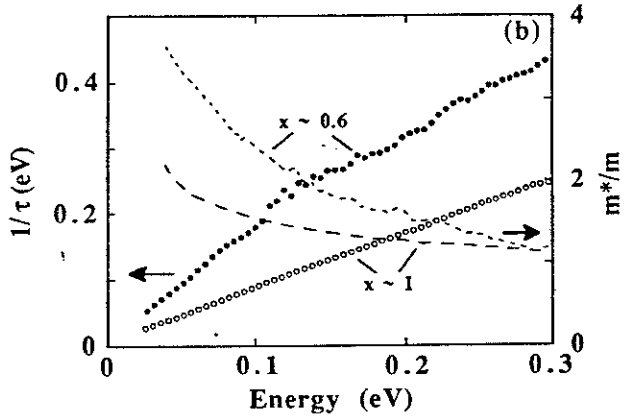

Fig. 50. Frequency-dependent effective mass and scattering rate derived from the a-axis conductivity for a $YBa_2Cu_3O_7$ (open circles and long dashes) and a $YBa_2Cu_3O_{6.6}$ crystal. The measurements were at room temperature. [Ref. 80.]

is reduced because the nesting is improved as the insulating state (a half-filled band in a one-electron picture) is approached. As yet, no connection between the nesting and superconductivity has been made.

5. $La_{2-x}Sr_xCuO_4$

A similar result has been reported for $La_{2-x}Sr_xCuO_4$ by Uchida *et al.*[33] Their results for four different doping levels are shown in Fig. 51. Recall that the $x = 0.15$

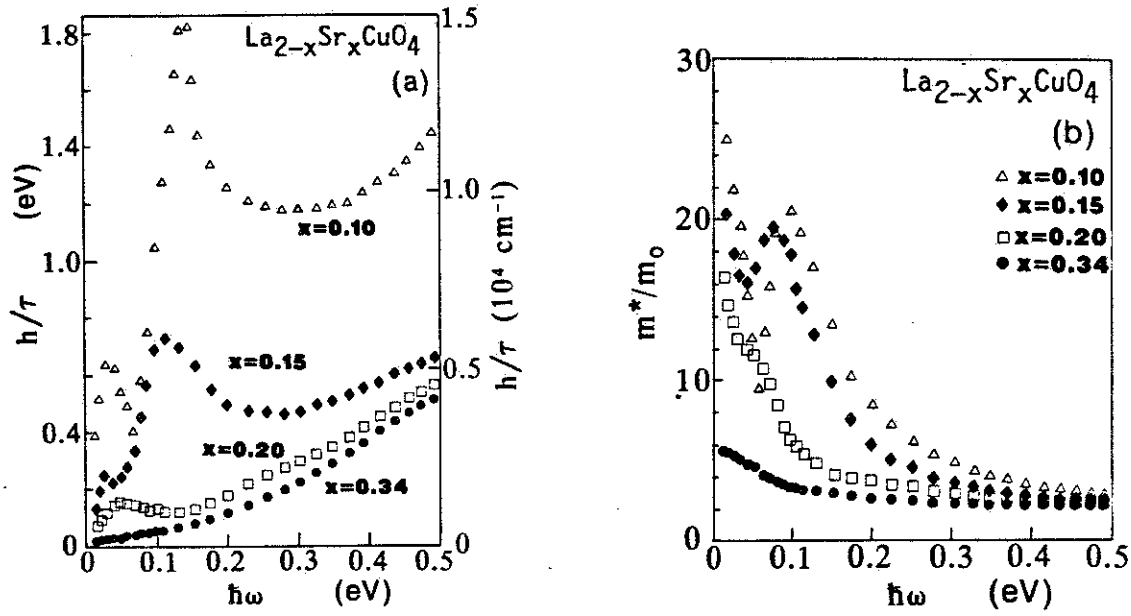

Fig. 51. a) Frequency dependent scattering rate and b) the effective mass ratio m^*/m for $La_{2-x}Sr_xCuO_4$. [Ref. 33.]

sample has the highest T_c. Neither the low-frequency enhancement of m^*/m_b nor the slope of $1/\tau$ with doping correlates with the superconductivity; instead we see a steady decrease of these quantities with doping level.

V. THE INFRARED PROPERTIES OF THE SUPERCONDUCTING STATE

A. Introduction

In the superconducting state, the infrared reflectance of the high T_c materials is puzzling. Fig. 52 shows the reflectance in the superconducting state of six different materials with T_c ranging from 20 K to near 100 K. The low-frequency reflectance is close to unity in all the materials with a steplike onset of absorption at higher frequency. In most materials, measurable absorption starts in the 150 cm^{-1} region and there is a pronounced onset of strong absorption between 350 and 600 cm^{-1}. In ordinary superconductors such an onset would be caused by a superconducting gap. The onset of absorption in the high T_c materials does not correlate with T_c when the T_c is reduced by doping.[27] Also, as Fig. 52 shows, there is no direct correlation between T_c and the various onsets. Timusk and Tanner[107] have presented evidence suggesting that in $YBa_2Cu_3O_{7-\delta}$ the feature at 400 - 500 cm^{-1} is not the superconducting gap, but is due to phonons. In this Section we will first discuss the infrared signature of the superconducting condensate and then turn to the question: is there evidence for a gap in the conductivity of the high T_c materials?

B. The effect of condensation: a delta function conductivity at zero frequency

The most striking manifestation of superconductivity in the infrared is a sharp increase of reflectance at low frequency at temperatures just below the superconducting transition. It can be shown, from a detailed Kramers-Kronig analysis,[15] that these changes in the reflectance result from changes of the low-frequency conductivity. The Drude-like band, some 100–200 cm^{-1} wide, centered at zero frequency, decreases rapidly in both amplitude and width at the superconducting transition, and is replaced by the delta function response at the origin due to the superconducting condensate.

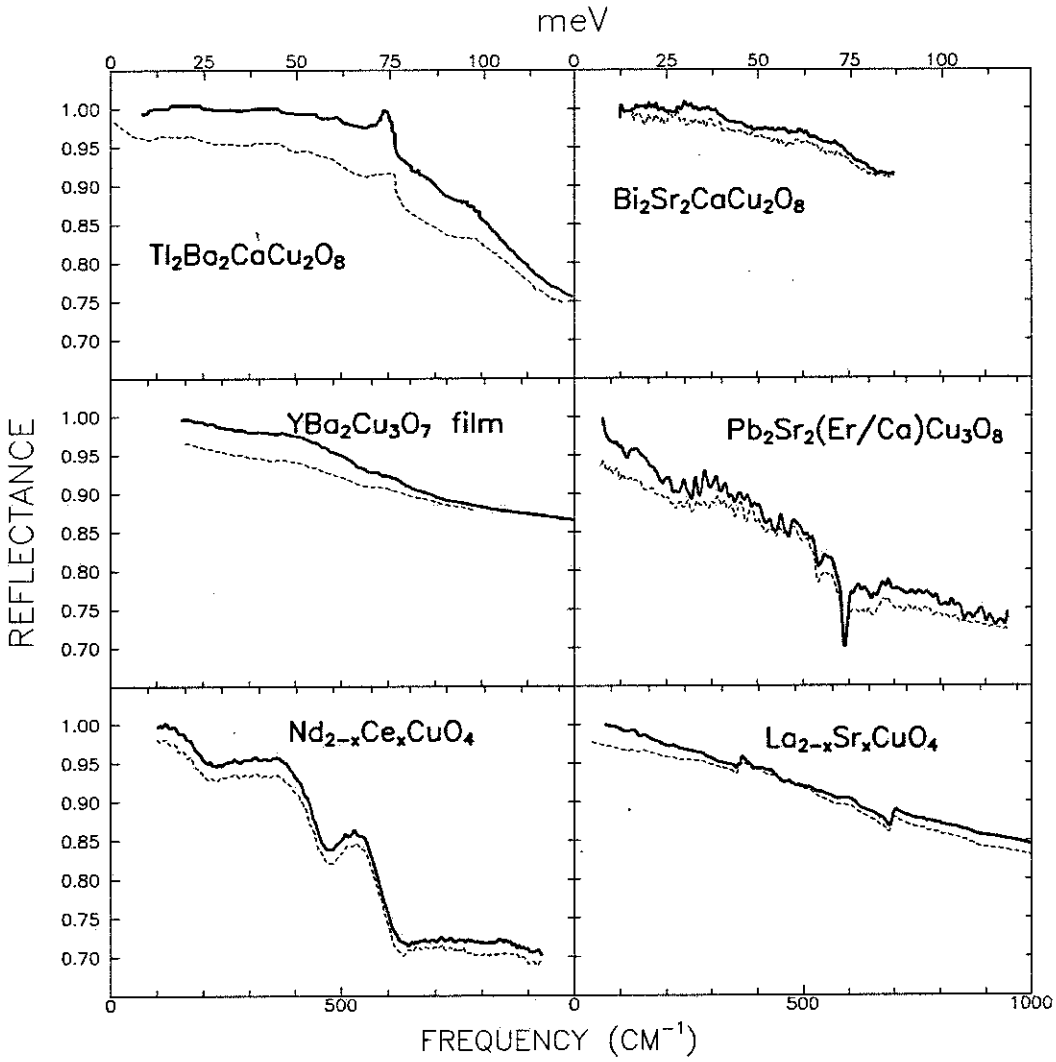

Fig. 52. The reflectance of six high T_c superconductors in the superconducting (solid curves) and normal states (dashed curves).

Fig. 53 illustrates the changes, according to BCS theory, expected for the conductivity when a material becomes superconducting. The two diagrams, both assuming a gap of $2\Delta = 280$ cm^{-1}, are for two values of the Drude damping $\gamma = 280$ cm^{-1}, a dirty superconductor, and $\gamma = 28$ cm^{-1}, a clean superconductor. The normal state conductivity is shown as a dashed line, the superconducting state (at $T = 0$) as a solid line. Similar curves for a variety of models are shown in Bickers *et al.*[128] and Nicol *et al.*[113] In the dirty superconductor a sharp feature appears at 2Δ, whereas for the clean superconductor the spectral feature is much weaker, since nearly all the Drude oscillator strength is in the superconducting delta function.

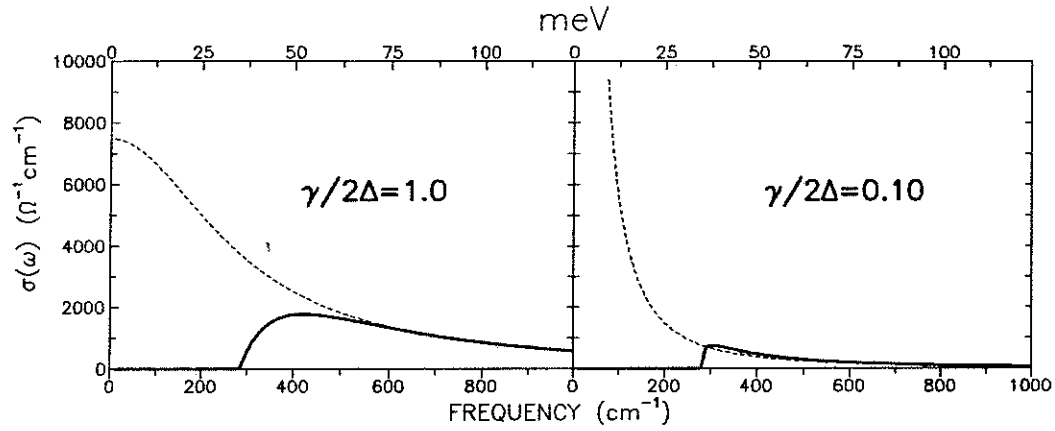

Fig. 53. The conductivity of a classical BCS superconductor in the a) dirty and b) clean limits.

The amount of conductivity that is transferred from the infrared to the delta function at zero frequency is given by:

$$\int_0^\infty [\sigma_{1n}(\omega) - \sigma_{1s}(\omega)]d\omega = 0. \tag{22}$$

It is evident from Fig. 53 that as the material becomes cleaner, *i.e.*, as the gap becomes larger in comparison to the damping rate of the carriers, more of the conductivity is transferred to zero frequency. This is the clean limit of superconductivity.

The delta function conductivity cannot be observed directly by optical techniques but the imaginary part of the conductivity, associated with the real part by Kramers-Kronig relations, has a marked effect on the optical properties. The complex conductivity due to the superfluid can be written[1]

$$\sigma(\omega) = \frac{\omega_{ps}^2}{8}\delta(\omega) + i\frac{\omega_{ps}^2}{4\pi\omega} = \frac{-i\omega[\epsilon(\omega) - 1]}{4\pi}. \tag{23}$$

This gives:

$$\epsilon_1(\omega) = 1 - \frac{\omega_{ps}^2}{\omega^2} \tag{24}$$

This quadratic frequency dependence has been checked directly against $\epsilon_1(\omega)$ obtained from the reflectance by Kramers-Kronig transformation.[15] Fig. 54 shows the results for a thin film of $YBa_2Cu_3O_{7-\delta}$ where $\epsilon_1(\omega)$ is plotted against the square of the frequency. The slope yields a plasma frequency of 9000 ± 400 cm^{-1} (1.11 eV). A fit of the low-frequency conductivity in the normal state to the Drude formula gave a *normal-state* plasma frequency of 8800 cm^{-1}. The fact that the two numbers are

almost equal means the normal-state Drude fit describes the superconducting-state conductivity well. The alternate picture, the marginal Fermi liquid model, needs an additional parameter, the energy gap, to describe the fraction of the conductivity that condenses. In both models, the conductivity sum rule guarantees that all the net spectral weight that is removed from the infrared spectrum goes to the delta function.

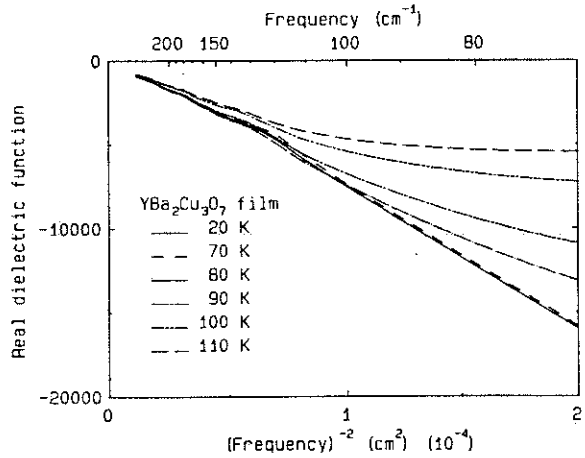

Fig. 54. The real part of the dielectric function plotted against ω^{-2}. A straight line seen in the superconducting state is a signature of the delta function response at the origin. The slope gives the penetration depth. [Ref. 15.]

The slope of ϵ_1 vs. ω^{-2} is a direct determination of the London penetration depth, λ_L which is related to the plasma frequency in the superconducting state by $\lambda_L = 1/2\pi\omega_{ps}$, with ω_{ps} in cm^{-1}. The penetration depth has been determined by a variety of techniques for the $YBa_2Cu_3O_{7-\delta}$ material, with values ranging from 1.3 to 1.4 eV. A complete summary of plasma frequency determinations for $YBa_2Cu_3O_{7-\delta}$ by various methods is given by Bozovic.[20] Some of the results are summarized in Table 3, based on Ref. 20. The μSR number is based on single-crystal work.[137]

The plasma frequency is related to the concentration of the carriers and their effective mass by $\omega_{ps}^2 = 4\pi ne^2/m^*$. Here n is the density of superconducting carriers and m^* their effective mass. A rough estimate of the density of carriers can be obtained from formal valence arguments, assuming that in $YBa_2Cu_3O_{7-\delta}$ there is one free carrier per unit cell. Using the free electron mass, we get a plasma frequency of 2.82 eV. This larger figure agrees rather well with near-infrared measurements but not with far-infrared or static measurements such as magnetization or μSR.

Table 3. Plasma frequency for the a-b-plane of $YBa_2Cu_3O_{7-\delta}$ determined in various ways.

Method	ω_p (eV)	Remarks
Far ir	1.32	Far ir oscillator models
μSR	1.41	Muon spin resonance
χ	1.32	Static magnetization
Near ir	2.93	Includes mid-ir spectral weight

Part of the difference can be accounted for by the presence of chains in this material.[78,79,19,80] Roughly half of the oscillator strength, it is argued, originates from the chains. The remaining difference can be interpreted in terms of an "optic mass" that acts, because of the interaction by carriers with some excitations, to increase their mass by having to drag along the cloud of excitations. The mass enhancement is the ratio of the squares of the low- and high-frequency plasma frequencies, *i.e.*, $(2.0/1.3)^2 = m^*/m = 2.3$. This is a rough estimate since it is difficult to determine the exact contribution of the chains to the conductivity. The procedure commonly used, subtracting σ_{1a} from σ_{1b}, assumes implicitly that the *plane* conductivity is isotropic. As discussed in Section II, the orthorhombic structure of the planes themselves suggest that this assumption may not be correct. Detailed discussion of the spectral weight distribution can be found in papers by Orenstein *et al.*[27] and Cooper *et al.*[80]

C. Temperature dependence below T_c

In addition to the purely inductive response of the superconducting condensate the excited quasiparticles can absorb energy from a finite-frequency external field. This gives rise to a peak in the dynamic low-frequency conductivity just below T_c as first shown by Palmer and Tinkham for $\sigma_1(\omega)$ in lead films.[138] This peak is, in BCS superconductors, a result of interference between Cooper pair wave functions and its observation provided early experimental support of the BCS theory. A similar coherence peak is predicted for the nuclear relaxation rate. However since the NMR peak is absent in the high T_c superconductors, it is important to examine the existence of a conductivity peak in more detail.

The frequency-dependent conductivity below T_c depends on three factors: the quasiparticle density, the BCS coherence factors, and the relaxation rate $1/\tau$.[139] The quasiparticle density and the coherence factors can be calculated from BCS theory but the relaxation rate depends on the details of the mechanism that scatters the electrons. In BCS superconductors the scattering is from impurities or phonons, with the impurity scattering dominating near T_c in many samples. This makes the scattering rate independent of the temperature. In the high temperature superconductors there is evidence that this is not the case and that the relaxation rate is dropping rapidly below T_c. We will now discuss the recent evidence for this.

The width of the Drude conductivity peak provides a direct measure of the quasiparticle relaxation rate. Although a frequency dependence of the scattering rate is expected to accompany the temperature dependent conductivity,[23] the low-frequency conductivity is approximately Drude-like.[120] Subtracting out the midinfrared conductivity, Romero *et al.*[120] have evaluated the scattering rate for low frequencies in $Bi_2Sr_2CaCu_2O_8$ and $Bi_2Sr_2CuO_6$. Fig. 55 shows the results. The top panel shows the dc resistivity measured directly with a four probe technique (solid line) and the amplitude of the Drude peak inferred from the far infrared conductivity (open squares and circles). For both materials the agreement is good.

The lower panel of Fig. 55 shows the scattering rate in cm^{-1} inferred from the Drude analysis. Both materials show, as expected, a linear relaxation rate with temperature. It is significant that both materials, the superconducting and the non-superconducting one, show the *same* slope, in other words the same coupling constant λ, despite their huge difference in T_c (the T_c of the $Bi_2Sr_2CuO_6$ may be 0 K). It is clear that the scattering rate is an intrinsic property of the copper oxygen planes. (Note that the higher T_c of the two-plane material could be a result of the much larger carrier density.)

The most striking feature of Fig. 55 is the rapid drop in scattering rate below T_c for the superconducting material. Whereas the non-superconductor seems to continue the linear decrease to low temperature, with a sign of saturation below 50 K, by 60 K the $1/\tau$ of the superconductor has dropped by an order of magnitude from the normal state (100 K) value.

This important result suggests that as the superconducting gap opens up at T_c the process that is responsible for the T-linear resistivity is suppressed. This is quite unlike phonon scattering of normal superconductors. To first order nothing happens to the phonons as the material becomes superconducting and one would expect the

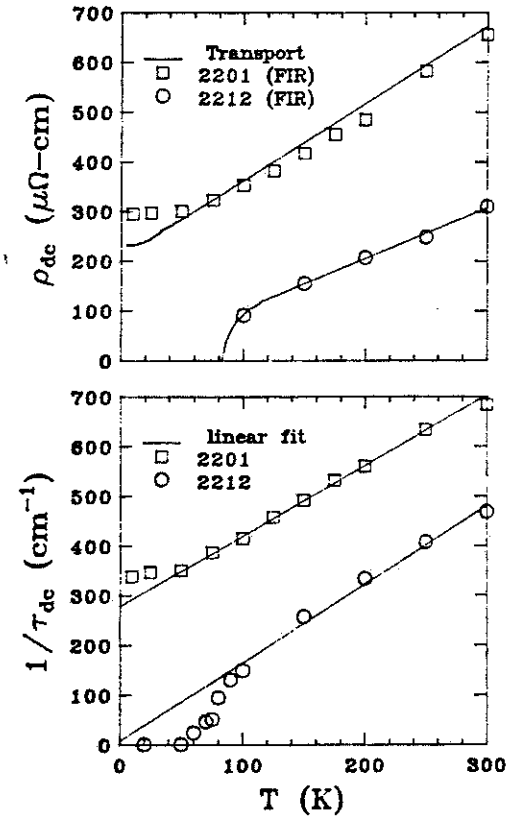

Fig. 55. Top: Comparison of the dc resistivity from Drude parameters based on far infrared transmission with transport measurements. Bottom: Temperature dependence of the quasiparticle relaxation rate. The scattering rate is linear with temperature in the non superconducting $Bi_2Sr_2CuO_6$but drops rapidly below T_c in $Bi_2Sr_2CaCu_2O_8$. [Ref. 120.]

quasiparticle lifetime not to change dramatically at T_c. Detailed calculations show that in BCS strong-coupling superconductors, such as lead, the scattering rate actually increases for a range of temperatures just below T_c.[139] The rapid suppression of the quasiparticle scattering rate at T_c is a unique property of high T_c superconductors.

Recent microwave surface impedance measurements, while not a direct measurement of $1/\tau$, have also been interpreted in terms of the collapse of carrier scattering at T_c.[140,141] The work of Bonn *et al.*[141] shows, for a high quality single crystal of $YBa_2Cu_3O_{7-\delta}$, a dramatic increase of microwave conductivity below T_c. It is interpreted in terms of a gap developing in the spectrum of excitations responsible for the large normal state resistivity of $YBa_2Cu_3O_{7-\delta}$.

A gap in the spectrum of excitations that couple the charge carriers suggests that these excitations are electronic in nature and may in fact be the charge carriers themselves. This suggestion has been made early in the field of high temperature

superconductivity by Anderson[109] and more recently by Varma and Littlewood in the context of the marginal Fermi liquid. There is no doubt that these recent results support the idea of electronic mechanisms of interaction between the charge carriers on the copper oxide planes.

D. The optical conductivity in the superconducting state

The question of the existence of a gap in the optical conductivity has been at the center of debate among the various experimental groups almost from the start of the high T_c field. In this Section we will focus on the structure in the optical conductivity in the superconducting state, structure that has been associated with the superconducting gap.

We will set aside the early gap identifications based on ceramics and on temperature-dependent features of reflectance. The ceramic work is difficult to interpret since it represents a mixture of a-b-plane and c-axis response. Work on single crystals and oriented films has shown that that the far-infrared response is dramatically different in the two directions, parallel to the planes and normal to the planes.[44,73,142,134,33] Thus attention has shifted to single crystals and oriented films and we will focus on these.

Similarly the interpretation of raw reflectance data is difficult. The striking changes in reflectance that occur when the materials become superconducting are a result of changes in both the real and imaginary parts of the dielectric function. The shift of oscillator strength from the far-infrared response of the charge carriers to the condensate delta function changes the dielectric function dramatically. (This statement is true independent of whether the low-frequency response is due to free carriers, to some sort of marginal Fermi liquid, or to other exotic behavior. In the normal state, there is broadening of the zero-frequency peak in $\sigma_1(\omega)$ due to interaction with some spectrum of excitations as well as due to elastic scattering from impurities and the surface. In the superconducting state, the charge carriers that are in the condensate no longer scatter, and the zero-frequency conductivity is a true delta function.) A simple superconductor, one where there is a true gap in the conductivity, has unit reflectance up to the gap followed by a region of absorption. In the high T_c materials the unit reflectance region is usually not present. To get a more complete picture of the low-frequency response we turn to a Kramers-Kronig analysis of the reflectance and examine the optical conductivity.

There are problems with Kramers-Kronig analysis of reflectance that are unique to superconductors. These arise from the assumptions, always necessary in evaluating the Kramers-Kronig integrals, of the analytical extension of the data at low frequency. One approach is to use some physically reasonable model of the low-frequency response and assume that the data will follow this behavior in the region where there are no measurements. Because of the exotic nature of the conductivity it is not obvious what form the low-frequency conductivity takes in the superconducting state. We will summarize some of the possible models for the electromagnetic response of conductors at low frequencies.

The various assumptions that have been made about the low-frequency behavior include:

1. The Drude assumption: In ordinary metals below a certain frequency the Hagen-Rubens law for reflectivity holds:

$$\mathcal{R} \approx 1 - \sqrt{\frac{8\omega}{\omega_p^2 \tau}}. \tag{25}$$

   where τ is a constant relaxation time. This is equivalent to assuming that the low-frequency conductivity is Drude-like. In cases where the dc conductivity has been measured for the sample and is found to agree with the Drude low-frequency value, *i.e.*, $\sigma_{dc} = \omega_p^2 \tau / 4\pi$, this can be justified. The procedure is obviously not valid in the superconducting state, where the dc conductivity is infinite, but it can often be used in the normal state.

2. The assumption of a gap: If the data show an approach to unit reflectance, one can *assume* that a gap in the conductivity exists and set the reflectance equal to unity below the apparent gap frequency. The Kramers-Kronig transforms will then yield zero conductivity below the gap frequency. Many experimental curves have been treated this way. A gap in the conductivity spectrum obtained by Kramers-Kronig analysis usually means that the author assumed unit reflectance for that region.

3. Power-law behavior: Since many superconducting samples show finite but decreasing absorption to the lowest frequencies, one can assume a power law absorption. The Hagen-Rubens expression of $(1 - \mathcal{R}) \propto \sqrt{\omega}$ is a special case. Other possibilities include:

i) Marginal-Fermi-liquid conductivity. Here one assumes that the scattering rate is linear in frequency. It can be shown that the reflectance will have the following approximate form[111]

$$\mathcal{R} = 1 - 4\sqrt{\pi\lambda\omega(\omega + \pi T)/\omega_p^2}.$$

For low temperatures and high frequencies $\pi T \ll \omega$ the formula simplifies to $(1 - \mathcal{R}) \propto \omega$.

ii) Two-fluid conductivity. If one assumes that there are normal Drude carriers embedded in the superconductor, one can show[108] that $(1 - \mathcal{R}) \propto \omega^2$.

iii) Two-fluid conductivity with embedded Lorentz oscillators. In this case it is easy to show that $(1 - \mathcal{R}) \propto \omega^4$

The optical conductivity of a series of high T_c materials in the superconducting state is shown in Fig. 56. All curves are for the *a-b* orientation. All show structure in the phonon region of the spectrum, structure that has been attributed to phonons and discussed in detail in Section VI. Here we are concerned with the existence of a gap in the conductivity, that is, a region of zero conductivity below a certain frequency.

We will examine the evidence for a gap in the various materials in turn. In reviewing the data one should note some of the experimental difficulties. First, at low frequency, in the 50–300 cm^{-1} region, where the gap is expected to lie, most infrared sources are weak. Combined with the small single-crystal samples, this weak intensity makes the signal-to-noise ratio poor. Secondly, diffraction effects from the edges of the sample become more important as the frequency is lowered. In the face of these problems, it is difficult to distinguish between unit reflectance and 99.5% reflectance, a typical value for a good sample at low temperature.

Some of the techniques used to overcome the experimental problems have included *in situ* evaporation of metallic overlayers[12] to correct for the roughness of the surface, the use of large thin films on polished single crystal surfaces,[15,14,22] the measurement of transmission,[143,31,61] or the measurement of direct absorption.[108,144] Of the various techniques, direct absorption is most relevant to the gap question since the signal produced is directly proportional to the quantity $1 - \mathcal{R}$ eliminating the need for the accurate measurement of $\mathcal{R}$. The drawback of the technique is the restriction to a narrow, fixed temperature range to accommodate the characteristics of the sensitive bolometers that are used.

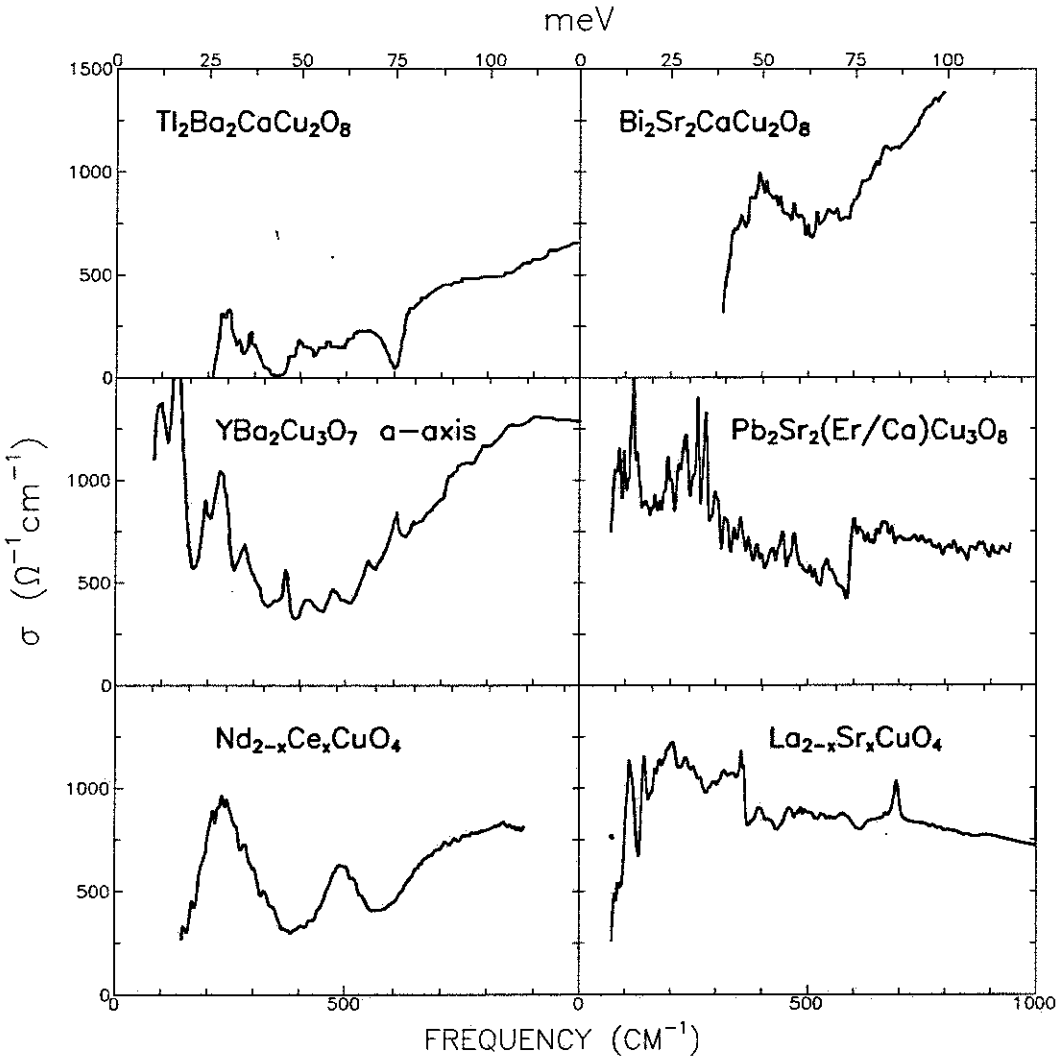

Fig. 56. The optical conductivity of six high T_c superconductors in the superconducting state.

1. $YBa_2Cu_3O_{7-\delta}$

a. The 150 and 450 cm^{-1} structures

The optical conductivity of this material has received the most attention. The first single crystal conductivity results were from Thomas *et al.*,[11] who found a region of depressed conductivity at low frequency and a gap-like onset of absorption in the 150 cm^{-1} region in several oxygen-deficient materials with a lowered T_c. Within the experimental 1% accuracy, the reflectance was unity up to this frequency. The value of the absorption onset was of the order of 3–4 k_BT_c and the feature was interpreted as the superconducting gap.

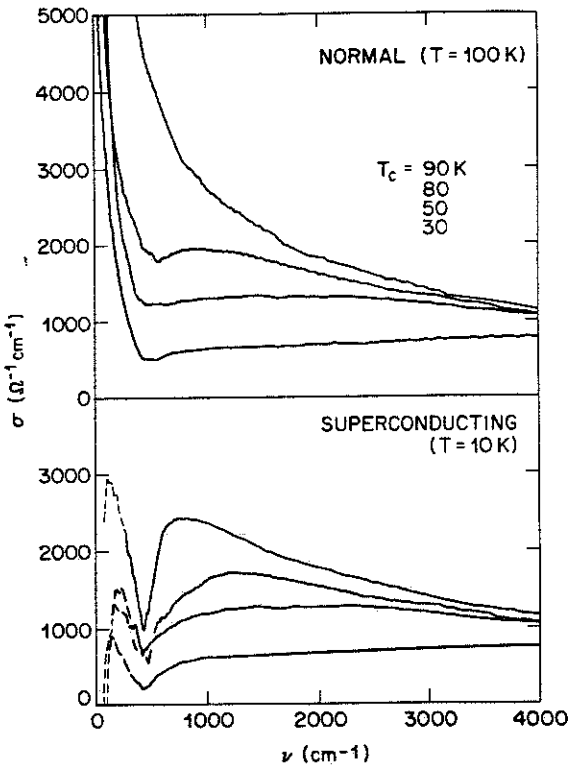

Fig. 57. The optical conductivity of four $YBa_2Cu_3O_{7-\delta}$ crystals with, starting from the top curve, T_c=90, 80, 50, and 30 K. The notch at 400 cm^{-1} and the onset at 150 cm^{-1} do not vary with T_c. [Ref. 27.]

This gap-like onset of conductivity at 150 cm^{-1} persisted in the fully oxygenated 90 K material as shown in Fig. 57 along with reduced T_c crystals.[27] The curves for the conductivity are very similar to those first shown by Thomas *et al.*[11] on oxygen deficient samples with strong absorption down to 150 cm^{-1}. In the 90 K material, $3.5k_BT_c = 221 cm^{-1}$ so the absorption extends well into the region where the energy gap is expected to be. Another striking feature of Fig. 57 is the notch at 450 cm^{-1} that does not change in frequency when the T_c is changed from 90 K to 30 K.

These observations, along with the earlier discovery of Reedyk *et al.*[55] in $Bi_2Sr_2CaCu_2O_8$ and Kamarás *et al.*[15] in $YBa_2Cu_3O_{7-\delta}$ that the infrared features persist well above T_c cast doubt on the identification of the 150 cm^{-1} onset as the superconducting gap.

b. Untwinned crystals

Midinfrared measurements on untwinned crystals were discussed in detail in Section II. Such measurements are more difficult in the far infrared because of the small size of the available crystals. Nevertheless several groups have presented results that

are relevant to the gap question. The first were the reflectance measurements of Schlesinger *et al.*[19] on mechanically detwinned material. The authors found that the absorption in the far infrared was stronger with radiation polarized in the b direction, along the chains, than in the a direction, normal to the chains. It was argued that transitions having a dipole moment parallel to the chains gave rise to the additional absorption.

To within the accuracy of the experiments (0.5%), for light polarized perpendicular to the chains, no absorption was found below 500 cm^{-1}, the same frequency that the "knee" in the reflectance spectra is observed in a variety of samples.[25] With the assumption of unit reflectance, Kramers-Kronig analysis showed $\sigma_1(\omega) = 0$ below 500 cm^{-1}. Schlesinger *et al.* took this as definitive evidence for a gap value of $8k_BT_c$ in $YBa_2Cu_3O_{7-\delta}$.

Recent direct absorption (bolometric) measurements by Pham *et al.*[144] on detwinned samples of $YBa_2Cu_3O_{7-\delta}$ throw serious doubt on this work. The experimental method is capable of yielding data more than an order of magnitude more accurate than the reflectance technique for highly reflecting samples in the infrared at low temperatures. The absolute absorption accuracy is 20% and the uncertainty in the zero of the absorption (*i.e.*, unit reflectance) is 0.02%, as opposed to the reflectance technique of Schlesinger *et al.* where 0.5% error is reported.

Pham *et al.*[144] find that the absorptivity, $1 - \mathcal{R}$, is finite for both polarizations down to their low frequency limit of 80 cm^{-1}. The absorption for $E \parallel b$ increases strongly in the far infrared, reaching ~3% at 300 cm^{-1}. The absorption for $E \parallel a$ was smaller but was definitely nonzero; over 140–400 cm^{-1} it is ~0.4%, rising slightly with increasing frequency. The absorption increases strongly above 500 cm^{-1}. The difference between zero absorption and 0.4% absorption has a dramatic effect on the conductivity returned by Kramers-Kronig analysis.

Fig. 58 shows the resulting optical conductivity for the a-direction of a single domain $YBa_2Cu_3O_{7-\delta}$ crystal. Instead of a gap, the data show a minimum of conductivity at 400 cm^{-1} and a rise toward lower frequencies. Superimposed on this smooth variation are sharp peaks, some of which can be attributed to optic phonons seen in the a-b polarization in the insulating parent compound. The low-frequency structure is reproducible but too strong to be due to ordinary optical phonons. While there are zone center phonons in this region, their contribution to the conductivity is small since the total phonon absorption is constrained by a sum rule involving ion masses.[144]

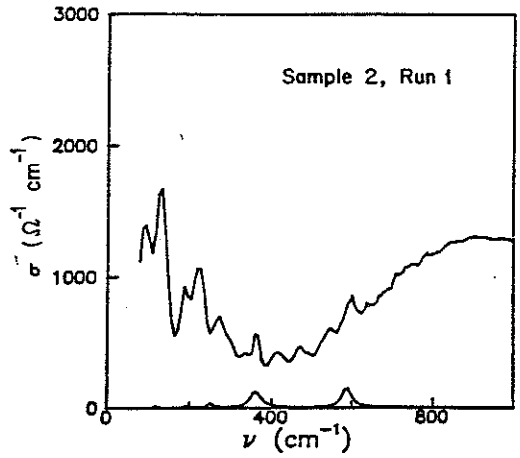

Fig. 58. Optical conductivity of a detwinned $YBa_2Cu_3O_{7-\delta}$ crystal in the a direction showing the absence of a true superconducting gap. Also shown is the calculated contribution of phonons polarized in the a-b plane. It appears that while some of the high-frequency structure can be attributed to ordinary phonons, that at low frequency $\sigma_1(\omega)$ is too strong. There is no evidence of a gap in the conductivity in this work. [Ref. 144.]

c. The c-axis conductivity

A discussion of the superconducting response of the $YBa_2Cu_3O_{7-\delta}$ material would not be complete without a discussion of the more difficult c-axis polarized measurements.[73,142] First measured by Collins *et al.* on a mosaic and subsequently by Koch *et al.* on a single crystal, the c-axis response is very similar to that of ceramic pellets. Phonons dominate the reflectance and the conductivity which are shown in Fig. 59 from Koch *et al.*[142] As in ceramic pellets, a plasma edge appears at low frequency where ϵ_1 crosses zero.[65,145] This phenomenon is responsible for the sharp reflectance edge at 80 cm^{-1}.

There appears to be depressed conductivity in the c-direction in the superconducting state below 250 cm^{-1}. If this is indeed the superconducting gap it appears to be smeared over a region of 200 to 250 cm^{-1}. More work needs to be done on a variety of samples to establish this as the superconducting gap. In particular one has to establish whether the conductivity seen in the c-direction of some 70 Ω^{-1}cm^{-1} is intrinsic. There is controversy about the dc resistivity in the c-direction; both metallic and insulating behavior has been reported. There is one report of c-axis optical conductivity in a depressed-T_c $GdBa_2Cu_3O_x$ crystal where *only* phonons are seen, with no free-carrier absorption at all.[146]

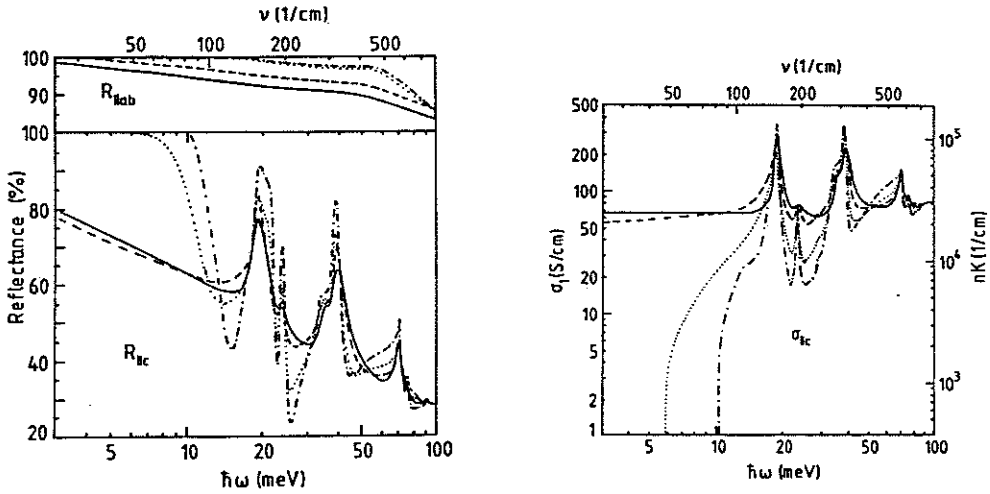

Fig. 59. Reflectance (left panel) and optical conductivity (right panel) of $YBa_2Cu_3O_{7-\delta}$ from Koch *et al.* for light polarized in the *c*-direction. In the normal state the spectrum is dominated by phonons while in the superconducting state a plasma edge at 80 cm^{-1} dominates the spectrum. There appears to be depressed conductivity up to 250 cm^{-1}. Solid curves 300 K, long dashes 110 K, dots 60 K, and dot-dash 10K. Note the logarithmic conductivity scale. [Ref. 142.]

2. $Bi_2Sr_2CaCu_2O_8$

In comparison to $YBa_2Cu_3O_{7-\delta}$ the low temperature infrared properties of other high-temperature superconductors have received less attention. $Bi_2Sr_2CaCu_2O_8$ has been studied both in reflectance[55,147,59,148,56] and in transmission.[143,31,61] We will discuss the reflectance work first and then turn to the transmission technique.

Reedyk *et al.*[55] found evidence of a gap in the conductivity, but this was a gap that was also present in the normal state. The reflectance was unity to within experimental error up to 300 cm^{-1} in the superconducting state. In the normal state, below 300 cm^{-1}, there was a narrow Drude like absorption followed by a "knee" at 300 cm^{-1}, at which point the absorption increased steeply. It was clear that the gap associated with the 300 cm^{-1} feature was unusual, since it persisted above the superconducting transition temperature.

The reflectance data are shown in Fig. 52 and the conductivity in Fig. 56. The conductivity shows an onset in the 250 cm^{-1} region followed by a shallow minimum at 500 cm^{-1}. A comparison with the $YBa_2Cu_3O_{7-\delta}$ curves shows that the structure is similar, but $Bi_2Sr_2CaCu_2O_8$, the material with the lower T_c, has structure at *higher* frequency. This of course is opposite of what one expects from a superconducting

gap. These results were confirmed recently by Kamarás *et al.*[56] on several samples over a wider range of frequencies.

Far-infrared transmission spectra have not been as popular a means of exploring the low-lying states as reflectance. BCS dirty limit calculations suggest that if the ratio of the film transmission in the superconducting state to the normal state (at the same temperature) is plotted, a peak occurs at the energy gap. In the clean limit this peak becomes weaker but sharper.[143]

In theory the transmission technique yields the same kind of information as Kramers-Kronig transformed reflectance, but there are practical problems finding infrared transparent substrates that are also suitable for thin film growth. The first measurements of transmittance were at high frequency on magnetron sputtered films of $YBa_2Cu_3O_{7-\delta}$ on $SrTiO_3$ by Bozovic *et al.*.[123] The first low-frequency measurements relevant to the gap question were by Hughes *et al.*[143] on magnetron sputtered films of $Bi_2Sr_2CaCu_2O_8$ on an infrared-transparent MgO substrate.

In order to get adequate transmission, Hughes *et al.* had to use films only a few hundred Å thick. Since MgO is not an ideal substrate for epitaxial growth, and the first few layers next to the substrate are of poor quality, the films did not show ideal superconducting behavior (zero transmission, extrapolated to zero frequency). The authors concluded that any superconducting gap had to be at frequencies in excess of 300 cm^{-1}, beyond the frequency of transparency of MgO. Gao *et al.*[32] reached similar conclusions from transmission studies of $YBa_2Cu_3O_{7-\delta}$ on MgO substrates.

The most recent transmission work by Forro *et al.*[31] and Romero *et al.*[61] was on high-quality single crystal flakes of $Bi_2Sr_2CaCu_2O_8$. The flakes are several penetration depths thick, so accurate transmission spectra required the high brightness infrared beam line of the Brookhaven Synchrotron Light Source.

Because they used free-standing films, Forro *et al.* were able to extend their measurements to 600 cm^{-1} and search for the predicted BCS dirty limit peak at 2Δ in the range from $1.5k_BT_c$ to $12k_BT_c$. They found no indication of the peak, even allowing for the scattering rate of 50 cm^{-1} which would make $2\Delta/\tau = 0.125$ at 400 cm^{-1} and place the sample in the clean limit. More recently Romero *et al.*[61] extended the measurements on free standing films to 3000 cm^{-1}, and did see a broad peak centered on 700 cm^{-1} ($12k_BT_c$), and suggested it could be interpreted as the 4Δ peak of the marginal Fermi liquid theory.[111,113]

However, they point out that in the $YBa_2Cu_3O_{7-\delta}$ material, where the optical constants are known, a calculated transmission also yields a peak in the 500–600 cm^{-1} range, associated with the "knee" and minimum in the reflectance. As discussed in Section II, this feature is most easily understood as resulting from a passband between two absorption bands, one at zero frequency and one in the midinfrared, with the feature becoming visible as the free carriers condense below T_c. If, in contrast, the 500 cm^{-1} "knee" in $YBa_2Cu_3O_{7-\delta}$ is a superconducting gap, then by the same token the 700 cm^{-1} feature in $Bi_2Sr_2CaCu_2O_8$ is a gap too. It should be clear that the transmittance and the reflectance measurements yield the same information: in both materials there is a steplike onset-feature in the frequency-dependent conductivity. In the transmission ratio this feature becomes a shoulder or peak; in reflection it yields a knee followed by a minimum at somewhat higher frequencies. Neither a peak in the transmission ratio nor a knee in reflectance are unambiguous markers of a superconducting gap in complex systems.

3. Other materials

A complete low-temperature reflectance study of $Tl_2Ba_2CaCu_2O_8$ was presented by Foster *et al.*[30] on laser-ablated *c*-axis oriented films on $LaAlO_3$ substrates. The films are of high quality with T_c between 98 and 100 K. The authors report no evidence of a superconducting gap but considerable structure in the phonon region, Fig. 52 shows the reflectance and Fig. 15 in Section II shows the conductivity in the superconducting state.

The reflectance curve is similar to that of other high T_c materials, with a pronounced knee at 600 cm^{-1}. This feature remains in the normal state up to room temperature. A Kramers-Kronig transform of the reflectance in Fig. 56 shows a remaining conductivity in the superconducting state that is lower than other high T_c materials, with a gap-like onset in the 200 cm^{-1} region. This material is unique in having very deep phonon minima, at 350 cm^{-1} and 600 cm^{-1}, somewhat similar to $Bi_2Sr_2CaCu_2O_8$.

The inset in Fig. 15 shows that the structures seen in the superconducting-state conductivity are already present in the normal state and are essentially unchanged at T_c. Foster *et al.* conclude that the onset of finite $\sigma_1(\omega)$ is unrelated to 2Δ.

The low-temperature spectrum of single-crystal $Pb_2Sr_2(Er/Ca)Cu_3O_8$, has been studied by Reedyk *et al.*[149] The conductivity is characterized by several sharp minima near the frequencies of Raman active phonons in the 400 - 600 cm^{-1} region. At lower frequency several of the sharp lines are due to direct absorption by phonons. The

overall midinfrared conductivity is similar to that of other high T_c superconductors and there is no evidence of the energy gap. Nearly all of the fine structure can be seen in the normal state. The reflectance is shown in Fig. 52 and the conductivity in Fig. 56.

Two superconductors with a low transition temperature are included in Fig. 52 and in Fig. 56. $Nd_{2-x}Ce_xCuO_4$ is a material in which the transport carriers may be electrons, so that it might be expected to have properties differing from the hole-doped cuprates. The spectrum shown is on a laser-ablated epitaxial film of high quality grown by Hughes *et al.*[150] Surprisingly, despite the differences, the low T_c, the electron doping, and the different structure near the copper plane, the absorption in the superconducting state is very similar to the other cuprates, resembling that of $Tl_2Ba_2CaCu_2O_8$ perhaps most closely. Both materials (along with $Bi_2Sr_2CaCu_2O_8$) show a strong coupling of the 600 cm^{-1} phonon to the electronic continuum state, in contrast to $YBa_2Cu_3O_{7-\delta}$ where the sensitive measurements of Pham *et al.*[144] show that this phonon appears in absorption like an ordinary optic phonon.

The last curve shown in Fig. 52 and 56 shows preliminary results[151] for a film of $La_{2-x}Sr_xCuO_4$. The material has optic phonons at 400 cm^{-1} and 700 cm^{-1}. The conductivity shows that the higher frequency mode is directly coupled to the radiation field, whereas the lower mode seems to have a Fano shape, a sign of electron-phonon coupling. As in the other systems, the reflectance approaches unity in the 100 cm^{-1} region, which transforms to a gap at the same frequency. Whether this is a superconducting gap cannot be decided at this stage, since more work needs to be done. It may well turn out to be possible to see a gap in the lower T_c materials for which the coherence lengths are longer, making it possible to approach the dirty limit with defect scattering, without destroying superconductivity.

E. Is there a gap in the conductivity?

From Fig. 56 it is apparent that there is no gap in the optical conductivity in the six high T_c materials for which low-temperature a-b-plane data are available. There is absorption down to the lowest frequency. Below 100 cm^{-1} the experiments rapidly lose their accuracy. Furthermore, most of the structure that is seen is present in the normal state and is, as we will suggest in the next Section, associated with phonons. The low-temperature optical conductivity in the 200–600 cm^{-1} region seems to be associated with the midinfrared band and does not seem to participate in the superconducting transition. It is still legitimate to ask if there is a gap in the overall

conductivity at lower frequency, below 200 cm^{-1} where the accuracy of the infrared work is low.

The most accurate measurements are the bolometric work of Pham *et al.*[108,144] and the thin film work of Kamarás *et al.*[15] and Schützmann, *et al.*[14] and Renk *et al.*[76] as well as the transmission work of Forro *et al.*[31] and of Romero *et al.*[61,62,120] With respect to the issue of the gap, the work falls into two groups. In some experiments (particularly in thin films) there is evidence for a break in the reflectance at 150 cm^{-1} and a constant reflectance below this frequency. If this is indeed an approach to a unit reflectance, there is a gap in these materials at 150 cm^{-1}. In other measurements the reflectance approaches unity with a power law and the authors conclude that there is no evidence of a gap.

There is reason to believe that the power-law absorption persists to lower frequency. It is well known that microwave surface impedance is consistent with an ω^2 dependence of the loss and the magnitude of the effect is consistent with bolometric far infrared absorption on the same samples.[152,74]

VI. THE ELECTRON-PHONON INTERACTION

In this Section we discuss the evidence for an electron-phonon interaction of an unusual kind in the high temperature superconductors. The electron-phonon interaction in these materials has many unusual features. For example, the dc resistance above T_c is essentially T-linear, suggesting that the charge carriers are scattered by some sort of thermally accessible excitation, like the phonons. As we have seen in Section IV (see Table 2) a weak-coupling value of $\lambda \sim 0.3$ is found for the strength of the interaction between charge carriers and thermal excitations.

Electron-phonon scattering is a natural explanation of this resistivity. Contradictions arise, however, when the data are examined in detail. First, the low-T resistivity is also quite linear, in some cases down to 20 K or so.[67] (In ordinary metals, the T-linear resistivity is a high-T phenomenon, with T^5 or T^3 behavior observed below the Debye temperature.) Second, the oxide superconductors have a large number of Einstein-like optical phonon branches at energies Ω of 150–1000 K, which should contribute to $1/\tau$ once $k_B T \simeq \hbar\Omega$. In contrast to this expectation, the resistivity remains linear up to nearly 1000 K, implying that the scattering of the free carriers is *completely unaffected* by these optical branches. This occurs despite the observation by Raman scattering of Fano-type line shapes[129,153] and frequency shifts at T_c[154]

implying strong coupling of the Raman-active modes to an underlying electronic continuum. For example Thomsen *et al.*[155] find a coupling constant to certain phonons with $\lambda = 0.6$ by analyzing Raman shifts on entry to the superconducting state.

A. Evidence from neutron scattering

The introduction of charge carriers is known to have considerable impact on the phonons. Neutron time-of-flight measurements,[156] which compare the phonon density of states of superconducting (metallic) samples with non-superconducting (insulating) ones, show pronounced enhancements in the 20 and 50 meV regions for the superconducting samples. An example is shown in the upper panel of Fig. 60, which compares superconducting $YBa_2Cu_3O_{7-\delta}$ with semi-insulating $Y_{1-x}Pr_xBa_2Cu_3O_{7-\delta}$. The bottom panel shows the difference between the superconducting and non-superconducting spectra. There are strong enhancements in the phonons in two energy regions, both believed to correspond to Cu-O bond motion. (A similar conclusion is reached when comparing the spectra of $YBa_2Cu_3O_7$ and $YBa_2Cu_3O_6$.[107])

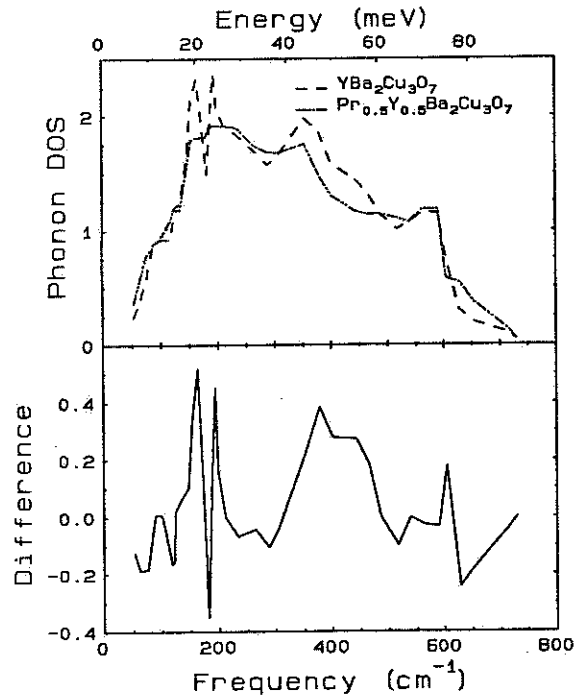

Fig. 60. The upper panel shows the phonon density of states for $YBa_2Cu_3O_{7-\delta}$ and $Y_{1-x}Pr_xBa_2Cu_3O_{7-\delta}$, as measured by Renker *et al.*[156] while the lower panel shows the difference between the two curves.

Phonon dispersion measurements[157] indicate a branch in the 50 meV region near the zone boundary which has anomalous behavior, attributed to the electron-phonon interaction. This mode is assigned to a "half-breathing mode" in which the oxygens in the x direction are moving in and out in alternate cells while the ones in the y direction are at rest. There is movement of the apical oxygen (O4) as well. The actual breathing mode is higher in frequency. The structure in the 20 meV region may be due to an anomalous splitting between the scissor modes of the planar oxygens in the two planes. (This mode makes the oxygen square into a parallelogram.) Additional effects are seen in neutron measurements of the kinetic energy of the Cu atoms, which changes considerably on entry into the superconducting state.[158]

B. Electron-molecular vibration coupling

With the above as background, we can now consider the effect of electron-phonon interactions on the infrared spectra.[159,107] The type of electron-phonon interaction considered is well-known in organic conductors but less common in other systems. In the organics, as first pointed out by Rice,[104,160–162] linear coupling of charge carriers to totally symmetric (A_g) phonons can lead to structure in the conductivity spectrum at the phonon frequencies. In this "charged phonon" mechanism or electon-molecular vibration coupling effect, the electron energies depend on the bond lengths, while at the same time the bond lengths depend on the local charge density. Infrared radiation at the A_g phonon frequencies can pump charge over long distances, giving rise to absorption that has electronic oscillator strength and that is polarized in the direction of easy electronic motion. This direction is in the quasi-one-dimensional stacking axis in the organics and in the a-b-plane in the Cu-O superconductors. When the electronic continuum overlies the phonon frequencies, characteristic Fano lineshape antiresonances occur in the continuum spectrum.

As an example, Fig. 61 shows the optical conductivity[163] of a quasi-one-dimensional organic conductor based on tetracyanoquinodimethane (TCNQ), trimethylammonium-iodide-TCNQ. This ternary compound[164] has a weakly metallic dc conductivity along the TCNQ stacking axis. Indentations in the optical conductivity can be seen at many of the A_g phonon frequencies of the TCNQ molecule on account of the interaction between charge motion and the vibrations.

In the high temperature superconductors, similar effects can lead to the reflectance "shoulders" at $\sim$ 150 and 440 cm^{-1} (19 and 55 meV). In $\sigma_1(\omega)$ they show up as an onset at the lower energy and a "notch" at the higher energy. This structure

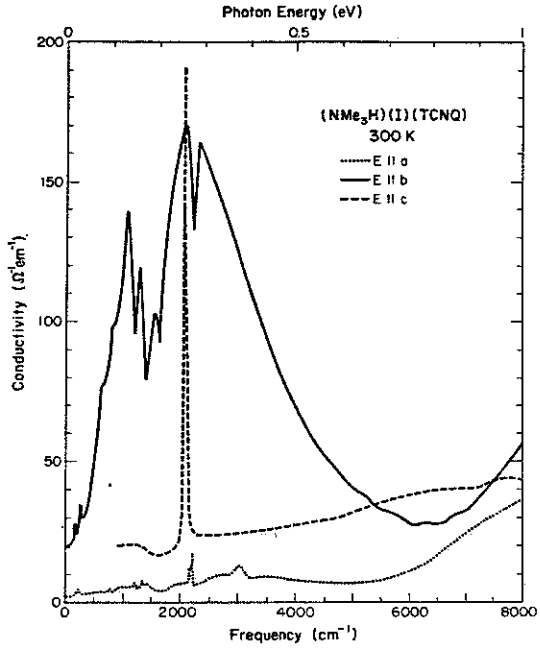

Fig. 61. Optical conductivity of trimethylammonium-iodide-TCNQ for three principal directions. The b-axis is the most conducting, with σ_{dc}~20 Ω^{-1}cm^{-1}. [Ref. 163.]

is illustrated for $YBa_2Cu_3O_{7-\delta}$ in Fig. 39, which shows data of Kamarás *et al.*[15], Fig. 57, from Orenstein *et al.*[27], and Fig. 58, which shows the single-domain results of Pham *et al.*[144] The conductivity has a broad band, with an apparent onset around 150 cm^{-1} and a clear notch-like minimum at 440 cm^{-1}.

The $Pb_2Sr_2LCu_3O_8$ series of compounds studied by Reedyk *et al.*[70] illustrate the difference between conventional phonon absorption and the electronically coupled charged phonon mechanism. Fig. 62 shows the optical conductivity of a sequence in the series from the insulating Pr doped material towards more metallic Er/Ca doped material. With increased metallicity the dc conductivity, shown as points on the conductivity axis, rises along with the far infrared conductivity. The behavior of the phonon lines is striking.

A typical optic phonon, for example the peak at 352 cm^{-1}, appears as a conductivity peak in the insulating material. At low doping levels the area under the peak not affected. But as the background conductivity rises above 600 cm^{-1}, the mode loses its oscillator strength, *i.e.*, the LO-TO splitting goes to zero due to screening. Different optic modes respond differently: for example the 304 cm^{-1} line survives up to the Er/Ca member whereas the 281 cm^{-1} line is noticeably weakened already for the Eu member.

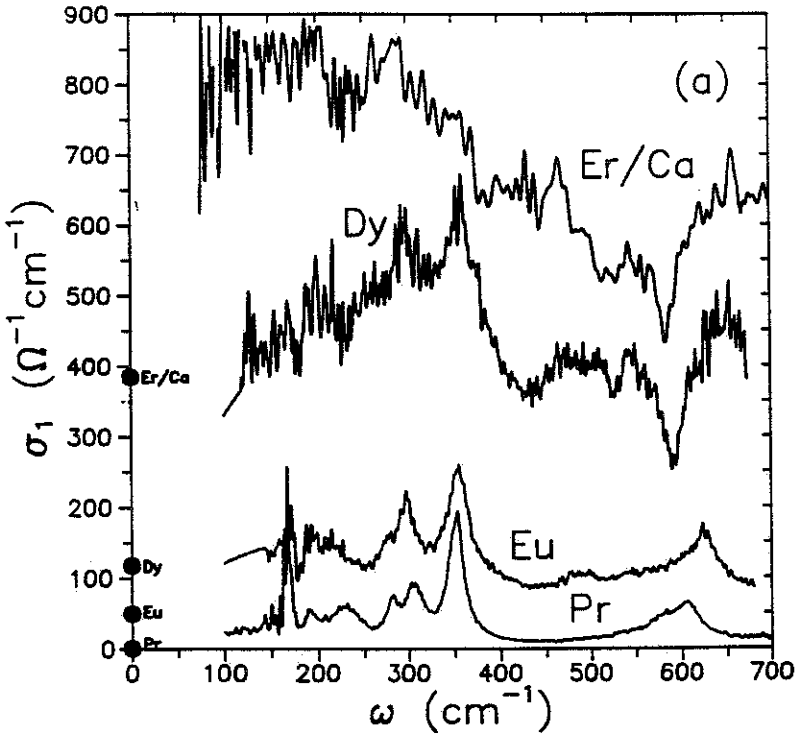

Fig. 62. Optical conductivity of $Pb_2Sr_2LCu_3O_8$ series of compounds where L is a lanthanide. Moving from the Pr doped material to the smaller rare earths the materials become more metallic and while the optic phonons such as the one at 352 cm^{-1} weaken, the electronically induced structure grows, for example the minimum at 585 cm^{-1}

Contrast the reduction of the optic phonon strength with growth, under the same conditions, of the three *minima* at 437, 525 and 585 cm^{-1}. Not visible in the insulating Pr doped materials, these lines grow in depth with doping. As Fig. 56 shows several other high T_c materials show these minima, particularly one near 595 cm^{-1}.

More examples of this type of behavior are shown in Fig. 56, where the optical conductivities in the phonon region for six different high T_c systems are shown. Note the sharp notch at the 595 cm^{-1} oxygen mode in $Tl_2Ba_2CaCu_2O_8$ for example.

C. The charged phonon model

The charged-phonon mechanism leads to the following dielectric function:

$$\epsilon(\omega) = \epsilon_\infty + \cdots + \frac{4\pi\chi_e(\omega)}{1 - D_0(\omega)\chi_e(\omega)/\chi_0}, \tag{26}$$

where ϵ_∞ is the high frequency dielectric constant, $\cdots$ represents other contributions (interband transitions, ordinary optical phonons, and non-interacting free carriers,

for example), and the last term is the effect of the charged phonons. In it, χ_e is the electronic susceptibility of the carriers in the absence of coupling, χ_0 is the zero-frequency susceptibility, and D_0 is the phonon propagator:

$$D_0(\omega) = \sum_\alpha \frac{\lambda_\alpha \omega_\alpha^2}{\omega_\alpha^2 - \omega^2 - i\omega\gamma_\alpha}, \tag{27}$$

with λ_α the dimensionless electron-phonon coupling constant, ω_α the unperturbed frequency, and γ_α the width of the α^{th} phonon mode. The total dimensionless electron-phonon coupling constant is $\lambda = \sum_\alpha \lambda_\alpha$ and the usual electron-phonon coupling function $\alpha^2F(\omega)$ is related to D_0 by

$$\alpha^2F(\omega) = \pi^{-1} \operatorname{Im} D_0(\omega).$$

D. Model calculation

Fig. 63 shows the application of this model to the 20 K midinfrared conductivity of Kamarás *et al.*,[15] shown in the upper panel. The middle panel shows $\sigma_1(\omega)$, calculated using the $\alpha^2F(\omega)$ in the lower panel. In making this calculation, χ_e for the carriers which interact with the phonons was taken as a Drude spectrum, with a plasma frequency of $\omega_p = 14,000$ cm^{-1} (1.7 eV) and a scattering rate of $1/\tau = 1500$ cm^{-1} (0.2 eV), intended as parameters characterizing the midinfrared conductivity of $YBa_2Cu_3O_{7-\delta}$. The $\alpha^2F(\omega)$ was chosen to resemble the difference spectrum in the bottom panel of Fig. 60 with the idea that the phonons which are strongly affected by the presence of charge carriers are those which interact with the carriers. The model $\alpha^2F(\omega)$ has two maxima, a narrow one at 150 cm^{-1} (20 meV) and a broader, more intense one at 440 cm^{-1} (55 meV). These two modes have coupling constants of 0.3 and 0.6, respectively, leading to a moderately strong-coupling value of $\lambda = 0.9$.

The dashed line in the center panel of Fig. 63 is the Drude spectrum, with no coupling to the phonons. When the coupling is included, the solid line results. The interaction with the phonons results in an antiresonance at the the frequency of the upper mode and a near-zero conductivity below the lower mode. The interaction with the phonons renders the metallic spectrum of the noninteracting case into a quasi-insulating one. The calculation is not particularly sensitive to the parameters in the model, in the sense that similar curves can be obtained with somewhat different parameters. In particular, it is possible to change systematically the coupling constant and the scattering rate and obtain very similar looking curves. Thus, the parameters used are only meant to be illustrative of what is possible.

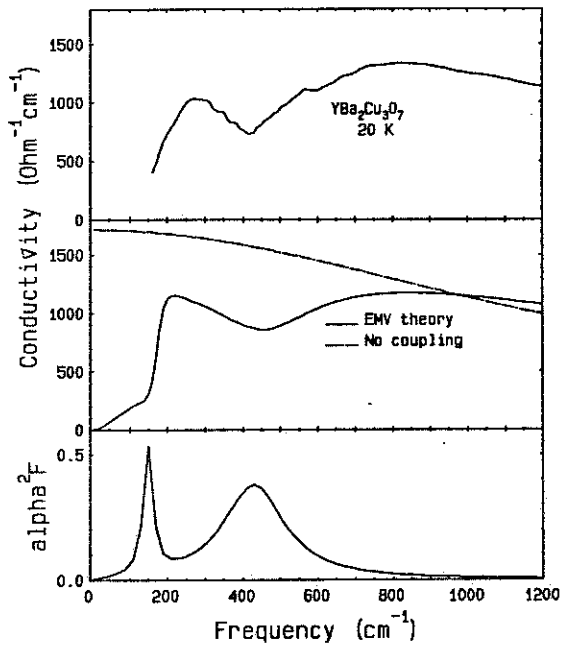

Fig. 63. The upper panel shows the frequency-dependent conductivity for $YBa_2Cu_3O_{7-\delta}$ at 20 K. Well below T_c, the free carriers have condensed, revealing the mid-infrared carriers. The center panel shows the result of taking a Drude conductivity (represented by the dash-dot line) and adding a linear coupling to phonons, using the $\alpha^2F(\omega)$ of the bottom panel. This $\alpha^2F(\omega)$ is meant to represent the experimental difference curve of Fig. 60, *i.e.*, the effect of introducing the electrons.

It is important to note that there is a second contribution to $\sigma_1(\omega)$ that is not explicitly shown in Fig. 63: the infinite dc conductivity of the superconducting condensate. The strong phonon effects seen in the spectrum occur in carriers which do not participate in the superconductivity. This midinfrared component is also seen above T_c when the free carriers have a Drude, rather than a delta-function, spectrum. A similar analysis can be carried out; again, the interaction is with the non-Drude midinfrared carriers. The interaction strength, measured by the depth of the minimum at 440 cm^{-1}, decreases with increasing temperature, but it is present all the way to room temperature.

Thus, the evidence of the phonons is that there are two components in the low-frequency spectrum of the high temperature superconductors: a free-carrier component, which interacts weakly with the phonons but which condenses to form the superconducting condensate below T_c, and a midinfrared component which interacts rather more strongly with the phonons and which is little affected by the onset of

superconductivity. The interaction with the phonons produces characteristic features in the conductivity spectrum of this second component.

E. The gap controversy

That the phonon-related features become more clearly revealed when the free carriers condense below T_c has lead to numerous cases of their being assigned to the superconducting gap. There are two reasons, however, which mitigate against the gap interpretation: the features are present in the normal state and their energy does not change very much with changes in T_c due to doping or different materials. This inert behavior is very well illustrated the results of Cooper *et al.*[25] and Orenstein *et al.*[27] shown in Fig. 57. This Figure shows the *a*-*b*-plane optical conductivity of four $YBa_2Cu_3O_{7-\delta}$ crystals that have T_c's between 30 and 90 K, on account of differing values of δ. (The reflectances of these samples are shown in Figs. 19 and 20.)

The two spectral features seen in the conductivity spectrum—the onset below T_c at ~140 cm^{-1} (0.018 eV) and the sharp notchlike minimum at 430 cm^{-1} (0.54 eV) that are visible both above and below T_c—*are unaffected by variations of a factor of 3 in carrier concentration and* T_c. The main change is simply in the value of the oscillator strength of the far- and midinfrared absorption and a shift of midinfrared oscillator strength to lower energies with increasing T_c.

The notch-like minimum is also seen at 420–450 cm^{-1} in $Y_{1-x}Pr_xBa_2Cu_3O_{7-\delta}$ with T_c between 30 and 90 K,[165] in $Bi_2Sr_2CaCu_2O_8$[55,56,62] and in $La_{2-x}Sr_xCuO_4$.[151] It would be surprising if the superconducting gap in all these materials had a value of 440 cm^{-1}, particularly as the gap ratio $2\Delta/k_BT_c$ would decrease (indicating weaker coupling) as T_c increases. The interpretation in terms of phonon effects, largely associated with oxygen motion around plane copper, is much more reasonable since phonon frequencies are little affected by temperature and since all of the materials (independent of T_c or doping level) have similar oxygen normal modes.

F. Difference from other phonon effects

We stress that the charged phonon mechanism is fundamentally different from other phonon effects in conductors. It is different from the Holstein phonon emission process, in which a charge carrier absorbs a photon, emits a phonon, and scatters with a momentum change equal to the phonon momentum. This Holstein effect gives rise to a step or threshold at the phonon energy, not to a notch-like antiresonance. A signature of the Holstein effect is a shift upwards by 2Δ of the phonon structure in

the superconducting state, which occurs because the photon must provide the energy both to break a Cooper pair and to create a phonon. A second phonon effect would be the direct excitation of a transverse optic phonon, such as occurs in insulators or compound semiconductors. Optical phonons are seen in many a-b-plane spectra as very weak structure, typically of order 0.1–0.5% in the reflectance. (The weak peaks around 350 and 560 cm^{-1} in Fig. 63 may be such phonons.) However, ordinary phonons have such a low oscillator strength compared to electronic phenomena that they cannot make a strong contribution to $\sigma_1(\omega)$.

The other effect that phonons can have on charge carriers is to contribute to the free-carrier scattering rate $1/\tau$. As already discussed, analysis of transport and infrared studies gives a weak coupling value for the coupling constant λ which governs the normal-state transport properties. With the temperature-dependent conductivity there is an associated frequency dependence of $1/\tau$. The simplest manifestation of this is a Holstein sideband at low temperature. The fraction of the area under the sideband compared to the area under the Drude curve is of the order of λ. The sideband, for coupling to a single oscillator, has an onset at $\hbar\Omega$, the energy of the excitation involved. In view of the weak coupling, the low frequency expected, and the high temperature of the experiments in the normal state, such a sideband is likely to be difficult to observe,[128] in contrast to the case in ordinary metals.[127]

VII. CONCLUSIONS

In the following we will first attempt to summarize what we believe to be our present knowledge of the infrared properties of the new high temperature superconductors. Secondly we will briefly reflect on what these properties tell us about the fundamental mechanism of high temperature superconductivity. In doing this we will exhibit some strongly felt opinions, opinions that nevertheless rest on experiments.

It is our conviction that the infrared properties of these materials, because of the wealth of detail they exhibit, show quite plainly that these are very complex systems. From one point of view this means that in wading through this mass of data, support can be found for every hypothesis. This has indeed been largely the use to which the data have been put in the past. One can, from the literature, find the superconducting gap determined to be anywhere from 1.6 k_BT_c to 8 k_BT_c. One can find evidence of coupling of the carriers to phonons, to high frequency excitations (0.5 eV peak!), or to a continuum extending from the phonon region to high frequencies.

In a more optimistic light, the great amount of detail of the infrared spectra offers opportunities for key experiments that will ultimately yield to understanding.

A. The free carriers

There is, we think, universal agreement about some of the properties of the free carriers. As Table 3 shows, the low frequency plasma frequency is known through several quite different experiments for the $YBa_2Cu_3O_{7-\delta}$ material. We also know that the coupling constant λ that governs the same charge carriers is quite small, as shown in Table 2.

Of course everyone knows that the temperature dependence of the dc resistivity is linear in T, for the $Bi_2Sr_2CuO_6$ material down to below 20 K.[67] Also well known is the fact that the Hall coefficient is temperature dependent, with the Hall number, $1/R_H$, being proportional to temperature. However, the far-infrared data show unambigously that this effect must in some way be associated with the magnetic field: direct measurement of the Drude peak shows that all the temperature dependence of the resistivity comes from a T-linear *scattering rate*; the carrier concentration is temperature independent.

The most important result on the scattering rate of the free carriers is the rapid decrease below T_c. Determined both from direct Drude line widths and from the microwave conductivity, these recent results,[140,62,141] if further confirmed, point strongly towards the domination of an electronic coupling between the charge carriers responsible for the transport current.

It is also clear from the infrared results that these same carriers form the superconducting condensate. The agreement in the spectral weights measured directly by integration and those inferred from the real part of $\epsilon(\omega)$ shows this. There is only a small leap from this idea to the conclusion that the same mechanism that gives us $1/\tau$ also is responsible for the superconducting pairing.

The question of the frequency dependency of $1/\tau$ is also clear at low frequency—there is no doubt that from the linear temperature dependence there follows a (weak) linear frequency dependence. The only problem is what portion of the infrared conductivity is to be attributed to the frequency-dependent Drude tail and what to the midinfrared band, if any. With weak coupling between the charge carriers, there is room for a midinfrared band. If all the absorption is attributed to the frequency-dependent scattering, no midinfrared band is needed. As we have seen, this idea leads to difficulties. We will address this question next.

B. The midinfrared band

There is an attractive simplicity in the hypothesis that all the observed conductivity results from one single process originating in a scattering rate that is linear with frequency. Also the fit, in the fully oxygenated $YBa_2Cu_3O_{7-\delta}$ system, to a conductivity that goes as $1/\omega$ is excellent.[112] Difficulties arise when this picture is looked at in detail. We have mentioned some of the problems in the previous Section on the midinfrared conductivity. The most serious difficulty with the one-component model is the apparent increase of the coupling strength (and mass renormalization) as T_c is *reduced* in the $YBa_2Cu_3O_x$ system. If either the marginal Fermi liquid hypothesis or the nested Fermi liquid model is to describe superconducting as well as normal-state properties, this problem has to be addressed.

At reduced carrier concentrations, a distinct midinfrared band becomes more and more evident, until at the lowest concentrations it is the only component left. Thus, it is clear that carriers on the two-dimensional CuO_2 layers can give an absorption band in the infrared. What, then, is the nature of the absorption? It may be that the marginal Fermi liquid picture is a limiting one, approached only in the fully oxygenated case. At lower oxygen concentrations, as the material in the normal state approaches a metal-insulating transition, a different picture may have to be invoked. It remains to be seen whether this low-doping range involves transitions at J, as discussed by Thomas *et al.*[48] states localized by disorder, as suggested by Phillips,[166] or polarons, as proposed by a number of workers.[167,94,168]

At higher concentrations, a separate midinfrared component still plays a role in a weak-coupling picture. It is worth noting that an electronic transition in this energy range occurs in band structure calculations,[169] in finite-lattice numerical results for Hubbard models,[170] and in the t-J model.[171,172]

C. The role of phonons

The role of phonons is an ambiguous one: on the one hand they are weakly coupled to the transport charge carriers, while on the other hand there is evidence of *strong* coupling of phonons to the midinfrared absorption.[159,107,173] The strong phonon bands seen as antiresonances in Fig. 56 are evidence of the complexity of this coupling. Not confined to one set of modes, in some systems the coupling seems to be to the 600 cm^{-1} oxygen mode, while in other systems this mode appears simply as a reststrahlen band and the coupling is to the "half-breathing" mode.

The photoinduced absorption experiments bring further evidence of a strong interaction between the phonons and the electronic degrees of freedom. Additional evidence comes from neutron spectroscopy and Raman scattering, as discussed above.

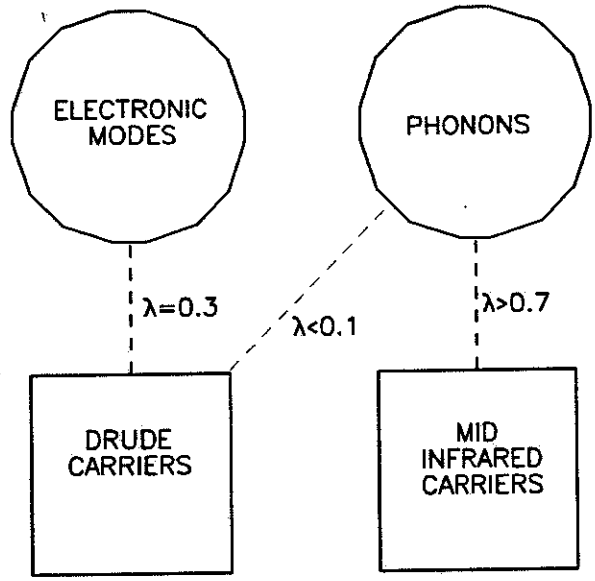

Fig. 64. The components that seem to be needed to account for the infrared properties of the high temperature superconductors.

We summarize this picture with a diagram shown in Fig. 64, drawn from a two-component perspective. This allows us to isolate the transport carriers from the phonons and gives us a second component to take care of the extra spectral weight that is needed to give the strong midinfrared band in the low doping level materials.

The coupling constants in Fig. 64 are estimates. The coupling between the Drude carriers and the excitation, likely electronic, is discussed in Table 2. The coupling of the free carriers to phonons has to very small to avoid a large negative intercept on the resistivity axis. Finally the coupling between the midinfrared carriers and phonons is estimated from the Raman widths and the coupling constants for the electron-phonon coupling to the midinfrared band.

D. The superconducting gap

As we suggested in our previous review,[1] the superconducting gap is one of the most elusive inhabitants of the high T_c zoo. Two years later we are still in the dark about its magnitude. However as a result of the recent developments, both in theory (with the marginal Fermi liquid hypothesis) and in experiments (which have measured the scattering rate in the superconducting state) we know better *why* the gap is invisible.

It was clear quite early that, because of the short coherence lengths, the materials are close to the clean limit, making the gap feature in the conductivity small as shown in Fig. 53. Nevertheless it should be visible even if the gap were quite large. It now appears that at least in the good materials, the relaxation rate drops by at least an order of magnitude at T_c, *before the gap has a chance to develop.* Thus the materials seem to plunge immediately into the extreme clean limit.

Secondly, since the first gap-related structure, according to the marginal Fermi Liquid hypothesis[114,111] appears at 4Δ in the clean limit, it is likely to be weak and, if our two component picture is correct, is certain to be lost in the strong midinfrared conductivity in the 600–1200 cm^{-1} region. If the two component picture is incorrect, if all the conductivity is to be gapped at T_c, there is a real problem to explain the finite optical conductivity down to 150 cm^{-1} seen in all the materials in the superconducting state.

In our opinion, there is no definitive evidence for a superconducting gap in the high temperature superconductors. While probes like photoemission appear to give evidence for the presence of a gap in the density of states, other methods, such as tunneling, show states within the gap region. It appears to us that infrared spectroscopy, despite four years of intense labor, has not yet revealed any definite value for the gap.

Acknowledgements

The authors would like to thank the following people for many helpful discussions: Philip Allen, Doug Bonn, John Berlinsky, Jules Carbotte, Larry Carr, Lance Cooper, Vic Emery, David Emin, Shahab Etemad, Alan Heeger, Steve Herr, Peter Hirshfeld, Catherine Kallin, Kati Kamarás, Pradeep Kumar, Peter Littlewood, Laszlo Mihaly, Andy Millis, Elisabeth Nicol, Joe Orenstein, John Preston, Maureen Reedyk, Michael

Rice, Danilo Romero, John Ruvalds, Gordon Thomas, Chandra Varma, Yaneer Bar-Yam, and Vladimir Železný. Work at McMaster is supported by the National Science and Engineering Research Council (NSERC), the Canadian Institute of Advanced Research (CIAR) and the Ontario Centre for Materials Research (OCMR). Work at Florida is supported by the NSF, Solid State Physics, DMR-9101676.

References

1. T. Timusk and D.B. Tanner in *Physical Properties of High Temperature Superconductors I,* D.M. Ginsberg, editor, (World Scientific, Singapore, 1989) p. 339.
2. J. Zaanen, G.A. Sawatzky, and J.W. Allen, *Phys. Rev. Lett.* **55**, 418 (1985).
3. D.C. Mattis and J. Bardeen, *Phys. Rev.* **111**, 412 (1958).
4. C. Thomsen and M. Cardona in *Physical Properties of High Temperature Superconductors I,* D.M. Ginsberg, editor, (World Scientific, Singapore, 1989) p. 509.
5. R. Feile, *Physica C* **159**, 1 (1989).
6. Koichi Kitazawa and Setsuko Tajima in *Some Aspects of Superconductivity,* (Nova Science Publishers, New York, 1990), to appear.
7. G.A. Thomas, in *Proceeding of the Scottish Universities Summer School on Physics of High-Temperature Superconductors,* D.P. Dunstall, editor, to appear.
8. K.F. Renk in *Studies of High Temperature Superconductors,* A.V. Narlikar, editor, (Nova Science Publishers, New York, 1991), Vol. 10. to appear.
9. K. Kamarás, C.D. Porter, M.G. Doss, S.L. Herr, D.B. Tanner, D.A. Bonn, J.E. Greedan, A.H. O'Reilly, C.V. Stager, and T. Timusk, *Phys. Rev. Lett.* **60**, 969 (1988).
10. T. Timusk, S.L. Herr, K. Kamarás, C.D. Porter, D.B. Tanner, D.A. Bonn, J.D. Garrett, C.V. Stager, J.E. Greedan, and M. Reedyk, *Phys. Rev. B* **38**, 6683 (1988).
11. G.A. Thomas, J. Orenstein, D.H. Rapkine, M. Capizzi, A.J. Millis, R.N. Bhatt, L.F. Schneemeyer, and J.V. Waszczak, *Phys. Rev. Lett.* **61**, 1313 (1988).
12. D.A. Bonn, A.H. O'Reilly, J.E. Greedan, C.V. Stager, T. Timusk, K. Kamarás, and D.B. Tanner, *Phys. Rev. B* **37**, 1574 (1988).

13. R.T. Collins, Z. Schlesinger, F. Holtzberg, P. Chaudhari, and C. Feild, *Phys. Rev. B* **39**, 6571 (1989).

14. J. Schützmann, W. Ose, J. Keller, K.F. Renk, B. Roas, L. Schultz, and G. Saemann-Ischenko, *Europhys. Lett.* **8**, 679 (1989); U. Hoffmann *et al.*, *Solid State Comm.* **70**, 325 (1989).

15. K. Kamarás, S.L. Herr, C.D. Porter, N. Tache, D.B. Tanner, S. Etemad, T. Venkatesan, E. Chase A. Inam, X.D. Wu, M.S. Hegde, and B. Dutta, *Phys. Rev. Lett.* **64**, 84 (1990).

16. K.F. Renk, H. Eschrig, U. Hoffman, J. Keller, J. Schützmann, and W. Ose, *Physica C* **165**, 1 (1990).

17. Z. Schlesinger, R.T. Collins, F. Holtzberg, C. Feild, G. Koren, and A. Gupta, *Phys. Rev. B* **41**, 11237 (1990).

18. Y. Watanabe, Z.Z. Wang, S.A. Lyon, D.C. Tsui, N.P. Ong, J.M. Tarascon, and P. Barboux, *Phys. Rev. B* **40**, 6884 (1989).

19. Z. Schlesinger, R.T. Collins, F. Holtzberg, C. Feild, S.H. Blanton, U. Welp, G.W. Crabtree, Y. Fang, and J.Z. Liu, *Phys. Rev. Lett.* **65**, 801 (1990).

20. Ivan Bozovic, *Phys. Rev. B* **42**, 1969 (1990).

21. R.T. Collins, Z. Schlesinger, F. Holtzberg, C. Feild, U. Welp, G.W. Crabtree, J.Z. Liu, and Y. Fang *Phys. Rev. B* **43**, 8701 (1991).

22. D. van der Marel, H.-U. Habermeier, D. Heitmann, W. König, A. Wittlin, *Physica C* **176**, 1 (1991).

23. C.M. Varma, P.B. Littlewood, S. Schmitt-Rink, E. Abrahams, and A. Ruckenstein, *Phys. Rev. Lett.* **63**, 1996 (1989); *ibid,* **64,** 497, (1990) (E).

24. A. Virosztek and J. Ruvalds, *Phys. Rev. B* **42**, 4064 (1990); *Physica B* **165&166**, 1267 (1990).

25. S.L. Cooper, G.A. Thomas, J. Orenstein, D.H. Rapkine, M. Capizzi, T. Timusk, A.J. Millis, L.F. Schneemeyer, and J.V. Waszczak, *Phys. Rev. B* **40**, 11358 (1989).

26. B. Koch, H.P. Geserich, and T. Wolf, *Solid State Comm.* **71**, 495 (1989).

27. J. Orenstein, G.A. Thomas, A.J. Millis, S.L. Cooper, D.H. Rapkine, T. Timusk, L.F. Schneemeyer, and J.V. Waszczak, *Phys. Rev. B* **42**, 6342 (1990).

28. S.L. Cooper, G.A. Thomas, J. Orenstein, D.H. Rapkine, A.J. Millis, S.-W. Cheong, A.S. Cooper, and Z. Fisk, *Phys. Rev. B* **41**, 11605 (1990).

29. Yun-Yu Wang, Goufu Feng, and A.L. Ritter, *Phys. Rev. B* **42**, 420 (1990).

30. C.M. Foster, K.F. Voss, T.W. Hagler, D. Mihailović, A.J. Heeger, M.M. Eddy, W.L. Olsen, and E.J. Smith, *Solid State Comm.* **76**, 651 (1990).

31. L. Forro, G.L. Carr, G.P. Williams, D. Mandrus, and L. Mihaly, *Phys. Rev. Lett.* **65**, 1941 (1990).

32. F. Gao, G.L. Carr, C.D. Porter, D.B. Tanner, S. Etemad, T. Venkatesan, A. Inam, B. Dutta, X.D. Wu, G.P. Williams, and C.J. Hirschmugl *Phys. Rev. B* **43**, 10383 (1991).

33. S. Uchida, T. Ido, H. Takagi, T. Arima, Y. Tokura, and S. Tajima, *Phys. Rev. B* **43**, 7942 (1991).

34. Ji-Guang Zhang, Xiang-Xin Bi, E. McRae, P.C. Eklund, B.C, Sales, and Mark Mostoller, *Phys. Rev. B* **43**, 5389 (1991).

35. J.H. Kim, I Bozovic, J.S. Harris, Jr., W.Y. Lee, C.-B. Eom, and T.H. Geballe, preprint.

36. J. Orenstein, G.A. Thomas, D.H. Rapkine, C.B. Bethea, B.F. Levine, R.J. Cava, E.A. Reitman, and D.W. Johnson, Jr., *Phys. Rev. B* **36**, 729 (1987).

37. S.L. Herr, K. Kamarás, C.D. Porter, M.G. Doss, D.B. Tanner, D.A. Bonn, J.E. Greedan, C.V. Stager, and T. Timusk, *Phys. Rev. B* **36**, 733 (1987).

38. S. Tajima, S. Uchida, S. Tanaka, S. Kanbe, K. Kitazawa, and K. Fueki, *Jpn. J. Appl. Phys.* **26**, 432 (1987).

39. J. Orenstein, G.A. Thomas, D.H. Rapkine, C.B. Bethea, B.F. Levine, B. Batlogg, R.J. Cava, D.W. Johnson, Jr., and E.A. Rietman, *Phys. Rev. B* **36**, 8892 (1987).

40. S. Etemad, D.E. Aspnes, M.K. Kelly, R. Thompson, J.M. Tarascon, and G.W. Hull, *Phys. Rev. B* **37**, 3396 (1988).

41. S.L. Herr et al. in *High Temperature Superconducting Materials: Preparations, Properties and Processing,* William Hatfield and J.J. Miller, editors, (Marcel Dekker, Inc., New York, 1988), p. 275.

42. G.L. Doll, J.T. Nicholls, M.S. Dresselhaus, A.M. Rao, J.M. Zhang, G.W. Lehman, P.C. Eklund, G. Dresselhaus, and A.J. Strauss, *Phys. Rev. B* **38**, 8850 (1988).

43. S. Tajima, S. Uchida, H. Ishii, H. Takagi, S. Tanaka, U. Kawabe, H. Hasegawa, T. Aita, and T. Ishiba, *Mod. Phys. Lett. B* **1**, 353 (1988).

44. R.T. Collins, Z. Schlesinger, G.V. Chandrashekhar, and M.W. Shafer, *Phys. Rev. B* **39**, 2251 (1989).

45. S. Uchida, H. Takagi, and Y. Tokura, *Physica C* **162-164**, 1677 (1989).

46. S. Tajima, T. Ido, S. Ishibashi, T. Itoh, H. Eisaki, T. Arima, H. Takagi, S. Uchida, *Phys. Rev. B* **43**, 10496 (1991).

47. S.L. Herr, K. Kamarás, D.B. Tanner, S.-W. Cheong, G.R. Stewart, and Z. Fisk, *Phys. Rev. B* **43**, 7847 (1991).

48. G.A. Thomas, D.H. Rapkine, S.L. Cooper, S-W. Cheong, A.S. Cooper, L.F. Schneemeyer, and J.V. Waszczak, *Phys. Rev. B,* to be published.

49. G.A. Thomas, D.H. Rapkine, S.L. Cooper, S.-W. Cheong, and A.S. Cooper, *Phys. Rev. Lett.* **67**, 2906 (1991).

50. M.S. Hybertsen and L.F. Mattheiss, *Phys. Rev. Lett.* **60**, 1661 (1988); H. Krakauer and W.E. Pickett, *Phys. Rev. Lett.* **60**, 1665 (1988); F. Hermann R.V. Kasowski, and W.Y. Hsu, *Phys. Rev. B* **38**, 204 (1988).

51. M. Tanaka, T. Takahashi, H. Katayama-Yoshida, S. Yamazaki, M. Fujinami, Y. Okabe, W. Mizutani, M. Ono, and K. Kajimura, *Nature* **339**, 691 (1989).

52. Yun-Yu Wang and A.L. Ritter, *Phys. Rev. B* **43**, 1241 (1991).

53. B.O. Wells, Z.-X. Shen, D.S. Dessau, W.E. Spicer, C.G. Olson, D.B. Mitzi, A. Kapitulnik, R.S. List, and A. Arko, *Phys. Rev. Lett.* **65**, 3056 (1990).

54. A. Maeda, M. Hase, I. Tsukada, K. Noda, S. Takebayashi, and K. Uchinokura, *Phys. Rev. B* **41**, 6418 (1990).

55. M. Reedyk, D.A. Bonn, J.D. Garrett, J.E. Greedan, C.V. Stager, T. Timusk, K. Kamarás, and D.B. Tanner, *Phys. Rev. B* **38**, 11981 (1988).

56. K. Kamarás, S.L. Herr, C.D. Porter, J.S. Kim, B. Andraka, G.R. Stewart, D.B. Tanner, M. Reedyk, D.A. Bonn and T. Timusk, preprint.

57. O.V. Kosogov, M.V. Belousov, V.A. Vasil'ev, V.Y. Davydov, K.G. Dyo, A.A. Kopylov, V.D. Petrikov, and V.V. Tret'yakov, *JETP Lett.* **48**, 530 (1989).

58. J. Humlicek, E. Schmidt, L. Bocanek, M. Garriga, and M. Cardona, *Solid State Comm.* **73**, 127 (1990).

59. A.M. Rao, P.C. Eklund, G.W. Lehman, D.W. Face, G.L. Doll, G. Dresselhaus, M.S. Dresselhaus, *Phys. Rev. B* **42**, 193 (1990).

60. P. Calvani, M. Capizzi, S. Lupi, P. Maselli, D. Peschiaroli, and H. Katayama-Yoshida, *Solid State Comm.* **74**, 1333 (1990).

61. D.B. Romero, G.L. Carr, D.B. Tanner, L. Forro, D. Mandrus, L. Mihály, and G.P. Williams, *Phys. Rev. B* **44**, 2818 (1991).

62. D.B. Romero, C.D. Porter, D.B. Tanner, L. Forro, D. Mandrus, L. Mihaly, G.L. Carr, and G.P. Williams *Solid State Comm.,* submitted.

63. D.B. Tanner, D.B. Romero, K. Kamarás, G.L. Carr, L. Forro, D. Mandrus, L. Mihály, and G.P. Williams, in *Electronic Structure and Mechanisms for High-Temperature Superconductivity,* G.C. Vezolli *et al.*, editors, (Plenum Press, New York, 1991).

64. R.E. Glover and M. Tinkham, *Phys. Rev. B* **107**, 844 (1956); **108**, 243, (1957).

65. D.A. Bonn, J.E. Greedan, C.V. Stager, T. Timusk, M.G. Doss, S.L. Herr, K. Kamarás, C.D. Porter, D.B. Tanner, J.M. Tarascon, W.R. McKinnon, and L.H. Greene, *Phys. Rev. B* **35**, 8843 (1987).

66. Frederick Wooten, *Optical Properties of Solids* (Academic Press, New York, 1972).

67. S. Martin, A.T. Fiory, R.M. Fleming, L.F. Schneemeyer, and J.V. Waszczak, *Phys. Rev. B* **41**, 846 (1990).

68. Ivan Božović, J.H. Kim, J.S. Harris, Jr., and W.Y. Lee, *Phys. Rev. B* **43**, 1169 (1991).

69. G. Jehl, T. Zetterer, H.H. Otto, J. Schützmann, S. Shulga, and K.F. Renk, *Europhys. Lett.,* to be published.

70. M.Reedyk, T. Timusk, J.S. Xue, and J.E. Greedan, *Phys. Rev. B,* to be published.

71. D.B. Tanner, S.L. Herr, K. Kamarás, C.D. Porter, N. Tache, S. Etemad, T. Venkatesan, A. Inam, X.D. Wu, M.S. Hegde, and B. Dutta, in *Proceedings of the Third European Conference on Low Dimensional Conductors and Superconductors,* S. Barišić and E. Tutiš, editors, (Fizika, Zagreb, 1990), pp. 205–209.

72. Steven L. Herr, K. Kamarás, C.D. Porter, N. Tache, D.B. Tanner, S. Etemad, T. Venkatesan, E. Chase, A. Inam, X.D. Wu, M.S. Hegde, and B. Dutta, in *Superconductivity Applications for Infrared and Microwave Devices*, K.B. Bhasin and V.O. Heinen, editors, (SPIE, Bellingham, Washington, 1990), pp 44–51.

73. R.T. Collins, Z. Schlesinger, F. Holtzberg, and C. Feild, *Phys. Rev. Lett.* **63**, 422 (1989).

74. K.F. Renk, J. Schützmann, A. Prückl, W. Ose, B. Roas, L. Schultz, and G. Saemann-Ischenko, in *Electronic Properties of High-T_c Superconductors and Related Compounds,* H. Kuzmany, M, Mehrig, J. Fink, editors, (Springer Series in Solid State Sciences, Vol 99, Springer- Verlag, Berlin - Heidelberg, 1990), p. 275.

75. H. Lengfellner, Gi. Schneider J. Betz, M. Hogan, W. Prettl, and K.F. Renk, *Europhys. Lett.* **15**, 343 (1991).

76. K.F. Renk, B. Gorshunov, J. Schützmann, A. Prückl, B. Brunner, J. Betz, S. Orbach, N. Klein, G. Müller, and H. Piel, *Europhys. Lett.* **15**, 661 (1991).

77. R.T. Collins, Z. Schlesinger, M.W. Shafer, and T.R. McGuire, *Phys. Rev. B* **37**, 5817 (1988).

78. J. Tanaka, K. Kamya, M. Shimizu, M. Simada, C. Tanaka, H. Ozeki, K. Adachi, K. Iwahashi, F. Sato, A. Sawada, S. Iwata, H. Sakuma, and S Uchiyama, *Physica C* **153–155**, 1752 (1988).

79. M.P. Petrov, A.I. Grachev, M.V. Krasin'kova, A. A. Nechitailov, V.V. Prokofiev, V.V. Poborchy, S.I. Shagin, and N.F. Kartenko, *Solid State Comm.* **67**, 1197 (1988).

80. S.L. Cooper, A.L. Kotz, M.A. Karlov, M.V. Klein, W.C. Lee, J. Giapintzakis, and D.M. Ginsberg, *Phys. Rev. B,* to be published.

81. T.A. Friedmann, W.M. Rabin, J. Giapintzakis, J.P. Rice, and D.M. Ginsberg, *Phys. Rev. B* **42**, 6217 (1990).

82. U. Welp, S. Flesher, W.K. Kwok, J. Downey, Y. Fang, and G.W. Crabtree, *Phys. Rev. B* **42**, 10189 (1990).

83. For a review of NMR data see C.H. Pennington and C.P. Schlichter in *Physical Properties of High Temperature Superconductors II,* D.M. Ginsberg, editor, (World Scientific, Singapore, 1990) p. 269.

84. B. Bucher, J. Karpinsky, E. Kaldis, and P. Wachter, *Physica C* **167**, 324 (1990).

85. S. Tajima, S. Uchida, A. Masaki, H. Tagaki, K. Kitazawa, and S. Tanaka, *Phys. Rev. B* **32**, 6302 (1985).

86. C.N. Berglund and H.J. Braun, *Phys. Rev.* **164**, 790 (1967).

87. X. Bi, P.C. Eklund, E. McRae, J. Zhang, P. Metcalf, J. Spalek, and J.M. Honig, *Phys. Rev. B* **42**, 4756 (1990).

88. D.A. Crandles, T. Timusk, J.E. Greedan, *Phys. Rev. B,* to be published.

89. Y. Watanabe, D.C. Tsui, J.T. Birmingham, N.P. Ong, and J.M. Tarascon *Phys. Rev. B* **43**, 3026 (1991).

90. Y.H. Kim, A.J. Heeger, L. Acedo, G. Stucky, and F. Wudl, *Phys. Rev. B* **36**, 7252 (1987).

91. J.M. Ginder, M.G. Roe, Y. Song, R.P. McCall, J.R. Gaines, E. Ehrenfreund, and A.J. Epstein, *Phys. Rev. B* **37**, 7506 (1988).

92. C. Taliani, R. Zamboni, G. Ruani, F.C. Matacotta, and K.I. Pokhodnya, *Solid State Comm.* **66**, 487 (1988).

93. Y.H. Kim, C.M. Foster, A.J. Heeger, S. Cox, and G. Stucky, *Phys. Rev. B* **38**, 6478 (1988).

94. C.M. Foster, A.J. Heeger, G. Stuckey, and N. Heron, *Solid State Comm.* **71**, 945 (1989).

95. H.J. Ye, R.P. McCall, W.E. Farneth, E.M. McCarron III, and A.J. Epstein, *Phys. Rev. B* **43**, 10574 (1991).

96. J.F. Frederici, B.I. Greene, D.H. Rapkine, and J. Orenstein, *Phys. Rev. B* **43**, 8617 (1991).

97. D. Mihailović, T. Mertelj, K.F. Voss, A.J. Heeger, and N. Herron, *Phys. Rev. B* **44**, 237 (1991).

98. Y.H. Kim, S-W. Cheong, and Z. Fisk, *Phys. Rev. Lett.* **67**, 2227 (1991).

99. X. Wei, L. Chen, Z.V. Vardeny, C. Taliani, R. Zamboni, A.J. Pal, and G. Ruani, *Physica C* **162-164**, 1109 (1989).

100. J. Orenstein and D.H. Rapkine, *Phys. Rev. Lett.* **60**, 968 (1988).

101. M.K. Crawford, G. Burns, and F. Holtzber, *Solid State Comm.* **70**, 557 (1989).

102. J. Orenstein and G.L. Baker, *Phys. Rev. Lett.* **49**, 1043 (1980).

103. W.R. Salaneck *et al.*, *Phys. Rev. Lett.* , 49, 801 (1982).

104. M.J. Rice, *Phys. Rev. Lett.* **37**, 36 (1976).

105. B. Horovitz, *Solid State Comm.* **41**, 729 (1982).

106. C.M. Foster, A.J. Heeger, Y.H. Kim, and G. Stucky, *Physica C* **162-164**, 1107 (1989).

107. T. Timusk, C.D. Porter, and D.B. Tanner, *Phys. Rev. Lett.* **66**, 663 (1991).

108. T. Pham, H.D. Drew, S.H. Moseley, and J.Z. Liu, *Phys. Rev. B* **41**, 11681 (1990).

109. P.W. Anderson, *Mater. Res. Bull.* **8**, 153 (1973); P.W. Anderson, *Science* **235**, 1196 (1987); P.W. Anderson, in *Frontiers and Borderlines in Many Particle Physics,* J.R. Schreiffer and R.A. Broglia, editors, (North-Holland, Amsterdam, 1989); R.B. Laughlin, *Science* **242**, 525 (1988); P.W. Anderson, *Phys. Rev. Lett.* **64**, 1839 (1990).

110. C.M. Varma, *Int. J. Mod. Phys. B* **3**, 2083 (1989).

111. P.B. Littlewood and C.M. Varma, *J. Appl. Phys.* **69**, 4979 (1991).

112. J. Ruvalds and A. Virosztek, *Phys. Rev. B* **43**, 5498 (1991).

113. E.J. Nicol, J.P. Carbotte, and T. Timusk, *Phys. Rev. B* **43**, 473 (1991).

114. J. Orenstein and S. Schmitt-Rink, in *Electronic Properties of High-T_c Superconductors and Related Compounds,* H. Kuzmany, M, Mehrig, J. Fink, editors, (Springer Series in Solid State Sciences, Vol 99, Springer- Verlag, Berlin - Heidelberg, 1990).

115. M.K. Kelly, P. Barboux, J.-M. Tarascon, D.E. Aspnes, W.A. Bonner, and P.A. Morris, *Phys. Rev. B* **38**, 870 (1988).

116. M. Garriga, J. Humlicek, J. Barth, R.L. Johnson, and M. Cardona, *J. Opt. Soc. Am. B* **6**, 470 (1989).

117. J. Kircher, M.K. Kelly, S. Rashkeev, M. Alouani, D. Fuchs, and M. Cardona *Phys. Rev. B* **44**, 217 (1991).

118. M. Gurvitch and A.T. Fiory, *Phys. Rev. Lett.* **59**, 1337 (1987).

119. M. Reedyk and T. Timusk, unpublished.

120. D.B. Romero, C.D. Porter, D.B. Tanner, L. Forro, D. Mandrus, L. Mihaly, G.L. Carr, and G.P. Williams *Phys. Rev. Lett.,* submitted.

121. P.B. Allen, T.B. Beaulac, F.S. Khan, W.H. Butler, F.J. Pinski, and J.H. Swihart, *Phys. Rev. B* **34**, 4331 (1986).

122. S. Martin, A.T. Fiory, R.M. Fleming, L.F. Schneemeyer, and J.V. Waszczak, *Phys. Rev. Lett.* **60**, 2194 (1988).

123. I. Bozovic, D. Kirillov, A. Kapitulnik, K. Char, M.R. Hahn, M.R. Beasley, T.H. Geballe, Y.H. Kim, and A.J. Heeger, *Phys. Rev. Lett.* **59**, 2219 (1987).

124. Z. Schlesinger, R.T. Collins, D.L. Kaiser, and F. Holtzberg, *Phys. Rev. Lett.* **59**, 1958 (1987).

125. T. Holstein, *Phys. Rev* **96**, 539, (1954); *Ann. Phys. (N.Y.)* **29**, 410, (1964).

126. P.B. Allen, *Phys. Rev. B* **3**, 305 (1971).

127. In conventional strong-coupling metals, such as lead, a Holstein sideband due to electron-phonon coupling has been observed in the normal state infrared spectra. See R.R. Joyce and P.L. Richards, *Phys. Rev. Lett.* **24**, 1007 (1970), G. Brändli and A.J. Sievers, *Phys. Rev. B* **5**, 3550 (1972), and B. Farnworth and T. Timusk, *Phys. Rev. B* **14**, 5119 (1976) for details.

128. N.E. Bickers, D.J. Scalapino, R.T. Collins, and Z. Schlesinger, *Phys. Rev. B* **42**, 67 (1990).

129. F. Slakey, S.L. Cooper, M.V. Klein, J.P. Rice, E.D. Bukowsky, and D.M. Ginsberg, *Phys. Rev. B* **38**, 11934 (1989).

130. S. Sugai, *Solid State Comm.* **72**, 1193 (1989).

131. C.G. Olson, R. Liu, D.W. Lynch, R.S. List, A.J. Arko, B.W. Veal, Y.C. Chang, P.Z. Jiang and A.P. Paulikas, *Phys. Rev. B* **42**, 381 (1990).

132. Y. Hwu, L. Lozzi, M. Marsi, S. La Rosa, M. Winokur, P. Davis, M. Onellion, H. Berger, F. Gozzo, F. Lévy, and G. Margaritondo, *Phys. Rev. Lett.* **67**, 2573 (1991).

133. A. Virosztek and J. Ruvalds, *Phys. Rev. B* **42**, 4064 (1990); *Physica B* **165&166**, 1267 (1990).

134. J.H. Kim, I. Bozovic, D.B. Mitzi, A. Kapitulnik, and J.S. Harris Jr., *Phys. Rev. B* **41**, 7251 (1990).

135. J.W. Allen and J.C. Mikkelsen, *Phys. Rev. B* **15**, 2952 (1977).

136. L.D. Rotter, Z. Schlesinger, R.T. Collins, F. Holtzberg, C. Field, U. Welp, G.W. Crabtree, J.Z. Liu, and Y. Fang G. Vandervoort, and S. Fleshler, *Phys. Rev. Lett.* **67**, 2741 (1991).

137. D.R. Harshman, L.F. Schneemeyer, J.V. Waszczak, G. Aeppli, R.J. Cava, B. Batlogg, L.W. Rupp, E.J. Ansoldo, and D.L. Williams, *Phys. Rev. B* **39**, 851 (1989).

138. L.H. Palmer and M. Tinkham, *Phys. Rev.* **165**, 588 (1968).

139. E.J. Nicol, J.P. Carbotte, and T. Timusk, *Phys. Rev. Lett.,* submitted.

140. M.C. Nuss, P.M. Mankiewich, M.L. O'Malley, and E.H. Westwick, *Phys. Rev. Lett.* **66**, 3305 (1991).

141. D.A. Bonn, P. Dosanjh, R. Liang, W.N. Hardy, *Phys. Rev. Lett.,* submitted.

142. B. Koch, M. Dürrler, H.P. Geserich, Th. Wolf, G. Roth, and G. Zachmann, in *Electronic Properties of High-T_c Superconductors and Related Compounds,* H. Kuzmany, M, Mehrig, J. Fink, editors, (Springer Series in Solid State Sciences, Vol 99, Springer-Verlag, Berlin - Heidelberg, 1990), p. 290.

143. R.A. Hughes, T. Timusk, S.L. Cooper, G.A. Thomas, J.J. Yeh, and M. Hong, *Phys. Rev. B* **40**, 5162 (1989).

144. T. Pham, H.D. Drew, S.H. Moseley, and J.Z. Liu, *Phys. Rev. B* **44**, 5377 (1991).

145. M.S. Sherwin, P.L. Richards, and A. Zettl, *Phys. Rev. B* **37**, 1587 (1988).

146. V. Železný, D.B. Tanner, and K. Kamarás, *Bull. Am. Phys. Soc.* **36**, 418 (1991).

147. S.H. Wang, B.P. Clayman, S. Gygax, R.R. Parsons, *Physica C* **162-164**, 1077 (1989).

148. K. Kamarás, S. L. Herr, C.D. Porter, D.B. Tanner, S. Etemad, and J.-M. Tarascon, *Phys. Rev. B* **43**, 11381–11383 (1991).

149. M.Reedyk, T. Timusk, J.S. Xue, and J.E. Greedan, (unpublished).

150. R.A. Hughes, Y. Lu, J.S. Preston, and T. Timusk, in *Proceedings of the Fifth Annual Conference on Superconductivity and Applications, Buffalo 1991,* (AIP Conference Proceedings) to be published.

151. Feng Gao, D.B. Romero, D.B. Tanner, J. Talvacchio, and M.G. Forrester, unpublished.

152. D. Miller, P.L. Richards, S. Etemad, T. Venkatessan, L. Nazar, B. Dutta, X.D. Wu, A. Inam, C.B. Eom, T.H. Geballe, N. Newman, and B.F. Cole, *Bull. Am. Phys. Soc.* **36**, 880 (1991).

153. F. Slakey, M.V. Klein, J.P. Price, and D.M. Ginsberg, *Phys. Rev. B* **42**, 2643 (1990).

154. B. Friedl, C. Thomsen, and M. Cardona, *Phys. Rev. Lett.* **65**, 915 (1990).

155. C. Thomsen, M. Cardona, B. Friedel, C.O. Rodriguez, I.I. Mazin, and O.K. Andersen, *Solid State Comm.* **75**, 219 (1990).

156. B. Renker, F. Gompf, E. Gering, D. Ewert, H. Rietschek, and A. Dianoux, *Z. Phys. B – Condensed Matter* **73**, 309 (1988).

157. W. Reichard, N. Pyka, L. Pintschovius, B. Hennion, and G. Collin, Int. Conf. on Superconductivity, Stanford, 1989, *Physica C.* **162 – 164**, 464 (1989).

158. H.A. Mook, M. Mostoller, J.A. Harvey, N.W. Hill, B.C. Chakoumakos, and B.C. Sales, *Phys. Rev. Lett.* **65**, 2712 (1990).

159. T. Timusk and D.B. Tanner, *Physica C* **169**, 425 (1990).

160. M.J. Rice, L. Pietronero and P. Bruesch, *Solid State Comm.* **21**, 757 (1977).

161. M.J. Rice, V.M. Yartsev, and C.S. Jacobsen, *Phys. Rev. B* **21**, 3437 (1980).

162. For a review see A. Painelli and A. Girlando, *J. Chem. Phys.* **84**, 5655 (1986).

163. D.B. Tanner, J.E. Deis, A.J. Epstein, and J.S. Miller, *Solid State Comm.* **31**, 671 (1979).

164. A. Cougrand, S. Flandrois, P. Delhaes, P. Depuis, D. Chasseau, J. Galtier, and J.L. Miane, *Mol. Cryst. Liq. Cryst.* **32**, 165 (1976).

165. N. Tache, D.B. Romero, D.B. Tanner, S. Etemad, and A. Inam, unpublished.

166. J.C. Phillips *Phys. Rev. Lett.* **43**, 11415 (1991).

167. M. J. Rice, and Y. R. Wang, *Phys. Rev. B* **36**, 8794 (1987); M.J. Rice and S. Jeydev, *Synth. Met.* **22**, 209 (1987).

168. David Emin in *Physics and Materials Science of High Temperature Superconductors-II,* R. Kossowsky, N. Raveau, and S. Patapis, editors, (Kluwer, Netherlands, 1992); submitted to *Phys, Rev. B.*

169. S.T Chui, R.V. Kasowski, and W.Y. Hsu, *Phys. Rev. Lett.* **61**, 885 (1988).

170. C.-X. Chen and H.-B. Schüttler *Phys. Rev. B* **43**, 3771 (1991).

171. W. Stephan and P. Horsch, *Phys. Rev. B* **42**, 8736 (1990).

172. D. Poilblanc, *Phys. Rev. B* **44**, 9562 (1991).

173. T. Timusk and D.B. Tanner, *Mod. Phys. Lett.,* to be published.